ADDIS ABABA UNIVERSITY

ADDIS ABABA INSTITUTE OF TECHNOLOGY SCHOOL OF CIVIL AND ENVIRONMENTAL ENGINEERING

AN EXPERIMENTAL INVESTIGATION ON THE EFFECT AND MECHANISM OF SIDE COVER FOR DEEP BEAMS

A Thesis in Structural Engineering by

Muhammed Jemal

July-2025

Addis Ababa, Ethiopia

The undersigned have examined the thesis entitled "**An Experimental Investigation on the Effect and Mechanism of Side Cover for Deep Beams**" presented by Muhammed Jemal, a candidate for the degree of master of science and hereby certify that it is worthy of acceptance.

Dr. Esayas G/Youhannes		18/07/25
Advisor	Signature	Date
Dr. Ing Adil Zekaria	for	July 18/2025
Internal Examiner	Signature	Date
Dr. Edom Adane		18/07/25
External Examiner	Signature	Date
Dr. Tensay Gebremedhin		18/07/25
Chair Person	Signature	Date

Tensay Gebremedhin Berhe (Dr.-Ing.)
I/Head, School of Civil &
Environmental Engineering

Vice Executive Dean Office for Academic Affairs
Addis Ababa University
College of Technology and Built Environment

A Thesis

Submitted in Partial Fulfillment of the Requirements for the Degree of Master of Science

UNDERTAKING

I certify that research work titled "An Experimental Investigation on the Effect and Mechanism of Side Cover for Deep Beams" is my own work. The work has not been presented elsewhere for assessment. Where material has been used from other sources it hasbeen properly acknowledged/ referred.

Muhammed Jemal

ACKNOWLEDGMENT

Praises and glory to the almighty Allah for showers of blessings, patience, and strength throughout my research work. I would also like to thank my parents for their unconditional support and encouragement during this research.

I would like to express my heartfelt gratitude to my advisor and mentor, Dr. Esayas Gebreyouhannes, for his invaluable support and guidance throughout my journey. He has navigated me through the challenging experimental process with motivation and encouragement. He dedicated time from his busy schedule to personally oversee many of the tests. His logical and innovative approach to research has enabled us to achieve the necessary results reliably. I am also thankful for the essential laboratory instruments, testing equipment, and construction materials he provided for specimen production, as well as for adapting existing lab equipment to suit the experimental design. This research would not have been possible without his support. His integrity, intelligence, and encouragement have genuinely inspired me. It is a true honor and privilege to learn from, be advised by, and be mentored by such a humble individual. I am incredibly grateful for everything he has contributed to my work.

I would also like to acknowledge the technicians and staff of the Construction Material Laboratory at AAiT—Demis M., Fikru B., Biniyam, and Wubet A.—for their assistance, patience, and understanding throughout the lengthy and demanding experimental process. Additionally, I extend my thanks to the technicians in the Mechanical Workshop, particularly Mr. Masresha, for his technical support whenever it was needed.

ABSTRACT

This study investigates the effect and underlying mechanism of side cover spalling in reinforced concrete deep beams subjected to shear. While prior research, such as that by [2], has focused on slender beams, this thesis addresses a critical gap by examining deep beams, whose shear behavior is governed by arch action rather than flexural beam theory. A series of six full-scale deep beams with varying side cover thicknesses and stirrup cage configurations were experimentally tested under three-point monotonic loading. Two configurations were explored: SA-series beams, which maintained a constant outer width and reduced the core with increasing cover, and SB-series beams, which preserved the core width while increasing total width by adding cover externally.

The primary aim was to determine whether large concrete covers compromise shear performance due to premature side cover spalling. Observations revealed that spalling initiates near peak load, particularly when the stirrup cage is confined by a reduced core, as in the SA-series. Despite observable spalling in all specimens, the presence of adequate core concrete and stirrup confinement significantly influenced the beams' ability to reach peak load without premature failure. Finite element modeling results from Vector2 were compared with the experimental findings. The Experimental findings highlighted the limitations of current two-dimensional analyses in capturing out-of-plane spalling.

Importantly, the results demonstrate that increasing the concrete side cover does not enhance the stiffness (except for the initial stiffness) or peak load capacity of deep beams. This finding sharply contrasts with the assumptions in most building design codes, such as ACI 318 and Eurocode 2, which treat the entire cross-sectional width—including the cover zones—as fully effective in resisting shear and flexure. The test results suggest that once the core (stirrup-confined zone) is sufficient, additional concrete cover adds little to structural performance and may even introduce weaknesses due to spalling risk. Additionally, SB-series beams display stable load-displacement behavior with limited post-peak softening, indicating improved ductility relative to SA-series specimens.

This research contributes to a more accurate understanding of D-region behavior in deep beams and underscores the need to re-evaluate code provisions related to effective shear/flexure width, particularly in the presence of large concrete covers.

Contents

List of Figures

List of tables

1 INTRODUCTION

1.1 Background

Reinforced concrete structures are renowned for their versatility and widespread application in civil engineering, offering a robust and durable solution for various construction needs. Reinforced concrete has gained immense popularity and widespread usage in the construction industry due to its inherent characteristics and the continuous advancements in materials and construction techniques. Several factors contribute to the widespread adoption and versatility of reinforced concrete structures, as evidenced by various research studies in the field. The ability of reinforced concrete to withstand these diverse loads is a testament to its adaptability and strength [1].

However, despite these advantages, reinforced concrete is not without its challenges. One significant issue that arises is spalling, which refers to the delamination of concrete in specific areas, primarily from the core. This phenomenon has traditionally been associated with members subjected to axial compression and torsional loading [2]. Stress-induced spalling occurs when internal stresses develop within the concrete member, leading to the detachment or breakage of the concrete cover. Factors such as tensile stress from the corrosion of reinforcing bars, compressive stress in concrete structures, and the interplay of mechanical loading and thermal stresses often contribute to this issue [3], [4].

The occurrence of stress-induced spalling can be attributed to various mechanisms and conditions. For instance, compressive stress in concrete structures can increase the risk of spalling by reducing tensile cracking in the tension zone of beams subjected to prestressing or inducing microcracking in slabs under uniaxial and biaxial loading conditions [4]. The development of compressive stresses in concrete elements can lead to reduced tensile strength in the tension zone, making the structure more susceptible to spalling. Additionally, the presence of mechanical and hydraulic stresses in concrete structures can contribute to stress-induced spalling. When these stresses exceed the tensile strength of concrete, the spalling phenomenon occurs, resulting in the detachment of concrete layers or pieces from the structure's surface [5]. The combination of mechanical loading, hydraulic mechanisms, and stress levels can lead to the development of internal stresses that trigger spalling in reinforced concrete elements.

Building code provisions play a crucial role in addressing stress-induced spalling by providing guidelines and requirements for concrete cover thickness, reinforcement detailing, and structural design considerations. The correlation between stress-induced side cover spalling and building code provisions lies in the provisions aimed at ensuring adequate concrete cover to protect the reinforcement from corrosion-induced stresses, which can lead to spalling [6]. Building codes often specify minimum concrete cover requirements to safeguard the reinforcement and prevent premature failure due to spalling [7].

The durability of concrete structures in aggressive environments is a critical consideration in structural design, particularly in ensuring the protection of steel reinforcement against threats of corrosion and fire. Building codes provide guidelines for determining the thickness of concrete cover to structural members based on various factors such as environmental conditions, durability requirements, bond requirements, fire resistance, and the structural class of the structure. These provisions aim to enhance the longevity and performance of reinforced concrete elements in challenging environments.

Eurocode 2 [8] recommends using concrete clear cover up to 55mm, with the thickness determined by exposure classes related to environmental conditions and structural requirements. ACI 318-19 [9]section 20.5.1.3 specifies cover depths up to 75mm unless greater concrete cover is needed for fire protection and corrosive environments. AASHTO LRFD Bridge Design Specifications 9th edition [10] suggests using concrete clear cover up to 120mm, reflecting the need for increased cover thickness in certain conditions to ensure the durability and safety of concrete structures in aggressive environments.

Ensuring the durability of concrete structures, especially in aggressive environments, is a paramount concern in structural engineering. One crucial aspect of enhancing durability is the provision of proper concrete cover to protect steel reinforcement from corrosion and fire hazards. However, while a thicker concrete cover is often associated with increased crack width in flexural reinforced concrete members [11], the effectiveness of this cover can be compromised if delamination occurs, leading to a loss of cross-section in the member. In such cases, the intended purpose of the concrete cover, which is to enhance durability, may be undermined, potentially resulting in premature failure of the structure. This raises the question of whether an increase in concrete cover thickness truly guarantees the durability of concrete structures.

The design for shear failures in concrete structures varies significantly based on dimensions, loading types, and material properties. Due to this variability, there is no exclusive means to design for shear, as the behavior of beams under shear is influenced by multiple factors, making it challenging to predict their behavior accurately. Despite the efforts of numerous researchers, there are still gaps in understanding the behavior of members subjected to shear forces. Existing theories for calculating the shear strength of reinforced concrete elements, as well as shear models and equations from design codes, typically consider the entire web width of a beam section as effective in resisting shear. However, these approaches often overlook the potential loss of concrete side cover, which can significantly reduce the effective shear-resisting width of the section. Additionally, they do not account for how variations in the overall beam width or web reinforcement cage width could impact the section's shear resistance behavior, especially considering cover delamination as a variable [2].

The importance of studying mechanism of spalling and its counter effects in reference to members failing in shear is highly related to the overall resistance of the member. Even though spalling ofconcrete side cover is considered a serviceability condition, its effects have a lot to adversely contribute to the ultimate shear resistance of RC members. Spalling leads to a decrease in cross section which leads to the member losing its strength and stiffness. In sections subjected to shearone of the factors contributing to its resistance is width of the cross section, Therefore, knowing the effect spalling has on a shear critical beam section will help to quantify the consequence of side cover spalling on the overall beam resistance [2].

1.2 Problem Statement

Shear failure of reinforced concrete beam is difficult to predict accurately. Despite of many years of experimental research and the use of highly sophisticated computational tools, it is not fully understood. A lot of variables contribute to the shear resistance of beams, and to predict the resistance their influence to the shear behavior should be studied thoroughly. Experimental investigations carried out on beams for shear behavior prediction led to an observation that spalling of side concrete cover was evidently occurring. It is seen that beam members subjected to shear are experiencing side cover spalling, for an in-plane transverse loading the beams are experiencing an out of plane thrust leading to spalling, but neither the reason nor the mechanism is fully explained as to why this is happening. This observation adds side cover as one of the important variables to be investigated for shear behavior prediction [2].

Spalling of concrete side cover is not only an issue of serviceability, with the loss of this side cover, the effective width of the beam is reduced to the centerline of the outermost transverse reinforcement, and could potentially cause premature concrete crushing if not accounted for in design. The fact that there is limited experimental data on the spalling of concrete side cover, especially for sections subjected to shear, creates a huge gap to be filled. The phenomenon and effect of spalling need to be assessed meticulously to better predict shear behavior of beams. Sideconcrete cover should also be explored as a variable as it could affect the effective width of a beam resisting shear [2].

The investigation of the effect of spalling on the shear capacity of slender beams has been studied by [2] in 2021. However, this effect has not been thoroughly explored in deep beams, where the assumption of the Euler-Bernoulli beam theory of the plane section remaining plane is not valid. The behavior of deep beams under shear forces is complex due to their small shear-span-to-effective-depth ratios, which can lead to heavy shear forces and more intricate deformation patterns compared to slender beams. [12] have studied the shear strength of RC deep beams with web openings based on a two-parameter kinematic theory, highlighting the challenges posed by the small shear span-to effective depth ratios in deep beams.

1.3 Objective of the Study

The main objective of this experimental research is to investigate side cover for deep beams subjected to shear and flexure. The influence of concrete side cover thickness and stirrup cage width for the same stirrup spacing are targeted. The specific objectives are:

- To investigate side cover spalling phenomenon.
- To investigate how spalling affects the ultimate shear resistance and the overallperformance of RC members.
- To investigate the effect of concrete side cover with reference to stirrup cage width and effective beam width.
- To investigate adequacy of current shear design provisions stipulated in building codes and shear theories.

1.4 Scope of the Study

This experimental study is limited to investigating side cover spalling for deep reinforced concrete beams subjected to three-point monotonic loading having concrete side cover thickness and stirrup cage width as a variable. The shear span to depth ratio (a/d) is kept constant at 1.92. Side cover variation is implemented in width direction only, the strength, quality and density of outer cover are kept the same as the concrete core of the beam. The specimens are only going to be subjected to an in- plane transverse loading, and any longitudinal loading to cause axial compression is avoided in the test region.

1.5 Methodology

This research follows four phases of investigative orders to meet the objectives set. The first phase includes the review of relevant literature related to shear theories, beams subjected to shear and side cover spalling in beams. The second phase of the study investigates provision of building codes for capacity predictions. Using the gaps observed from the reviewed literature as an input analytical simulation was carried out using micro plane based nonlinear three-dimensional finite element (FE) model in the third phase. The model was developed using ANSYS to simulate the behavior of two sets of RC beams. The first set of beams were with the same total width but varying cage width. The second set of beams were with the same cage width but varying total width. Two-dimensional non-linear finite element software was also used to assess the reliability of existing numerical tools. In the fourth phase an experimental program including 6 deep reinforced concrete beams is then carried out systematically assess the effect of side cover on the shear/flexure performance of deep RC beams.

2 LITERATURE REVIEW

2.1 Basic Mechanisms of Shear

Figure 2-1 and Figure 2-2 present free-body diagrams illustrating the mechanisms of shear transfer in reinforced concrete (RC) beams [13]. In beams without shear reinforcement shown in Figure 2-1, the applied shear (V) is distributed through three primary concrete-based resistance mechanisms: shear in the compression zone (V_{cy}), dowel action (V_d), and the vertical component of aggregate interlock stresses (v_a) along the inclined crack surface. The relative contribution of each component has been a subject of ongoing research and debate for decades. Factors influencing this distribution include compression zone depth, shear span to depth ratio, crack width roughness, concrete strength, and various other parameters. A minor additional component, residual tension across the crack, also contributes to shear resistance, though its effect is relatively small, particularly in cases of wide cracks. For beams incorporating shear reinforcement shown in Figure 2-2, an additional vertical force (Vs) is introduced by the stirrups, representing the steel contribution to overall shear resistance[14].

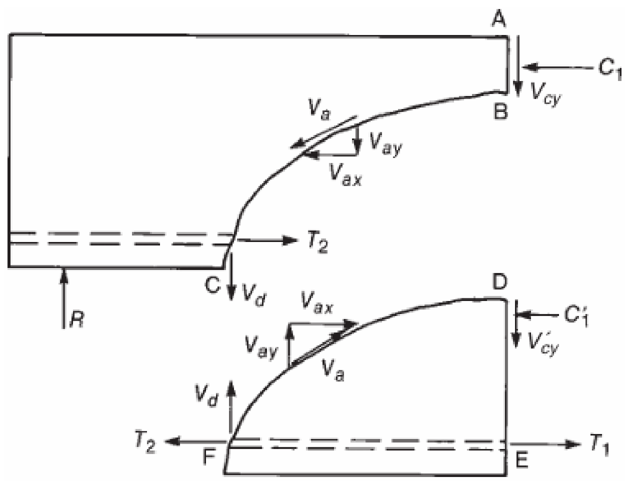

Figure 2-1 Internal forces in a cracked beam without stirrups[13]

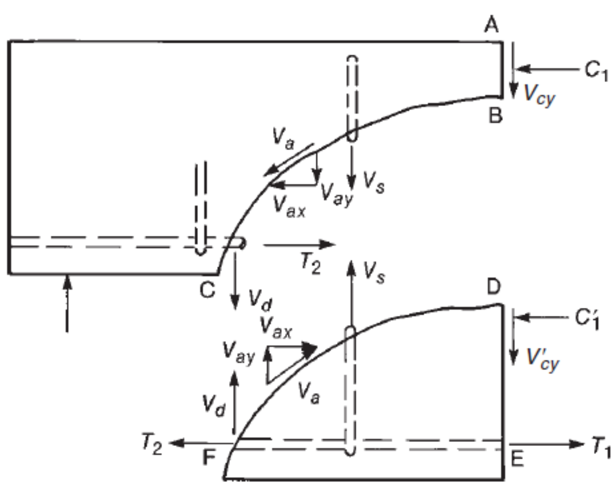

Figure 2-2 Internal forces in a cracked beam with stirrups[13]

2.1.1 Strut-And-Tie Mechanism

When the applied shear is close to the support, such as in deep beams and corbels, the proportions transferred by the aforementioned mechanisms change and the majority of the applied shear can be considered to be transferred by a strut-and-tie mechanism as shown in Figure 2-3. In this case, the tensile forces are carried by the flexural reinforcement, whilst the concrete is supposed to transfer shear only in compression. When the member is subjected to distributed load, the arch action is developed Figure 2-3 rather than just the strut-and-tie mechanism [14].

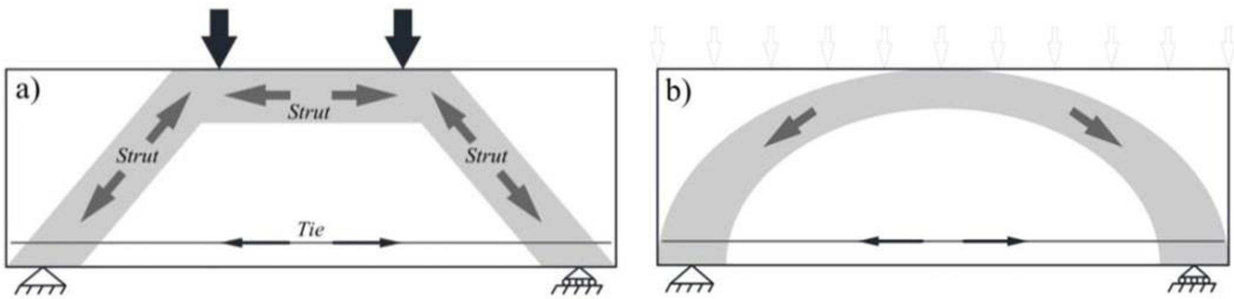

Figure 2-3 a. Strut and Tie Mechanism b. Arch action [14]

The strut-and-tie method can be used for the design of Disturbed regions (D-regions) of structures where the basic assumption of flexure theory, namely plane sections remaining plane before and after bending, does not hold true. Such regions occur near statical discontinuities arising from concentrated forces or reactions and near geometric discontinuities, such as abrupt changes in cross section etc. The strut-and-tie method of design is based on the assumption that the D-regions in concrete structures can be analyzed and designed using hypothetical pin-jointed trusses consisting of struts and ties interconnected at nodes[15].

Structural members may be divided into portions called B-regions, in which beam theory applies, including linear strains and so on, and other portions called discontinuity regions, or D-regions, adjacent to discontinuities or disturbances, where beam theory does not apply. D-regions can be geometric discontinuities, adjacent to holes, abrupt changes in cross section, or direction, or statical discontinuities, which are regions near concentrated loads and reactions. Corbels, dapped ends, and joints are affected by both statical and geometric discontinuities[13].

St. Venant's principle suggests that the localized effect of a disturbance dies out by about one member-depth from the point of the disturbance. On this basis, D-regions are assumed to extend one member-depth each way from the discontinuity. This principle is conceptual and not precise. However, it serves as a quantitative guide in selecting the dimensions of D-regions[13].

Prior to any cracking, an elastic stress field exists, which can be quantified with an elastic analysis, such as a finite-element analysis. Cracking disrupts this stress field, causing a major reorientation of the internal forces. After cracking, the internal forces can be modeled via a strut-and-tie model consisting of concrete compression struts, steel tension ties, and joints referred to as nodal zones. If the compression struts are narrower at their ends than they are at midsection, the struts may, in turn, crack longitudinally. For struts without reinforcement crossing their longitudinal axis, this may lead to failure. On the other hand, struts with transverse reinforcement to restrain the cracking can carry additional load and may fail by crushing. Failure may also occur by yielding of the tension ties, failure of the bar anchorage, or failure of the nodal zones. As always, failure initiated by yield of the steel tension ties tends to be more ductile and is desirable[13].

The struts-and-ties model can be used for the design of local regions by providing a clear concept of the stress flows, following which the reinforcing bars can be arranged. However, the struts-and-ties model does not provide a unique solution. Since this model provides multiple solutions, the best solution may elude an engineer. The best solution is usually the one that best ensures the serviceability of the local region and its ultimate strength. Such service and ultimate behavior of a local region are difficult to predict, because they are strongly affected by the cracking and the bond slipping between the reinforcing bars and the concrete. Since the 1980s, the struts-and-ties model has received considerable interest. Much research was carried out to study the various types of D regions. As a result, the struts-and-ties model has been considerably refined. The improvements include a better understanding of the stress flow, the behavior of the 'nodes' where the struts and ties intersect, and the dimensioning of the struts and the ties[16].

Struts

In a strut-and-tie model, the struts represent concrete compressive stress fields with the compression stresses acting parallel to the strut. Although they are frequently idealized as prismatic or uniformly tapering members struts generally vary in cross section along their length. This is because the concrete stress fields are wider at mid length of the strut than at the ends. Struts that change in width along the length of the member are sometimes called bottle-shaped due to their shape. The spreading of the compression forces gives rise to transverse tensions in the strut that may cause it to crack longitudinally. A strut without transverse reinforcement may fail after this cracking occurs. If adequate transverse reinforcement is provided, the strength of the strut will be governed by crushing[13].

Ties

The second major component of a strut-and-tie model is the tie. A tie represents one or several layers of reinforcement in the same direction[13]. The concrete in a tie does not resist any load. It aids in the transfer of loads from struts to ties or to bearing areas through bond with the reinforcement. The concrete surrounding the tie steel increases the axial stiffness of the tie by tension stiffening. Tension stiffening may be used in modeling the axial stiffness of the ties in a serviceability analysis. Ties may fail due to lack of end anchorage. The anchorage of the ties in the nodal zones is a critical part of the design of a D-region using a strut-and-tie model. Ties are normally shown as solid lines in strut-and-tie models[13].

Nodes and nodal zones

The points at which the forces in struts-and-ties meet in a strut-and-tie model are referred to as nodes. Conceptually, they are idealized as pinned joints. The concrete in and surrounding a node is referred to as a nodal zone. In a planar structure, three or more forces must meet at a node for the node to be in equilibrium[13].

2.1.2 Truss Mechanism

When the struts-and-ties concept was applied to a main region (B region), it is known as a truss model. For a reinforced concrete beam, truss model can be applied, not only to bending and axial loads, but also to shear and torsion[16]. When the applied load is far away from the support, such as slender flexural element, a truss action [17] as below is activated. This has a longitudinal compression chord on top through the concrete and a tension chord at the bottom formed by the longitudinal tension reinforcement. The shear forces are transferred up and down the beam depth by inclined compressive forces which can be carried by the concrete and vertical ties which are formed by the shear reinforcement.

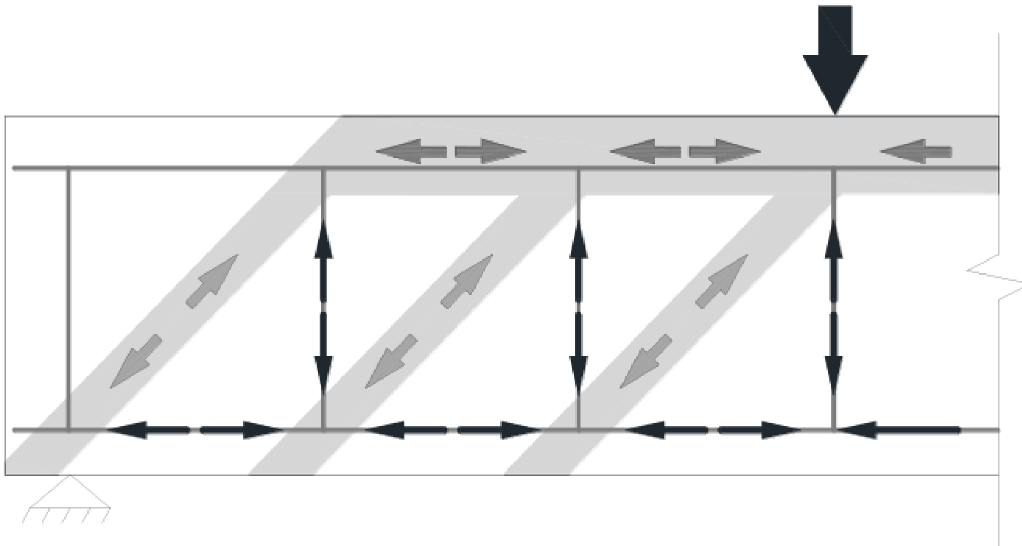

Figure 2-4 Truss Mechanism[14]

2.1.3 Modified Compression Field Theory

In 1986, Vecchio and Collins [18] conducted an experimental program on thirty RC-panels and developed the Modified Compression Field Theory (MCFT) to predict the load-deformation response of RC elements subjected to in-plane shear and normal stresses. MCFT is an improvement on the Compression Field Theory (CFT) that was developed in the seventies by Mitchell and Collins [19] as a theory to describe the behavior of RC elements under pure torsion. The main difference between CFT and MCFT is the utilization of the tensile strength of the concrete in MCFT. Depending on the measured stress and strain of the tested elements, Vecchio and Collins noticed that cracked concrete is capable of carrying a substantial amount of stress in the principal tensile direction. Therefore, the tensile strength of the cracked concrete, which was previously ignored, was added to the constitutive material models[14] .

MCFT was derived based on the simplified assumption that the average direction of principal compressive stress in the cracked concrete is related to the average direction of principal tensile strain and that the inclination of the critical cracks is parallel to the direction of the principal compressive stress. Additionally, the theory assumes that for any state of stress there is only one corresponding state of strain, and concrete and reinforcement are perfectly bonded together[14].

As MCFT was derived mainly on the basis of test results on concrete panels subjected to pure shear forces and with well distributed reinforcement, it cannot be used directly to predict the load-deformation of RC beams and columns subjected to a complex combination of bending, shear and axial loads. To predict the load-deformation of beam and column members, Vecchio and Collins [20] presented an analytical model called layered model based on an implementation of the MCFT. The model assumes that the beam can be represented as an assemblage of finite layers of concrete and longitudinal steel reinforcement. Each layer is analyzed individually with the compatibility requirement of plane sections before bending remain plane after bending[14].

Based on the layered model, Response-2000, a computer software that implements basic engineering beam theory, was developed at the University of Toronto by Bentz [21]. The program is capable to predict the load-deformation response of reinforced and prestressed concrete beams and columns. As mentioned in the program manual, Response-2000 is based on the principle of section analysis and assumes that plane sections before bending remain plane after bending[14].

Additionally, the program assumes that there is no transverse clamping stresses near point loads and supports. These assumptions might be correct for slender beams, which most likely fail in regions that are not near point loads or supports. However, in the case of disturbed regions, such as deep beams, these assumptions are far from correct and their implementation would lead most likely to inaccurate predictions[14].

2.2 Experimental Studies on Pure Torsion

Beams structurally loaded in torsion experience torsional moments acting on the cross section of the beam. This causes shearing stresses that circulates near the periphery, making concrete side cover an important parameter to investigate. Since the behavior of torsional shearing stress created by the application of twisting moment in structures can be corelated to shearing stresses formed by vertical forces, results documented in pure torsion are relevant for the study of pure shear. Side cover delamination factors observed in torsion should be investigated for shear as well[2].

In their 1974 study, Mitchell et al. , [19] introduced a theoretical model for analyzing the behavior of structural concrete subjected to pure torsion, supported by experimental testing on two specimens, PT5 and PT6. The primary objective was to investigate the impact of concrete cover spalling on torsional behavior. Both specimens were designed with identical internal reinforcement layouts and exhibited similar compressive strengths. The critical variable between them was the thickness of the concrete cover: specimen PT5 was constructed with a minimal cover of 2 mm, while specimen PT6 incorporated a significantly thicker clear cover of 40 mm. Consequently, the overall cross-sectional dimensions were 356 mm for PT5 and 432 mm for PT6, respectively.

Upon testing, PT6 exhibited substantial concrete spalling at approximately the same torque level as PT5. However, once spalling initiated, PT6 demonstrated limited capacity to resist further increases in torsional load. Additionally, after the yielding of the transverse reinforcement, PT6 developed more pronounced cracking compared to PT5. The experimental observations indicated that an increase in concrete cover thickness contributes to greater susceptibility to spalling and wider diagonal cracks but does not correspond to an improvement in the ultimate torsional strength of the member.

The failure modes, depicted in Figure 2-5, clearly show the spalling of the concrete cover and the exposure of transverse reinforcement at failure in both specimens. This observation confirms that concrete detached down to the plane of the stirrups. Furthermore, the measured torsional stiffness values for the specimens fell between the theoretical stiffnesses of sections with intact and fully spalled covers. Ultimately, the torsional strength was found to be governed by the capacity of the cross-section following the occurrence of spalling.

These findings reinforce the applicability of the Diagonal Compression Field Theory (DCFT) to predict the torsional behavior of reinforced concrete members, particularly emphasizing the critical role of post-spalling mechanisms in controlling ultimate strength.

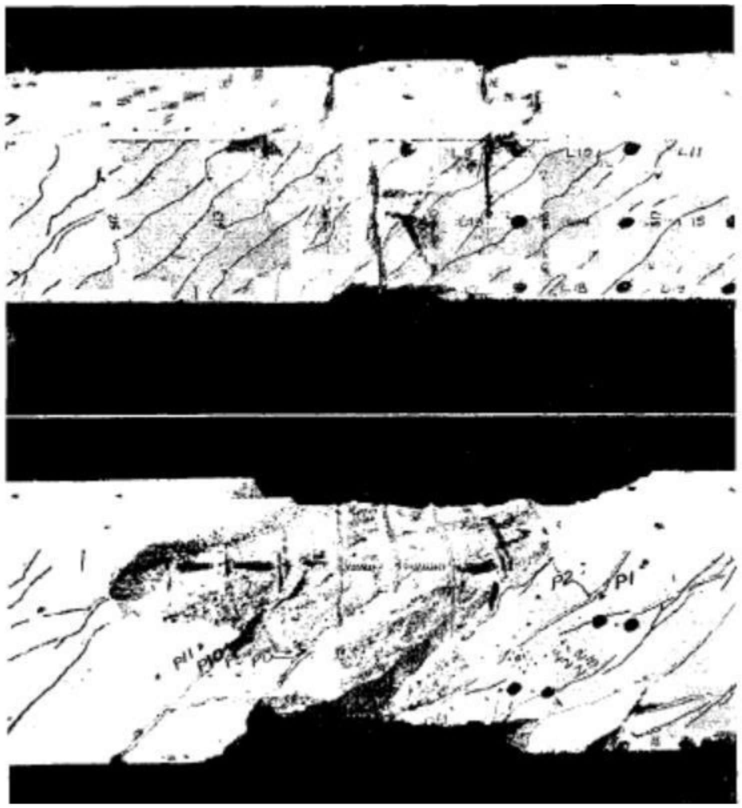

Figure 2-5 Beams PT5 and PT6 at failure[19]

Nagataki et al. [22] further investigated torsional behavior across specimens with cover thicknesses of 5 mm, 30 mm, and 55 mm. Severe spalling and larger diagonal crack widths were observed in specimens with 55 mm covers near ultimate loads, confirming the detrimental effect of excessive cover on torsional performance. Later studies such as [19] emphasized that while torsional resistance depends mainly on internal reinforcement, thick covers may detach without significantly improving strength.

Other studies like [23] showed that larger concrete covers significantly influenced both the ultimate torsional capacity and the overall torsional behavior of the beams. Specimens with thicker covers displayed a noticeable reduction in torsional strength, especially at post-peak stages, primarily due to the spalling of cover concrete under high torsional stresses.

2.3 Experimental Studies on Shear-Torsion Interaction

In 1995, Rahal and Collins [24] conducted a comprehensive experimental study to evaluate the impact of increasing concrete cover thickness on the structural behavior of reinforced concrete (RC) sections subjected to combined shear and torsion. Seven large-scale beams were tested under varying shear-to-torque ratios and minimal flexural influence. The specimens were divided into two series: Series 1 (RC1-2, RC1-3, RC1-4) with a clear cover of 22.5 mm, and Series 2 (RC2-1, RC2-2, RC2-3, RC2-4) with a clear cover of 42.5 mm. Although the reinforcement cages remained identical, the outer dimensions of the beams were adjusted to account for the different cover thicknesses—300 mm × 600 mm for Series 1 and 340 mm × 640 mm for Series 2.

Beams were incrementally loaded until failure under predefined torque-to-shear ratios. Cover separation was identified by tapping the surface with a steel hammer, with a hollow sound indicating delamination. For Series 1 specimens, cover spalling was not observed until after the ultimate load had been reached, whereas in Series 2, spalling was detected before peak load. Notably, spalling typically initiated along the faces subjected to combined shear and torsional stresses. The failure modes, depicted in Figure 2-6 clearly shows total spalling of series 2 beams.

The study concluded that although the concrete cover contributes to torsional and shear resistance, increasing the cover thickness results in wider crack spacings and premature spalling. Beams with smaller covers-maintained integrity until maximum loading, while those with larger covers exhibited early cover detachment. Furthermore, the highest post-spalling strength was achieved when spalling remained localized to a single face. Alarmingly, spalling was observed even under pure shear loading conditions in beams with larger covers, indicating a potential vulnerability that warrants consideration in design practices emphasizing durability through increased cover thickness.

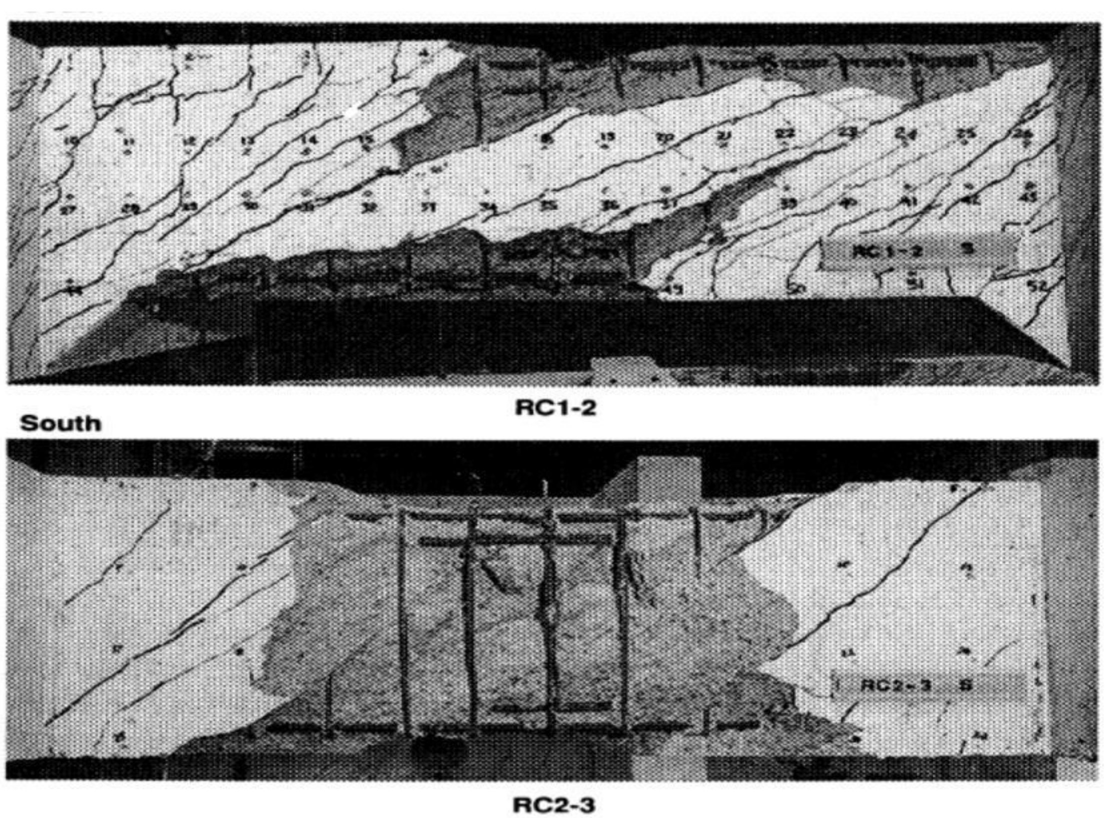

Figure 2-6 Observed Spalling on south and north faces of Specimen RC1-2 and RC2-3[25]

2.4 Experimental Studies on Pure Shear

In 2006, following their earlier investigation[24] on shear-torsion interaction, Rahal [25] conducted an experimental study to examine the influence of varying concrete side cover thickness on the shear behavior of reinforced concrete beams [2]. The study reported the results of seven specimens, divided into two series: Series I, comprising four test regions, and Series II, comprising three test regions. Within each series, the concrete side cover thickness varied, while the target concrete compressive strength differed between Series I (25 MPa) and Series II (40 MPa). The first specimen, cast using 25 MPa concrete, had a clear side cover of approximately 5 mm. The remaining specimens were prepared using two different concrete mixes, each featuring two distinct test regions. In Series I, side cover thicknesses varied from 5 mm to 75 mm, whereas in Series II, covers ranged from 25 mm to 75 mm. To maintain a constant effective depth (d), the top and bottom concrete covers were fixed at 40 mm across all specimens. All beams were 400 mm deep, 3 meters long, and were tested at a shear span-to-depth ratio (a/d) of 3.

Concrete spalling was typically initiated by the separation of the side cover from the core concrete confined within the stirrups. Consistent with previous observations from the shear-torsion study, initial spalling was not always accompanied by visible loss of concrete material. Consequently, detection relied on acoustic methods—tapping the surface with a steel hammer and interpreting a hollow sound as evidence of internal separation.

Specimens with 75 mm side covers exhibited a sharp increase in diagonal crack widths upon cracking and demonstrated less favorable post-cracking behavior. Nevertheless, at estimated service load levels, all specimens either remained uncracked or exhibited crack widths below the 0.3 mm threshold commonly recommended for serviceability. All beams ultimately failed in shear, with strain gauges indicating yielding exclusively in the transverse reinforcement. Spalling was observed near the ultimate load in specimens with thicker side covers. Typically, spalling was concentrated at the corners of the cross-section, leaving the central and upper regions largely intact. This localized spalling pattern paralleled observations from Rahal and Collins' previous study [24], despite differences in loading conditions. Furthermore, similar behavior was noted in earlier tests [25], where severe corner spalling occurred even under predominant shear.

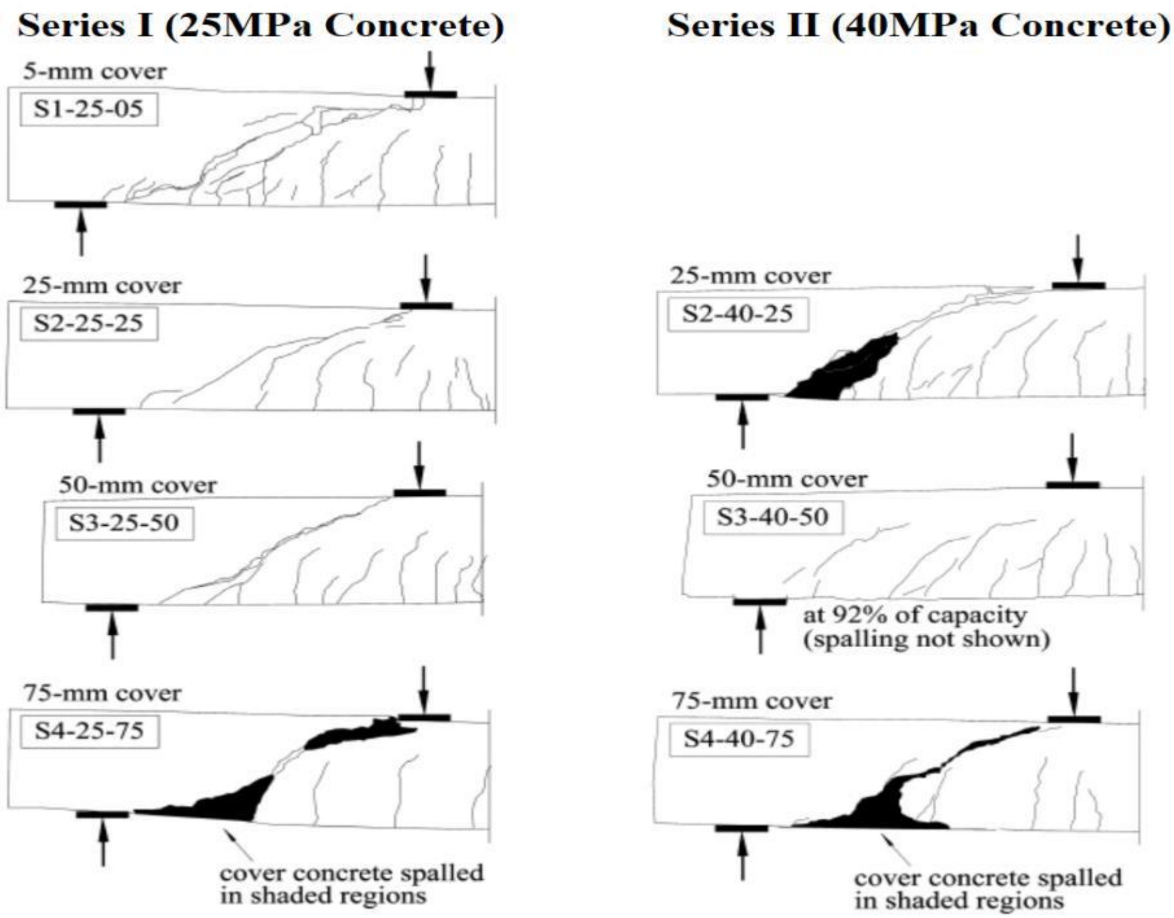

Figure 2-7 Series I and Series II Specimens at Ultimate Load[25]

It is important to distinguish this spalling pattern from that observed in beams subjected to pure torsion, where spalling typically affects the entire perimeter of the section rather than being localized at the corners.

The study concluded that increasing the concrete side cover and, consequently, the overall cross-sectional area, significantly enhanced the ultimate shear strength for beams made with 25 MPa concrete. However, similar benefits were not observed for beams cast with 40 MPa concrete. These results suggest that spalling has a more detrimental effect on higher-strength concrete members. Additionally, the study affirmed that the ACI shear provisions and general truss-based design methods provided conservative strength predictions based on unspalled cross-sectional areas. As such, spalling at code-calculated ultimate loads is unlikely to occur, and thus, recalculating the ultimate strength based on reduced, post-spalling dimensions—common in torsion design—is deemed unnecessary [25].

In 1974, Arbesman [26] conducted experimental tests at the University of Toronto to support the development of the Compression Field Theory (CFT), focusing specifically on the phenomenon of concrete cover spalling under shear loading. The study involved a beam specimen with two test regions, SA3 and SA4. SA3 had no clear side cover, while SA4 incorporated a 40 mm clear cover along the vertical sides. Although the external dimensions of the concrete sections remained identical between the two regions, the internal steel cage dimensions were reduced in SA4 to accommodate the increased cover thickness. Both specimens were heavily reinforced in shear, with a transverse reinforcement ratio, $\rho_v f_y / f_c'$ is 0.116. Full geometric properties and the corresponding observed and predicted shear capacities are presented in Figure 2-8.

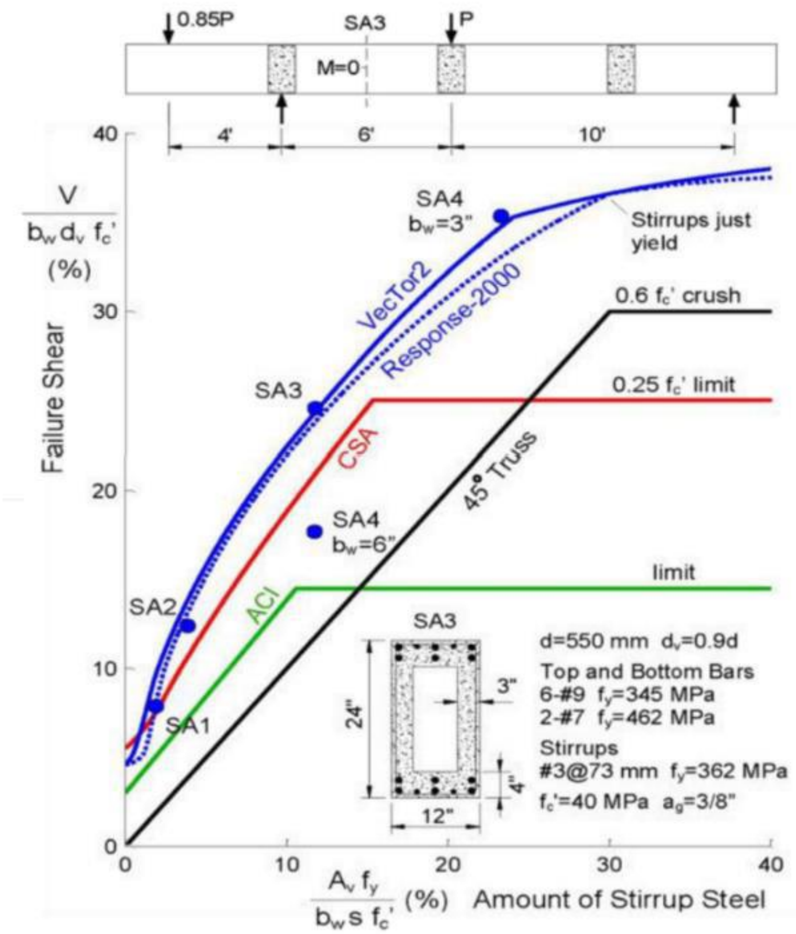

Figure 2-8 SA3 and SA4 Geometric Properties and Observed and Predicted Results[26]

Test results for SA4 demonstrated that side cover spalling initiated as soon as the stirrups began to yield, significantly reducing the effective width of the beam from 152 mm to 76 mm. Consequently, the capacity of SA4 dropped to 73% of that observed in SA3. When assuming an unspalled section width (152 mm), the experimental capacity of SA4 was substantially lower than predicted. However, when a reduced spalled width (76 mm) was assumed, the predicted strength closely matched the experimental value (see Figure 2-8, comparisons labeled “SA4, b_w=6” and "SA4, b_w=3”)

Figure 2-9 illustrates the top and bottom views of spalling observed in SA3 and SA4. It is notable that the region with the larger side cover resisted a 26% lower load compared to the region without cover, primarily due to severe spalling. However, it should also be noted that SA4 was tested after SA3, implying that pre-existing cracks from the earlier test could have influenced the failure behavior. Additionally, the study highlighted that reducing the stirrup cage dimensions—not solely the increase in concrete cover—may have contributed to the observed reduction in ultimate load resistance.

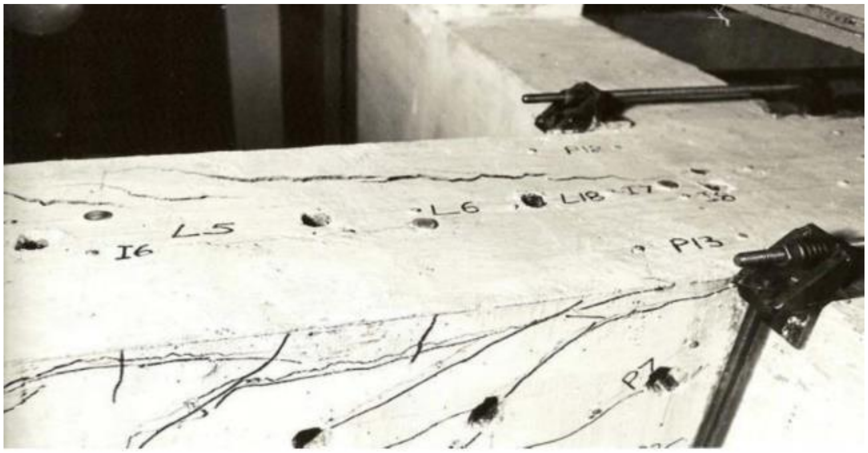

Side Cover Spalling Top View

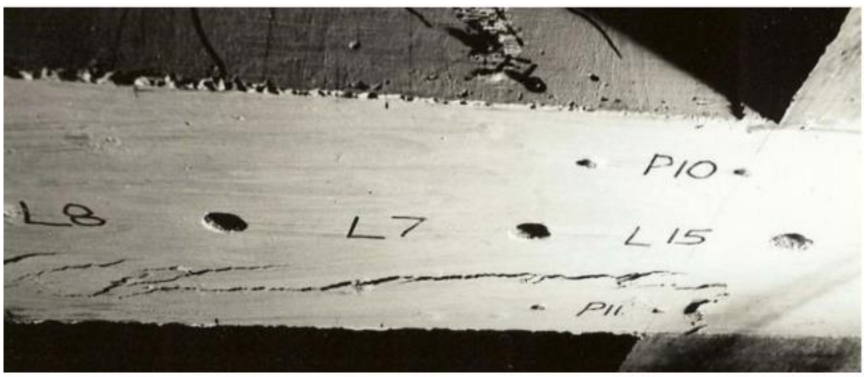

Side Cover Spalling Bottom View

Figure 2-9 SA3 and SA4 Side Cover Spalling Observation from Top and Bottom Views[26]

Although later research, such as Rahal's 2006 study [25], suggests that under standard code-calculated ultimate loads spalling is unlikely to significantly reduce shear capacity, Arbesman's findings [26] introduce some contradictions. Moreover, severe spalling near ultimate loads was shown to create unfavorable structural conditions that must be carefully considered during design.

Fisher et al. , [27] shed further light on the issue of side concrete cover spalling in beams subjected to shear. Their research involved an experimental investigation of four heavily reinforced coupling beam specimens, each with varying concrete strengths, reinforcement ratios, and side cover thicknesses. These specimens were tested to failure to assess the strength and stiffness of coupling beams in high-rise concrete buildings, as well as to examine the impact of load-induced side cover spalling on shear strength. Notably, the specimens were designed to exceed the shear limit prescribed by the ACI code.

Due to design requirements mandating that the longitudinal reinforcement of coupling beams be anchored within the layers of shear wall reinforcement, coupling beams typically feature significant side cover thicknesses. The four specimens—CBF1 through CBF4—measured 1600 mm in length and 600 mm in depth, constructed monolithically with 400 mm-wide shear wall end blocks. While CBF1 had a beam width of 316 mm with a minimal side cover of 3 mm, CBF2, CBF3, and CBF4 featured a beam width of 400 mm with a 45 mm side cover. The stirrup spacing was maintained at 60 mm for CBF1, CBF2, and CBF3, resulting in shear reinforcement exceeding the ACI Code's upper limit. Conversely, CBF4 employed a stirrup spacing of 120 mm, conforming to the code requirements. All specimens ultimately failed in shear, with failures characterized by stirrup yielding, crack slip, and diagonal concrete crushing.

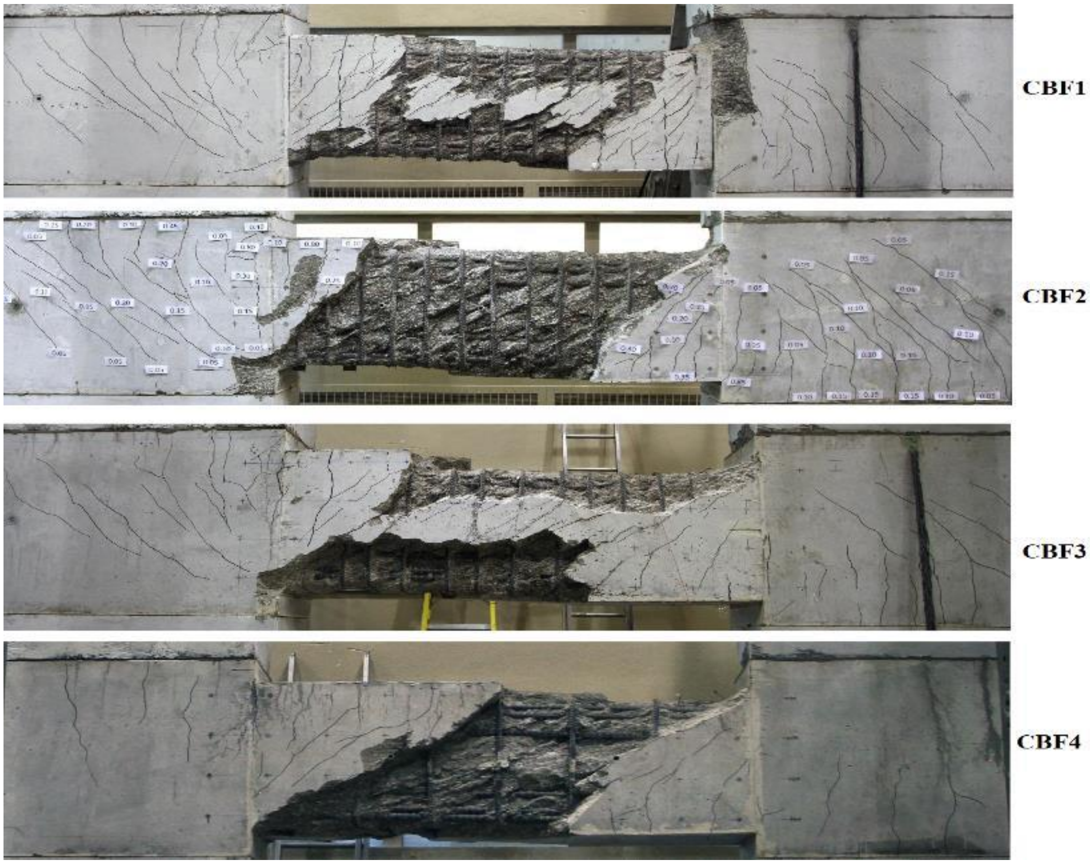

Figure 2-10 Coupling Beam Specimens at Ultimate Load[27]

Side cover spalling was observed in all four coupling beam specimens. Based on measurements obtained using LVDT and LED equipment's, spalling initiated at the flexural compression corners of the coupling beam as stirrups began to yield. This phenomenon progressed toward midspan at peak load, becoming visibly pronounced by the conclusion of testing. Side cover spalling led to localized variations in surface strain as the cover delaminated from the core.

The study concluded that side cover spalling had a negligible effect on shear strength for these particular specimens due to the unexpectedly high concrete strengths used. However, it could pose challenges for heavily reinforced elements designed near the diagonal concrete crushing threshold. The reduction in cross-sectional area may contribute to premature concrete crushing failure. Additionally, it was noted that the tightly spaced stirrup configurations in CBF1, CBF2, and CBF3 led to more significant cover delamination compared to the wider stirrup spacing of CBF4. The research findings emphasize that side cover spalling occurs in heavily reinforced, high-strength coupling beams, warranting its consideration in the design process. A significant reduction in shear strength due to spalling would only occur if the loss of cover caused the remaining concrete core to crush in diagonal compression before stirrup yielding or before an anticipated decrease in the angle of inclination of diagonal compressive stresses in the concrete.

Although side cover spalling was not a factor in a separate study conducted in 2009, Zakaria et al. , [28] investigated shear cracking behavior in reinforced concrete beams. Their research considered variables such as beam size, span-to-depth ratio, shear reinforcement characteristics—including stirrup spacing and configuration—side concrete cover, and longitudinal reinforcement ratio. The tested beams were grouped into three series, with the second series including three specimens subjected to an a/d ratio of 2 while varying side cover thickness, stirrup spacing, and configuration. The side cover values for the three specimens were 40 mm, 60 mm, and 80 mm. Observations revealed that the beams with larger side covers (60 mm and 80 mm) exhibited greater diagonal crack spacing compared to the beam with a smaller cover (40 mm). The study concluded that increasing the side concrete cover to stirrups resulted in larger diagonal crack spacing and, consequently, wider cracks. This suggests that variations in side cover not only impact structural performance through cover spalling but also influence shear cracking behavior, particularly crack width and spacing.

Tesfaye [2] tested seven full-scale shear-critical reinforced concrete beams under monotonic loading to failure. These beams varied in concrete side cover thickness, stirrup cage width, and stirrup spacing to observe the different effects on side cover spalling and shear capacity. All the Testing involved include surface displacement measurement devices, strain gauges, and load cells to capture deformation and strain responses during loading. Additionally, nonlinear finite element software VecTor 2 was employed to simulate beam behavior and validate the experimental results.

This investigation found that Spalling occurred near peak load, confirming that stirrups serve as planes of weakness where cover detachment initiates. Also Spalling was most severe in specimens with larger side covers, affecting crack propagation and shear resistance. Beams with thinner side covers (e.g., 25mm) exhibited less spalling and performed better in load resistance. Beams with larger covers (e.g., 75mm) suffered pre-peak spalling, particularly in specimens with reduced stirrup cage widths, leading to premature failure. Stirrup spacing played a role in determining the extent of spalling—tightly spaced stirrups contributed to more severe delamination.

2.5 Mechanisms of Spalling

Based on the findings presented in the reviewed studies, spalling has been observed in beams subjected to various loading conditions and combinations of influencing factors. Certain investigations have sought to identify and explain the potential underlying causes of this phenomenon.

The Diagonal Compression Field Theory, introduced in 1974 [19], analyzes spalling in beams subjected to torsion by evaluating the equilibrium of a corner element. It establishes that the compressive forces within the concrete exert outward pressure on the corner, whereas the tensile forces in the hoops counteract this effect by providing restraint. The theory further posits that under increased loading conditions, the concrete cover will inevitably detach, as the hoops alone cannot sustain it without inducing excessive tensile stresses within the concrete.

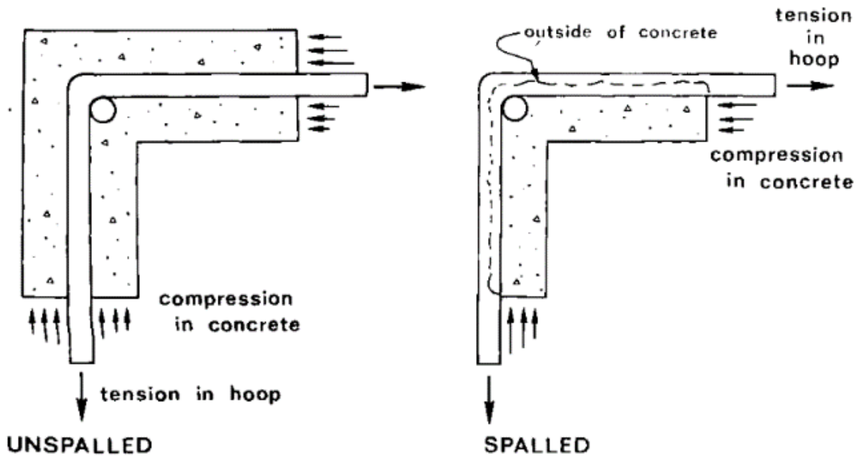

Figure 2-11 Spalling of concrete cover[19]

Similarly, the 1995 Shear-Torsion Interaction study [24] examines the effects of shear and torsion on the distribution of shear stresses within a section. It establishes that shear stresses v, induced by the vertical shear force V, align with the direction of V, whereas torsional shear stresses τ, resulting from torque T, circulate around the section. The study highlights that the elevated shear stress intensity leads to increased stress levels in both the concrete and reinforcement. Additionally, it identifies the possibility of spalling occurring in the concrete cover outside the stirrups due to these stress concentrations.

To maintain equilibrium, the concrete compressive stresses that resist shear and torsion after cracking must alter direction near the beam's corners, thereby generating tensile stresses perpendicular to these trajectories. If the shearing stresses and the thickness of the concrete cover are sufficiently high, these tensile stresses will exceed the concrete's tensile resistance, leading to delamination of the cover from the core concrete confined within the stirrups. Additionally, it has been observed that splitting primarily occurs along the plane of weakness formed by the stirrups and becomes most pronounced when the shearing stresses induced by vertical shear forces and torsional effects combine, as illustrated in Figure 2-12.

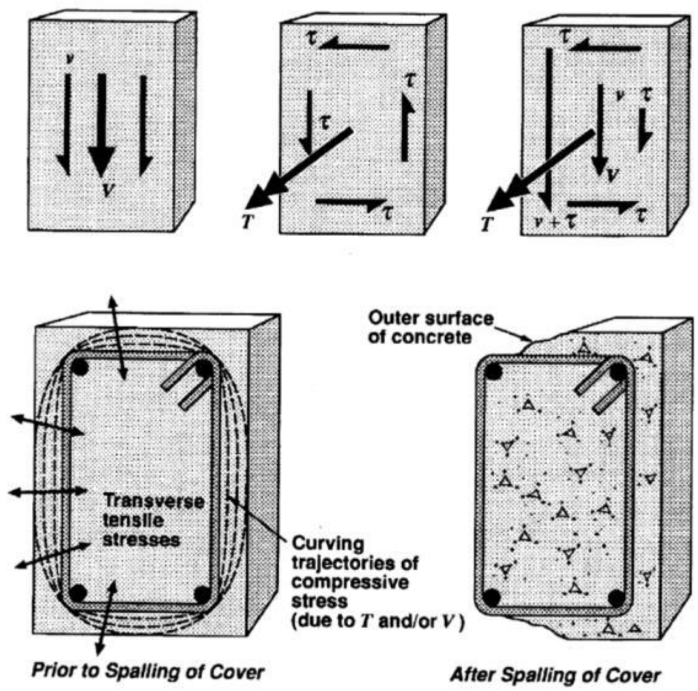

Figure 2-12 Stresses in sections subjected to combined Shear and Torsion

Similarly, Rahal [25] and Fisher et al. , [27] describe spalling in beams subjected to shear in a comparable manner. They explain that the force resisted by diagonal compressive stresses alters direction near the beam's corners, generating tensile stresses that act perpendicular to the direction of compression. This phenomenon, illustrated in Figure 2-13, highlights the interaction between shear-induced forces and localized tensile stress concentrations, contributing to the occurrence of spalling.

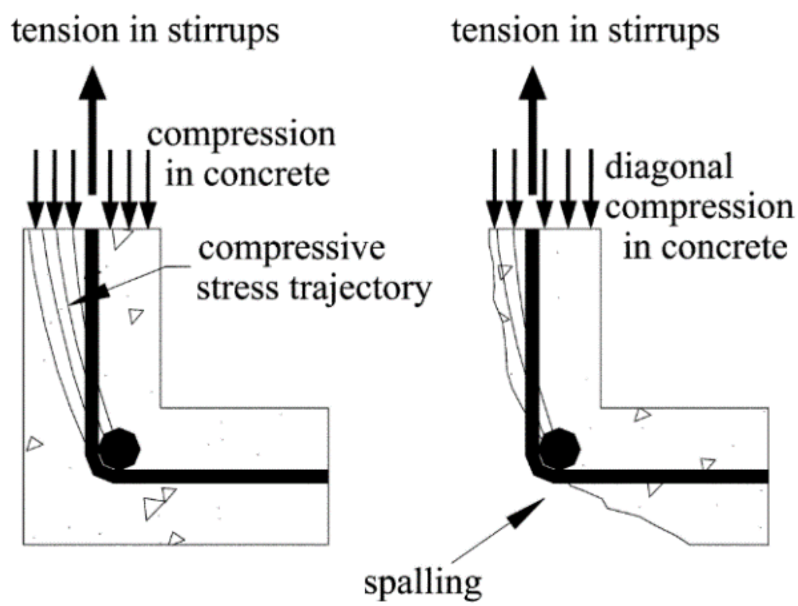

Figure 2-13 Spalling of concrete cover in beams subjected to shear[25]

For larger concrete covers, in addition to spalling, an increase in shear crack width was reported by [19] and in crack spacing by [24] was observed. The influence of side cover thickness on shear cracking behavior was analyzed by [28] who reported a greater shear crack spacing in specimens with larger covers. Their study indicated that with increased cover thickness, the ability of stirrups to control crack spacing at the surface of reinforced concrete members diminishes. Bond stresses arise due to stirrup slip through the concrete, transferring force from the stirrup to the surrounding concrete between cracks.

For a crack to form within the effective concrete area around the stirrup, the force transmitted through bond at the end of the transfer length must exceed the concrete's cracking strength. Consequently, increasing the side cover thickness leads to both a larger effective concrete area and greater force introduction into the surrounding concrete, promoting surface cracking. This process necessitates an extended transfer length, which results in larger crack spacing.

In a more recent experimental study conducted by Moccia et al. , [29], the spalling of concrete cover induced by reinforcement was further investigated. Their research examined spalling in reinforced concrete caused either by bond stress or internal pressure. Specifically, the study considered the effects of radial transverse pressure resulting from bond stress and the volumetric expansion of corroded reinforcement. Based on their findings, the researchers proposed a design approach utilizing a simplified mechanical model. One aspect of their investigation focused on how concrete cover thickness affects spalling resistance under varying conditions.

2.6 Research Gaps and Unresolved Variables

Existing studies report varying behaviors of reinforced concrete beams subjected to shear with different side concrete cover thicknesses, underscoring that side cover spalling remains an unresolved issue in shear-critical beams. While some research suggests that increased side cover can lead to reduced ultimate load resistance, findings remain inconsistent, highlighting gaps in experimental methodologies and analytical approaches.

Arbesman’s investigation [26] demonstrated that spalling can occur in beams with higher side cover, potentially reducing load resistance. However, the specimens in this study had a unique box beam geometry, which is atypical for conventional industry applications. To develop a more applicable experimental database, full-scale beams with typical industry designs must be tested to better understand spalling behavior. Additionally, stirrup cage width was reduced in the specimen with larger cover, leading to a 26% lower load resistance, which raises the question of whether this reduction was solely due to the increased side cover or also influenced by the reduced stirrup cage width. Both parameters require further investigation to determine their individual and combined effects on ultimate load resistance and overall structural performance. Moreover, the test sequencing may have affected results, as SA3 was tested first, leaving SA4 pre-cracked during testing—potentially compromising the reported outcomes. Spalling was observed near the beam corners, yet no extensive evaluation of propagation mechanisms was conducted.

The 1995 Shear-Torsion Interaction study [24] reported a correlation between side cover thickness and spalling occurrence, noting that beams with small cover exhibited spalling post-peak load, whereas beams with larger covers exhibited spalling before reaching peak load. However, spalling assessment in this study relied on hammer tapping tests, where a hollow sound indicated separation. This qualitative and subjective methodology calls into question the reliability of the reported findings. There is a need for a more scientific, quantifiable approach to assessing spalling, ensuring accurate measurement and analysis.

Rahal [25] observed spalling near beam corners in specimens with larger concrete cover but reported no reduction in load resistance. This conclusion contrasts with Arbesman's findings, indicating that the effect of side cover on shear performance remains inconsistent across studies. The discrepancies highlight the need for comprehensive investigations involving varied concrete strengths, reinforcement configurations, and loading scenarios.

An experimental investigation on coupling beams by Fisher et al. , [27] confirmed spalling in all tested specimens, extending beyond the corners to central and upper regions—a deviation from previous studies that primarily associated spalling with corner tensile stresses. This broader spalling distribution challenges prior explanations, suggesting that compressive stress redirection alone is insufficient to explain spalling. A more nuanced understanding of spalling mechanisms, particularly in regions distant from the corners, is necessary.

In addition to side cover thickness, stirrup spacing emerged as a critical factor. The study observed that tightly spaced stirrups aggravate spalling, supporting the concept of stirrups as planes of weakness. However, since the specimens tested were highly stressed coupling beams designed for lateral load resistance, results may not directly apply to beams designed for vertical load resistance. Future experimental programs should address typical structural beams to ensure findings are applicable to broader engineering practices.

Tesfaye's [2] recent research further investigated side cover spalling mechanisms through an extensive experimental study, testing shear-critical beams with varied side cover thicknesses, stirrup cage widths, and stirrup spacing. Findings confirmed that spalling occurs predominantly along stirrup planes, reinforcing the hypothesis that stirrups serve as weakness lines where delamination initiates. However, the intensity of spalling depends on stirrup spacing—beams with wider stirrup spacing exhibited less severe spalling compared to those with tightly spaced stirrups. Additionally, pre-peak spalling followed by premature failure was noted in beams with reduced stirrup cage widths, further validating concerns raised in earlier studies.

A critical issue in shear design provisions involves the determination of effective shear resisting sections. Four international design codes—ACI 318-19, Eurocode 2, CSA, and JSCE—all assume that the full beam width (b_w) contributes to shear resistance. However, Tesfaye's [2] findings reveal that spalling significantly reduces the effective concrete core resisting shear, particularly when shear-induced stresses exceed the tensile resistance of the concrete cover. The discrepancy between code predictions and experimental results suggests that existing design provisions should be reassessed for beams experiencing side cover spalling, ensuring accurate shear resistance estimates that account for spalling-induced reductions in the effective resisting section.

While Tesfaye's [2] study provided valuable insights into side cover spalling in slender beams, the behavior of deep beams subjected to shear remains an area requiring further exploration. Deep beams differ significantly in their shear transfer mechanisms, often exhibiting strut-and-tie action rather than diagonal cracking behavior found in slender beams. Given the observed influence of side cover thickness and stirrup spacing on spalling in slender beams, it is crucial to determine whether similar spalling mechanisms persist in deep beams or whether alternative failure patterns emerge due to their lower span-to-depth ratio. This research aims to extend Tesfaye's [2] findings into deep beam configurations, investigating shear-critical deep beams under various reinforcement arrangements and loading conditions to establish a comprehensive understanding of spalling effects across different beam geometries.

3 EXPERIMENTAL PROGRAM AND TESTING OF SPECIMENS

The experimental program is designed to examine the mechanism of side cover and its impact on performance of beams. To achieve this, six deep reinforced concrete beams were cast and subjected to monotonic one-point loading at the Materials Laboratory of Addis Ababa Institute of Technology.

The beams were constructed with varying concrete side cover thicknesses and stirrup cage widths to assess their influence on shear behavior and structural integrity. Prior to conducting the experimental program, a sectional analysis was performed using RESPONSE 2000, a program based on the Modified Compression Field Theory, developed at the University of Toronto by Evan C. Bentz and Michael P. Collins. Furthermore, a two-dimensional non-linear finite element analysis was conducted using VECTOR 2, a computational tool developed at the same institution, to supplement the experimental findings.

This section provides a detailed discussion on specimen design and construction, outlining the test assembly and instrumentation setup. Additionally, the material properties used in specimen production will be presented to ensure a comprehensive understanding of the experimental parameters.

3.1 Specimen Configuration

Test specimens are configured in such a way that concrete side cover and cage sizes are varied. The six main specimens are divided into two groups. The groups each have three specimens. Specimens in the first group (SA group) have the same total width with decreasing stirrup cage width to accommodate the increase concrete side cover. Specimens in the second group (SB group) have different total width with the same cage width and increasing concrete side cover. All main specimens have the same bottom cover thickness of 25mm and top cover thickness of 31.5mm (to maintain similar effective depth), concrete quality and strength, overall depth of 520mm and total beam length of 2.34m. An a/d ratio of 1.92 is maintained for all specimens. The last number on the specimen designates its side cover in mm. As presented in Table 3-1 and Table 3-2 below all specimens are designed with a 10mm diameter deformed longitudinal reinforcement for bottom faces of the cross section while 8mm diameter deformed reinforcing bars are used for transverse and top reinforcements.

Table 3-1 Configuration and Cross-Sectional Details of Test Specimens

Group	Specimens	Depth (mm)	Effective Depth (mm)	Width (mm)	Cage Width (mm)	Total Beam Length (mm)	Side Cover (mm)	Bottom Cover (mm)	Top Cover (mm)	Reinforcement		
										Bottom	Top	Transverse
Group 1	SA-25	520	495	270	212	2340	25	25	31.5	6ϕ10	2ϕ8	Ø8 c/c 69.5mm
	SA-50	520	495	270	162	2340	50	25	31.5	6ϕ10	2ϕ8	Ø8 c/c 69.5mm
	SA-75	520	495	270	112	2340	75	25	31.5	6ϕ10	2ϕ8	Ø8 c/c 69.5mm
Group 2	SB-50	520	495	320	212	2340	25	25	31.5	6ϕ10	2ϕ8	Ø8 c/c 69.5mm
	SB-75	520	495	370	212	2340	50	25	31.5	6ϕ10	2ϕ8	Ø8 c/c 69.5mm
	SB-100	520	495	420	212	2340	75	25	31.5	6ϕ10	2ϕ8	Ø8 c/c 69.5mm

Table 3-2 Reinforcement details of test specimens

Specimens	Transverse reinforcement in X and Y	Longitudinal tension reinforcement ratio (bottom rebar/width*effective depth)	Transverse reinforcement ratio (transverse rebar/width*spacing)	a/d
SA-25	Ø8 c/c 69.5mm	0.33578%	0.53595%	1.92
SA-50	Ø8 c/c 69.5mm	0.33578%	0.53595%	1.92
SA-75	Ø8 c/c 69.5mm	0.33578%	0.53595%	1.92
SB-50	Ø8 c/c 69.5mm	0.28331%	0.45221%	1.92
SB-75	Ø8 c/c 69.5mm	0.24503%	0.39110%	1.92
SB-100	Ø8 c/c 69.5mm	0.21586%	0.34454%	1.92

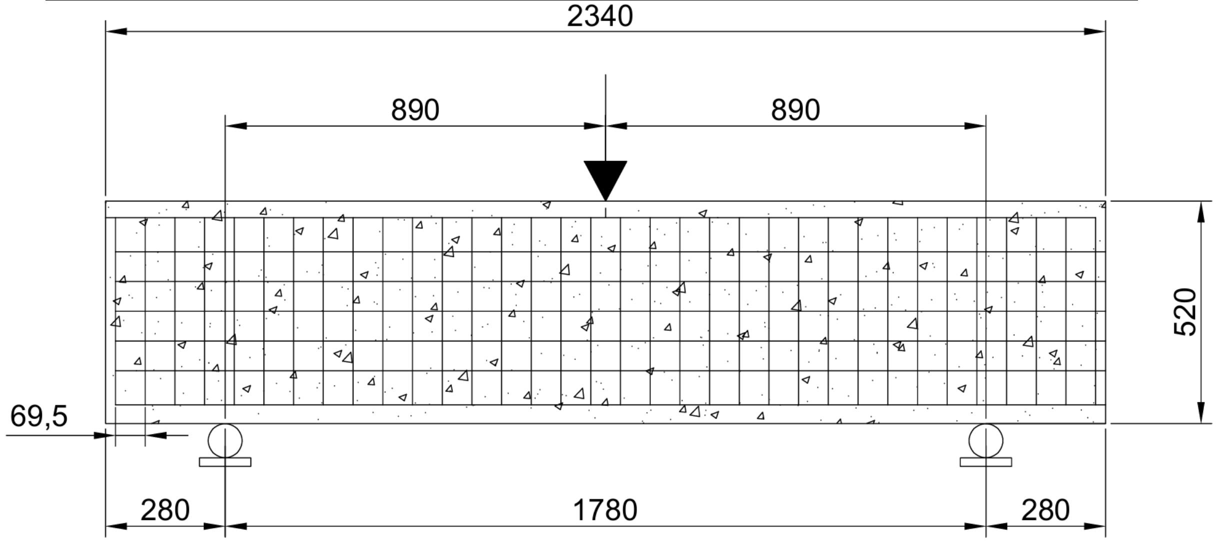

Figure 3-1 Longitudinal Profile of the test beam

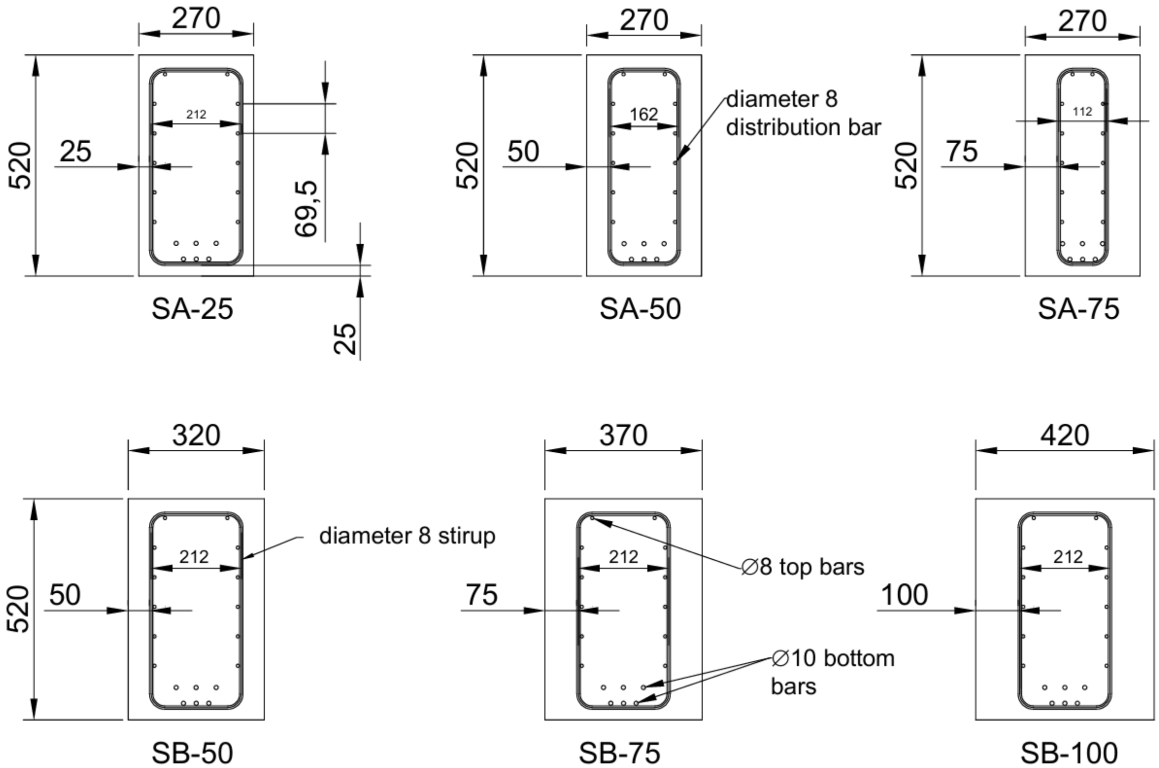

Figure 3-2 Cross Sectional Detail of the Specimens

3.2 Material Properties

3.2.1 Concrete

All six specimens were cast-in-place at Addis Ababa Institute of Technology (AAiT). The mix design, shown in Table 3-3 and Table 3-4, was formulated based on ACI guidelines to achieve a target compressive strength of 25 MPa for cubic samples. The concrete composition included coarse aggregate with a maximum particle size of 25 mm, Ordinary Portland Cement, and a slump range of 75 mm to 100 mm to ensure appropriate workability. Throughout the production process, strict quality control measures were implemented to maintain uniformity and consistency across all test specimens.

Table 3-3 Concrete mix design

Mix Design Specifications	
Slump	75 to 100mm
Target Cubic Compressive Strength	25MPa
Nominal Maximum Aggregate Size	25mm
Cement Type	Ordinary Portland Cement

Table 3-4 Amount Required for 1m3 of Concrete Volume

Amount Required for 1m^3 of Concrete Volume	
Cement	296.3 kg/m^3
Fine Aggregate	774.4 kg/m^3
Coarse Aggregate	1132.9 kg/m^3
Mixing Water	165.8 kg/m^3

A thorough material characterization and preparation was conducted before mixing of ingredients.

3.2.2 Coarse Aggregate

Different physical tests were done as per the construction material laboratory manual by Prof. Abebe Dinku [30] for the purpose of characterization and they are shown in Table 3-5. The gradation curve is shown in Figure 3-3.

Table 3-5 Material Properties of Course Aggregate Used

Coarse Aggregate Material Properties	
Maximum Aggregate Size	25mm
Gradation	Figure 3-3
Moisture Content	2%
Absorption	1.65%
Unit Weight	1571 kg/m^3
Fineness Modulus	2.8

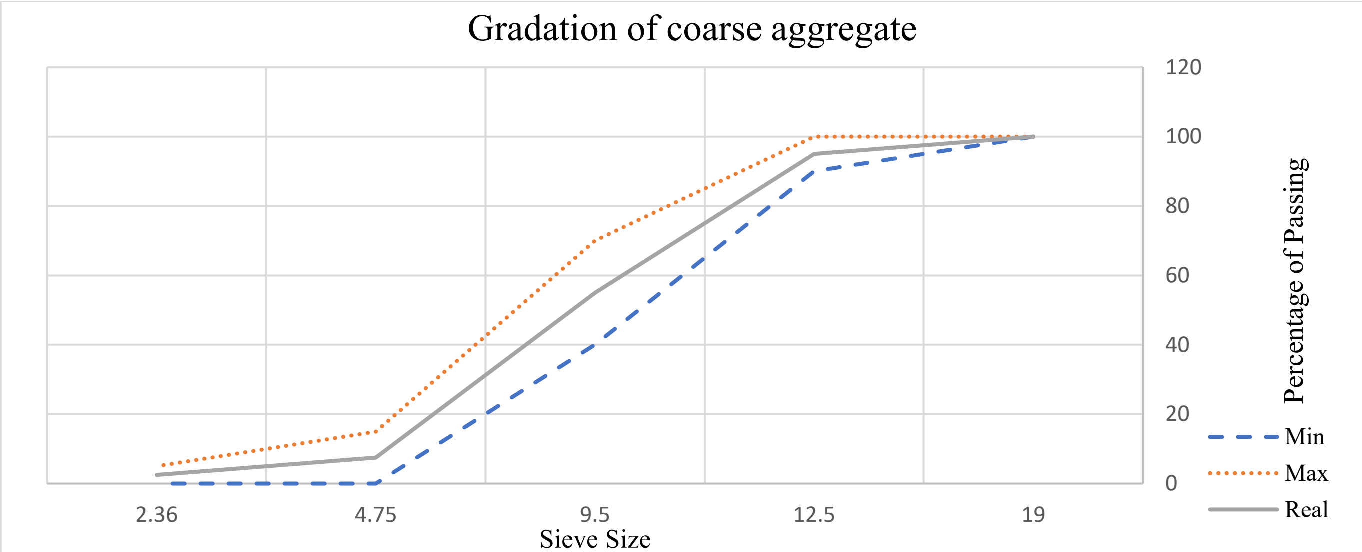

Figure 3-3 Gradation of Coarse aggregate used

3.2.3 Fine Aggregate

In the preparation of fine aggregate, the silt content was first checked as shown in Figure 3-4 and was found to be 2% and no need to wash to reduce the silt amount. Its property and gradation are presented as shown in Table 3-6 and Figure 3-5 respectively.

Figure 3-4 Silt Content Test for Fine Aggregate

Table 3-6 Material Properties of Fine Aggregate Used

Fine Aggregate Material Properties	
Silt Content	2%
Moisture Content	8%
Absorption	0.7%
Finess Modulus	2.9

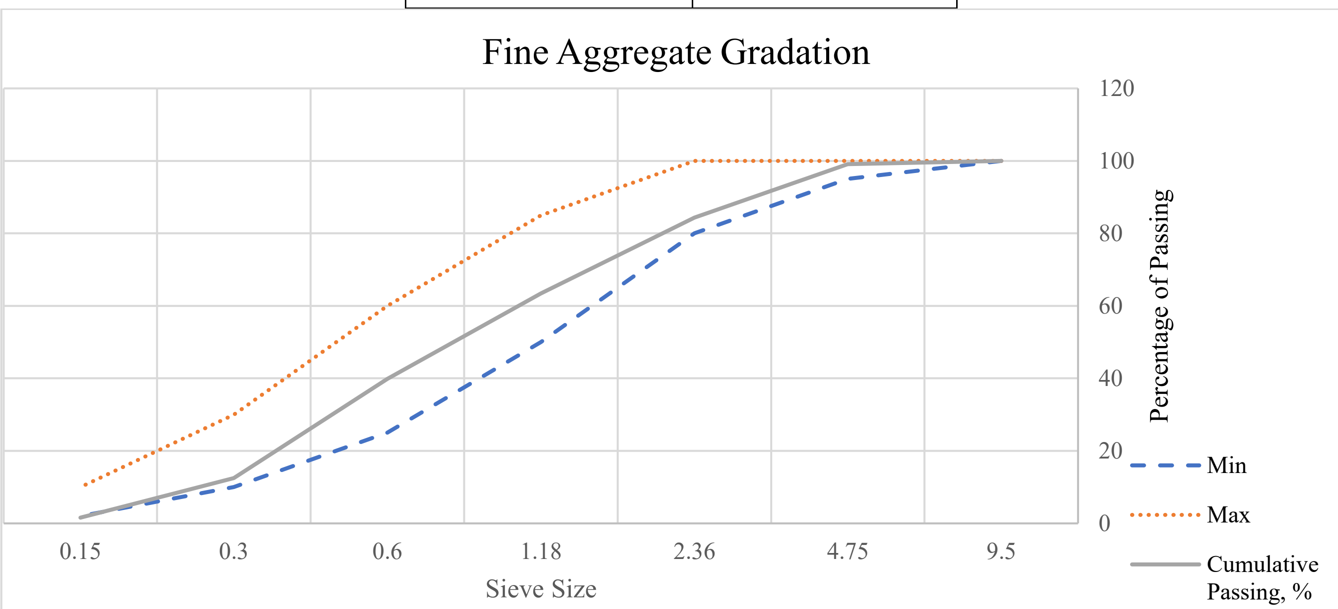

Figure 3-5 Gradation of Fine Aggregate used

3.2.4 Reinforcement Steel

In all specimens a 10mm diameter deformed reinforcement was used as longitudinal bar while deformed 8mm diameters were used as transverse reinforcements. Uniaxial tensile tests were performed on rebar samples from the different diameters used. Results from the uniaxial test are reported in Table 3-7. More detail can be found in Appendix C.

Table 3-7 Mechanical Properties of Reinforcements

Specimen	Internal Diameter(d_1) (mm)	Average Yield Strength (MPa)	Average Ultimate Strength (MPa)	Elongation (%)	Yield Strain(με)
$\phi 8$	7.46	547.9	667.71	24.4	2600
$\phi 10$	9.56	563.97	744.1	24.5	2722

3.3 Specimen Production/Fabrication

The process of specimen fabrication consists of three primary stages. Initially, formwork is prepared and assembled to establish the required structural framework. This is followed by the fabrication of the reinforcement cage, which is subsequently positioned within the formwork after the necessary accessories have been installed. Finally, the specimen preparation is completed by pouring and casting the concrete within the configured setup

3.3.1 Formwork

Plywood formwork, with 16mm thickness shown in Figure 3-6, cut in appropriate pieces for each specimen dimension was used in the making of the required formwork. The plywood was purchased from a local market and was assembled as shown in Figure 3-7.

Figure 3-6 Plywood used for Formwork Construction

As part of the proposed approach, the formwork was arranged so that the beams would be cast adjacent to one another, utilizing a shared plywood formwork on the side.

Figure 3-7 Formwork Assembly for Specimens

3.3.2 Reinforcing Cages

The reinforcing cages for the test assembly were also constructed at the construction yard of AAiT's Construction Material Laboratory. The reinforcing bars were cut to a required length using an electric grinder and bent to the designed shape according to the proposed detailing. The bars were tied together manually using rebar ties.

Figure 3-8 Reinforcement cages placed in the formwork

In order to maintain cover provisions between the cage and the formwork, a mortar spacer produced at the casting site were applied, shown in Figure 3-8, on to both the bottom and side layer of reinforcing bars.

3.3.3 Concrete Casting

For the trial beam concrete mixing was done using a small mixer found at the lab. However Concrete casting for the main specimens took place outside of the laboratory using a tilting drum mixer, shown in Figure 3-9, which had a greater volume capacity per mix than the mixer found inside the lab. All eight specimens were cast in the same day. It took three mixes of the tilting drum mixer to cast all specimens along with their respective cube and cylinder samples. The concrete constituents proportioned in Table 3-2 were mixed in an orderly manner and slump was checked for every mix to check consistency. Petrol vibrator with 50mm diameter was used during casting to consolidate the concrete in both the specimens and test samples (Cylinders and Cubes).

While casting the main specimens nine cube samples (150mm*150mm*150mm) and nine-cylinder samples (150mm diameter and 300mm height) were prepared to check compressive and tensile strength of concrete respectively. Samples were cured in the same environmental condition as the specimens. Consequently, a consistent concrete strength was achieved for all specimens.

Figure 3-9 Materials and mixer ready for casting

3.3.4 Specimen Preparation

After the curing process the specimens were prepared to be tested. First the formwork was removed as shown in Figure 3-10. This preparation included cleaning the beam surfaces, cleaning the holes created and painting the specimens white as shown in Figure 3-11, for better visibility of cracks during testing.

Figure 3-10 Beam specimens just after removal of formwork

Figure 3-11 Getting ready the beams and transporting

3.4 Test Setup

The experimental program is testing six shear-critical deep reinforced concrete beams under a three-point monotonic loading system. Each beam was simply supported on two steel roller supports, positioned at both ends. The reinforced reaction frame at the Construction materials laboratory was utilized to conduct the tests until structural failure was reached. A concentrated point load was applied at the mid-span of each beam using a manually operated hydraulic jack as shown in the Figure 3-12 with a maximum loading capacity of

1000 kN, exerting force against the bottom of the resistance-enhanced reaction frame to simulate real structural loading conditions. The transducers were calibrated using measuring caliper shown in Figure 3-17.

As the hydraulic jack was manually operated, maintaining a fixed loading rate was not possible. However, the loading rate was regulated within a consistent range by controlling the number of strokes applied per minute.

Figure 3-12 Hydraulic Jack

Instrumentation for the experimental program was designed to help meet the research's objective by obtaining relevant response data from the experiment. Measurements obtained during testing were, applied load in kN from load cell, mid span deflection in mm from displacement measuring transducer, surface displacement measurements from surface mounted transducers and out of plane strain measurement from strain gauges attached on aluminum strips. The general test setup is shown in Figure 3-26.

The TDS-630 datalogger shown in Figure 3-13 was used to monitor and record data. Load reading from the load cell shown in Figure 3-3, midspan deflection reading from the transducer shown Figure 3-14 and out of plane strain measurements from straingauges were recorded in 1 second interval and extracted in an excel format using the TDS-630 datalogger shown in Figure 3-16.

Figure 3-13 Load cell

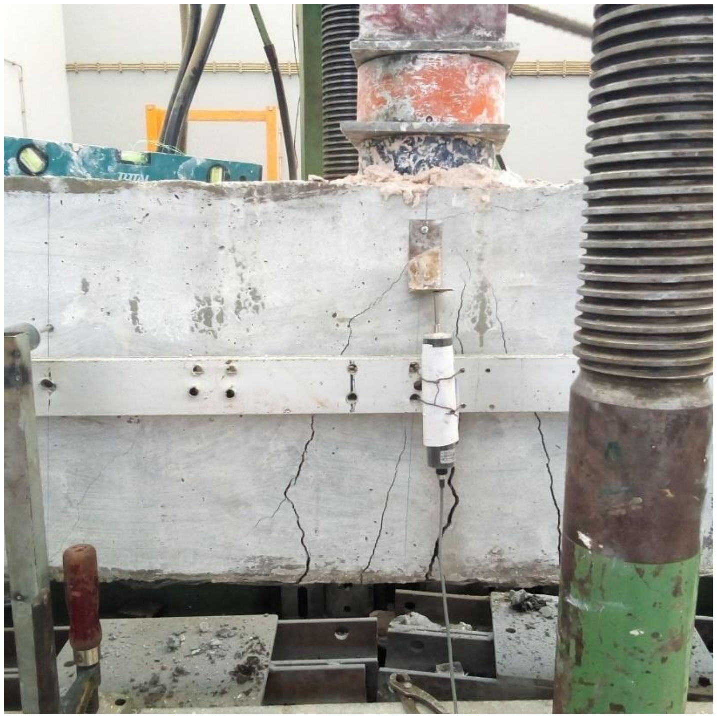

Figure 3-14 Displacement Transducer (For Mid-Span Deflection)

Figure 3-15 Displacement Transducer (For out of plane measurements)

Figure 3-16 TDS-630 Datalogger

Figure 3-17 Distance Measuring Caliper

3.4.1 Out of Plane Measuring Instruments

The out of plane measurement used on the trial beam consisted of two transducers as shown in Figure 3-18 and Figure 3-19 located at midpoint between support and load on opposite side of the beam. they were placed on part of the strut where maximum out of plane was expected.

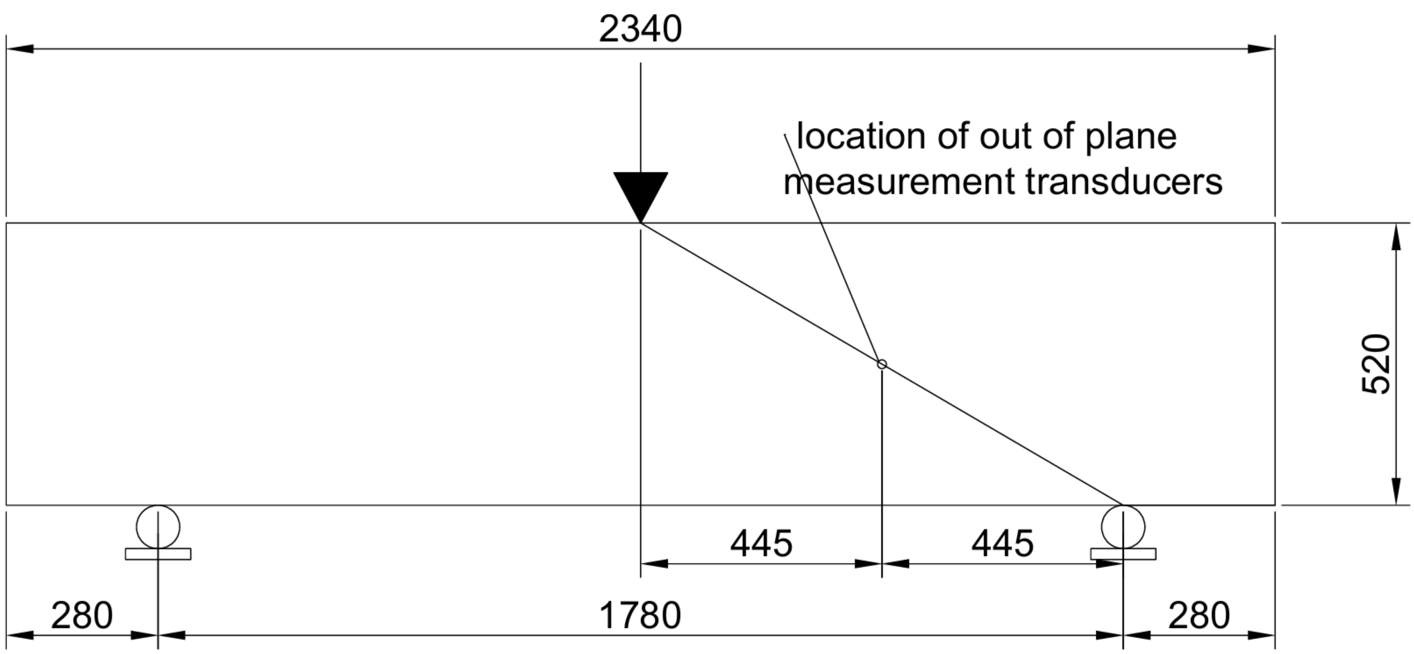

Figure 3-18 Sketch Out of Plane Deformation Measurement Locations

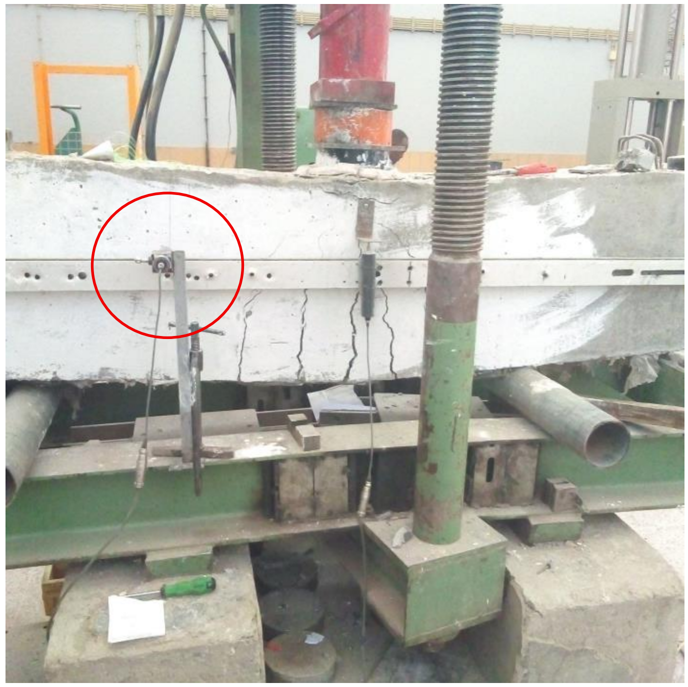

Figure 3-19 Out of Plane Deformation Measurement Locations

3.4.2 Surface Mounted Displacement Measurements

A 300mm*300mm square grid shown in Figure 3-20 was used as a guide to place surface displacement measuring instruments. This square grid was positioned in a region where shear failure is expected to govern, it was placed between the support and loading point as shown in Figure 3-21 on the beam symmetrically in two alternative sides. Linearly varying differential transformers (LVDT) (Displacement Transducers) were installed along the compression strut and perpendicular to the strut. and one horizontal installation was placed at the midline of the proposed grid.

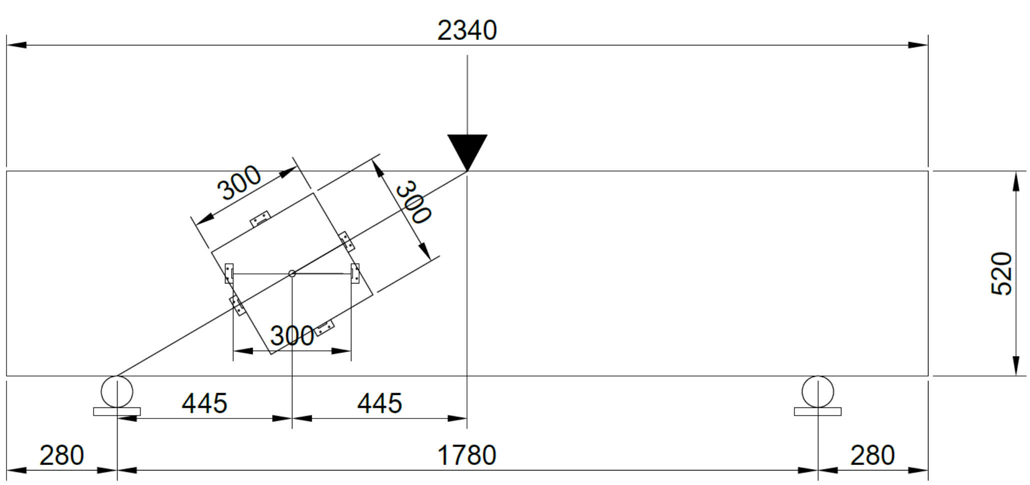

Figure 3-20 Surface Mounted Displacement Measuring Instrument Setup

Holes for mounting instrumentation steel plates were pre-drilled in each specimen prior to installation of test assembly components. The displacement transducers were logged in to the geodatalog which is connected to a computer data acquisition system named "Datacom", which was tailored to record data in 1 second interval to match with the TDS-630 data logger shown in Figure 3-22. The results obtained were then collected in an excel format from the connected computer. A total of three LVDTs were used on one side of the beam, the average surface shear strain was obtained from the relative movement of the two diagonally placed displacement measurements while longitudinal displacement was obtained from the horizontally placed LVDT. The same set up is reciprocated at the alternative side.

Figure 3-21 Surface Mounted Displacement Measuring Instruments

Figure 3-22 Geodatalogger Connected to a Computer Data Acquisition System

4 RESULT AND DISCUSSION

Six deep reinforced concrete beams were subjected to failure testing. This section presents a comprehensive analysis and prediction for each specimen based on the gathered data. Additionally, software simulations and building code predictions are included, along with detailed explanations of their respective responses. The influence of various variables is also thoroughly examined through equivalent comparisons.

4.1 Test Observation

4.1.1 Testing Procedure

Once the beams were ready for testing, they were transported from the casting area to the construction material laboratory by using a forklift. Within the laboratory, forklift and hydraulic floor cranes were used to place the beams on the reaction frame. The reaction frame had two roller supports which were adjusted for the required testing length of the beam. After placement, the beam alignment was then adjusted to the center of the reaction frame.

The test assembly followed a thorough procedural set of steps to avoid eccentric loading and to ensure proper reading of measuring instruments for their intended purpose. Primarily, the holes for mounting surface displacement measuring instruments were drilled.

Plumb bob and bubble level were used while setting up for the loading platform above the beam which included the load cell, hydraulic jack and thick load bearing/distributing plates which were used in between for an even load distribution and to avoid local crushing on the beam surface.

Since the setup and preparation prior to testing required a lengthy amount of time, it took two days to complete the testing of one specimen. The first day, the beam is setup for the planned measurements and the instruments are installed. Testing took place the second day after the setupinstruments were properly connected to their respective data recording systems. After initializing readings, the beam is loaded to failure under monotonic loading. During testing the beam was monitored distantly for safety reasons but a camera was mounted nearby to document the tests. At the end of each test day the accessories for loading and instrumentations were removed and post failure status of the beam was documented by taking pictures and measuring crack properties. In the test observations graphs below “EX” refers to the plotting of experimental data.

4.1.2 Test Observation - Specimen SA-25

As shown in the graphs in Figure 4-1, SA-25 exhibited the highest initial stiffness (100 kN/mm over 0–5 mm) and a nearly linear load increase up to the first crack at 1.2 mm. Its full-range curve, shown in Figure 4-2 ,peaked at 438 kN around 12 mm displacement. Post-peak, the beam-maintained loads of 400–420 kN up to 20 mm before gradually softening—a long plateau indicative of excellent ductility. Spalling of the 25 mm side cover was minimal and occurred only near peak load, confirming that a relatively small cover with a wider core and well-confined stirrups delays cover detachment and maximizes energy absorption. The Vector 2 2D NLFEA model predicted initial stiffness reasonably well but overestimated peak capacity by 15%, failing to capture out-of-plane spalling effects that govern ultimate strength.

This suggests fair agreement in stiffness modeling between Vector2 and the physical specimen in the early (elastic) stage. Vector2 underestimates the experimental peak deflection (5mm Vs 50mm). This discrepancy may be due to limitations in Vector2's Material model. the experimental curve shows a smooth transition into a softening plateau — possibly due to progressive cracking and redistribution. The Vector2 result shows more abrupt drops and fluctuations after the peak — likely due to numerical instability or localized failure not captured accurately in 2D modeling. Figure 4-3 shows the first crack at elastic range and Figure 4-4 and Figure 4-5 shows the beam just after the peak load with the top of the center of the beam spalled.

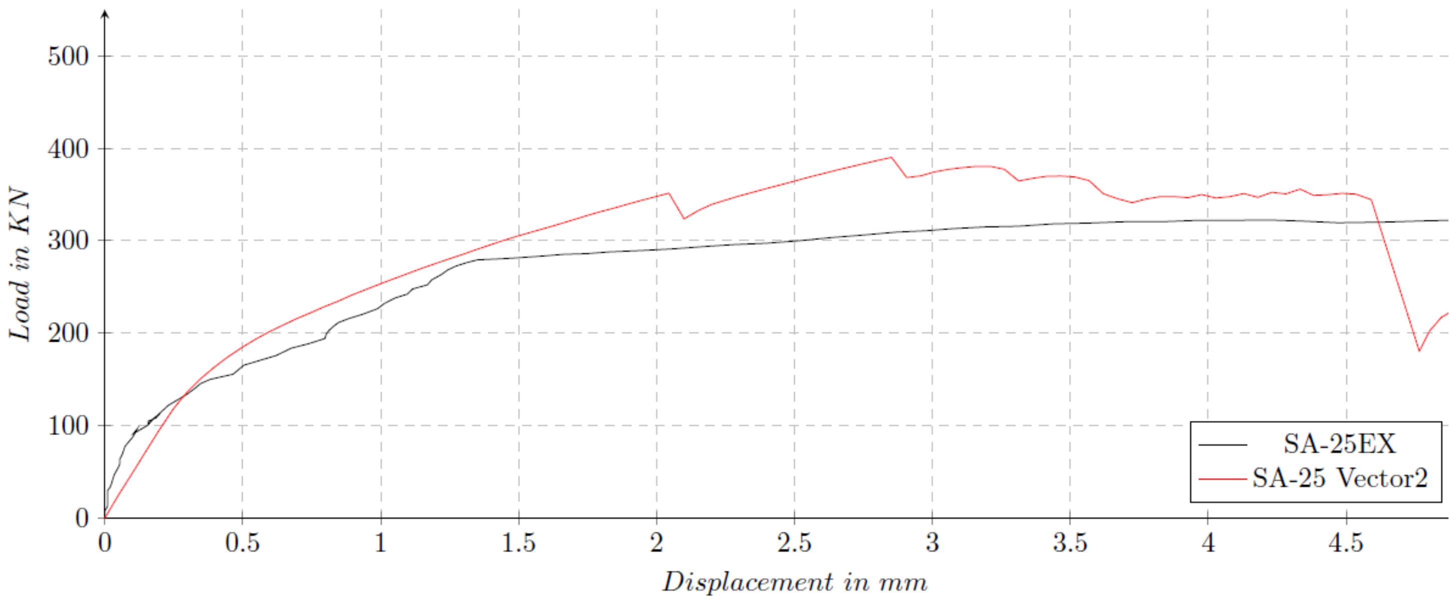

Figure 4-1 Load Vs. Mid-Span Deflection for SA-25 up to 4.5mm deflection

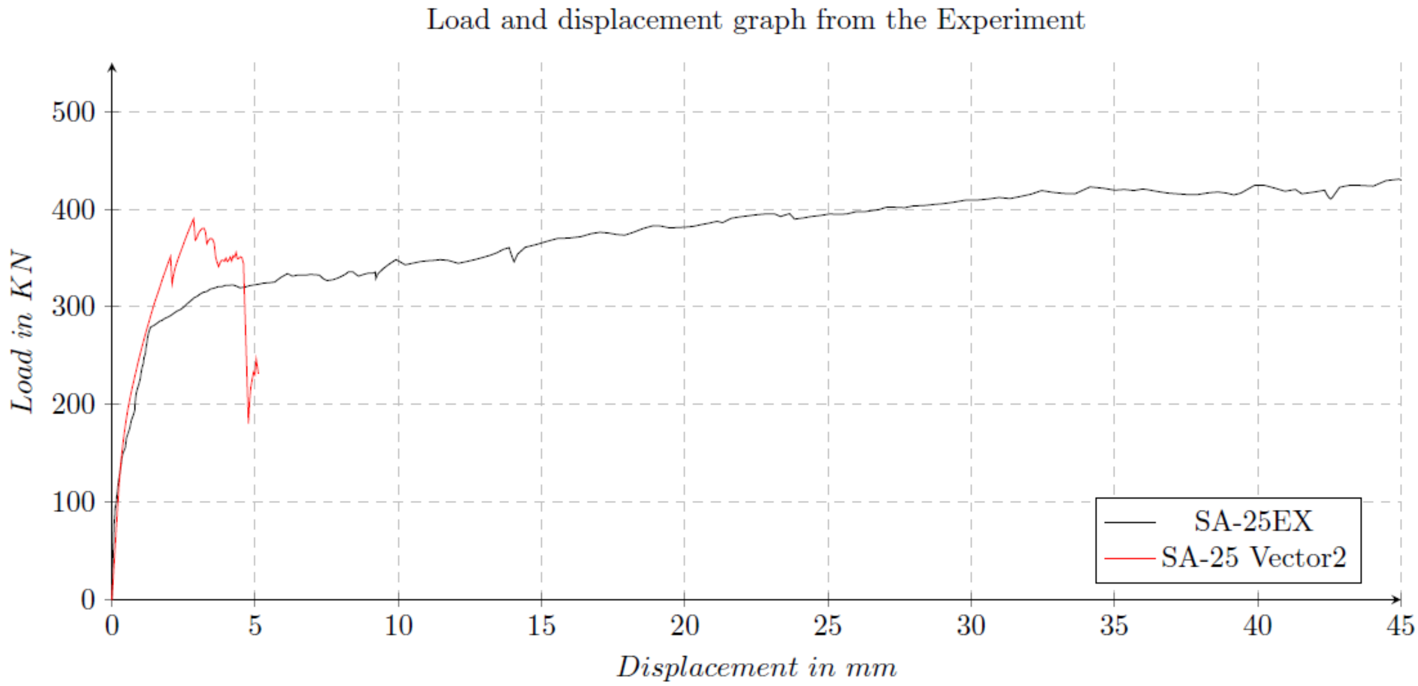

Figure 4-2 Load Vs. Mid-Span Deflection for SA-25 up to failure

Figure 4-3 bottom Crack (SA-25)

Figure 4-4 Side Cover Spalling Limited at the Top under peak load (SA-25)

Figure 4-5 top of the beam after the test

4.1.3 Test Observation - Specimen SA-50

With a 50 mm cover and correspondingly narrower core, SA-50's initial stiffness dropped to 75 kN/mm, and nonlinearity appeared as early as 1.0 mm. As shown in Figure 4-8 the cracking was limited to the middle bottom part of the beam which is the same as the previous beams. As shown in Figure 4-6 and Figure 4-7, the beam reached a peak load of ~369 kN at ~14 mm displacement. Its post-peak plateau (340–360 kN to ~25 mm) was shorter than SA-25's, reflecting moderate ductility. Side cover spalling initiated just before the ultimate load, producing small load oscillations in the curve. Overall, SA-50 demonstrates that reducing core width in favor of thicker cover diminishes both stiffness and strength. Vector 2 again matched the pre-crack stiffness but predicted a peak near 450 kN, overestimating strength by 22% and neglecting early spalling-induced softening. After the peak load there was clear delamination as seen in Figure 4-9 and Figure 4-10 .

Like in the SA-25 model, Vector2 continues to underestimate the ductility of the beam due to simplified material behavior and 2D modeling limitations. The mismatch in post-peak behavior indicates that Vector2 may not realistically capture progressive cracking or crushing in concrete, especially where 3D stress states or side cover effects are significant.

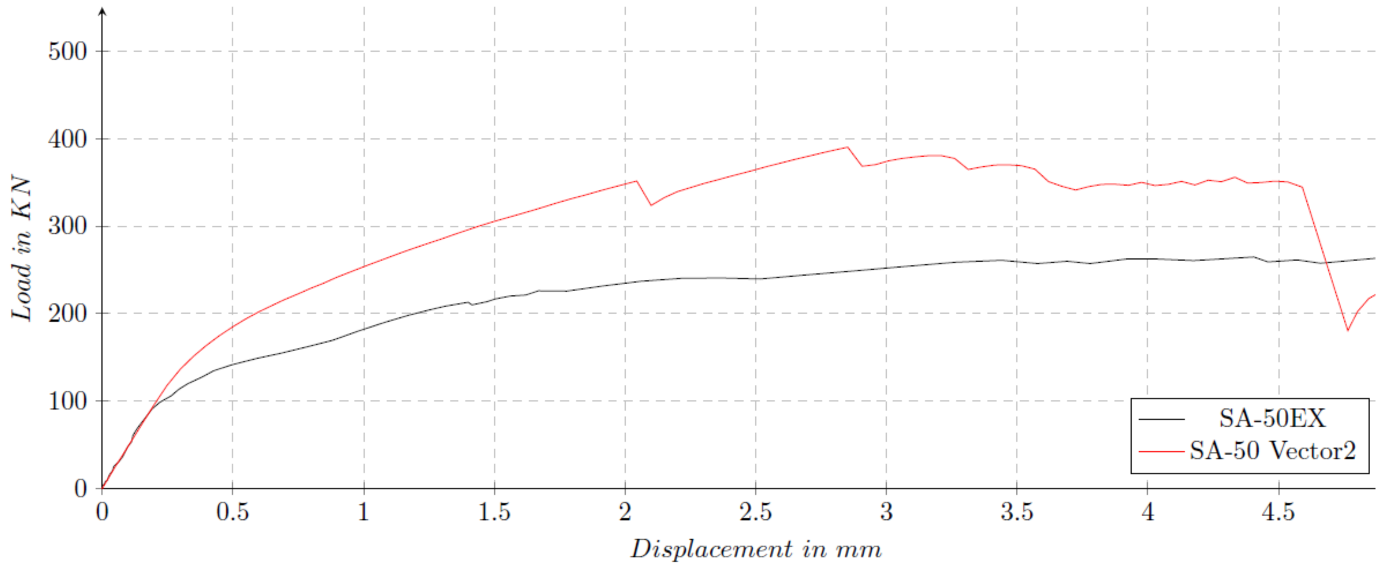

Figure 4-6 Load Vs. Mid-Span Deflection for SA-50 up to 5mm

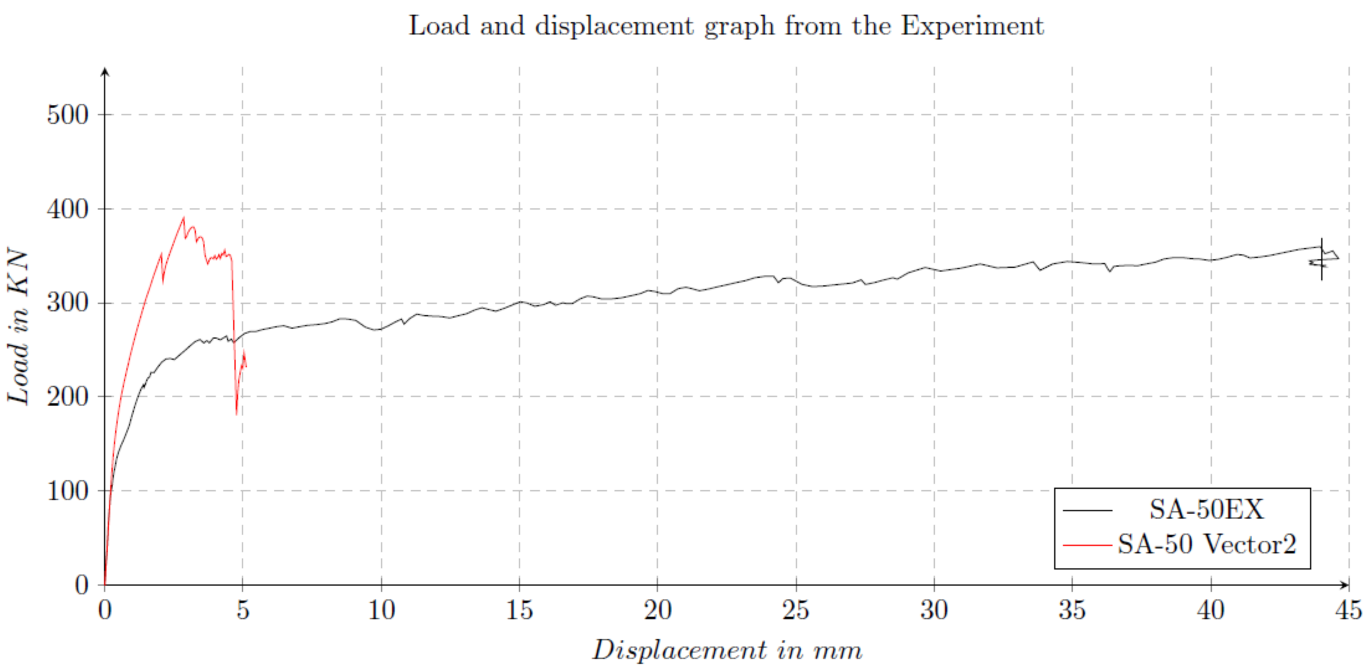

Figure 4-7 Load Vs. Mid-Span Deflection for SA-50 up to failure

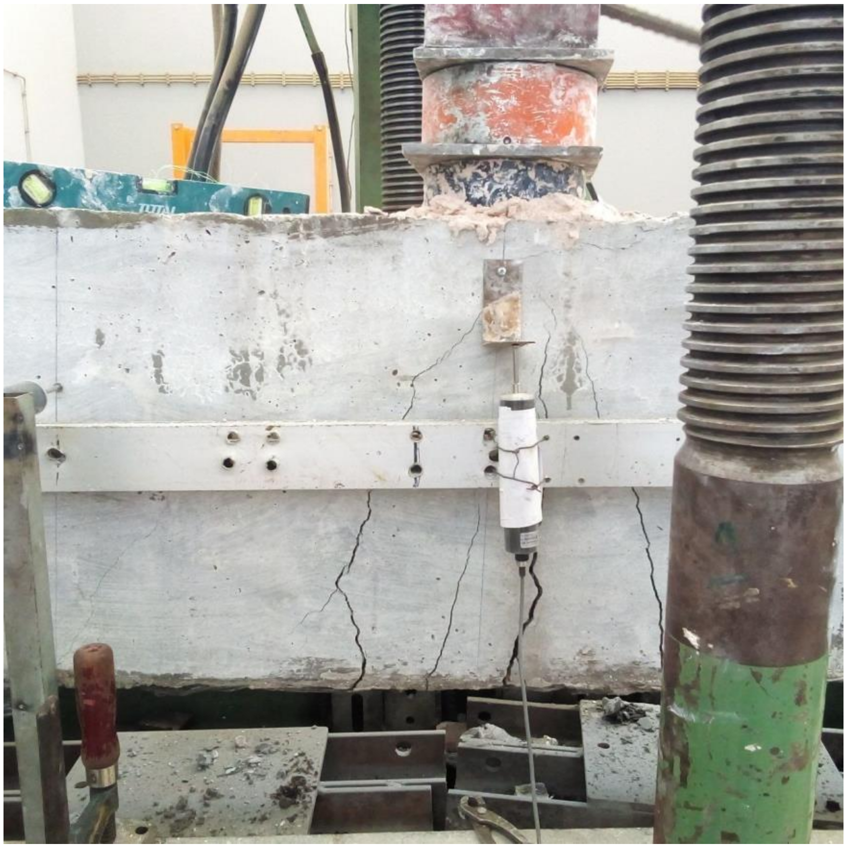

Figure 4-8 Mid span cracking before peak load

Figure 4-9 Spalling under load around peak load

Figure 4-10 Top view of SA-50 after the test

4.1.4 Test Observation - Specimen SA-75

SA-75 showed the weakest performance among SA-series beams as shown in Figure 4-11 and Figure 4-12. Its initial stiffness was only 60 kN/mm, with significant nonlinearity by 0.7 mm. The peak load of 342 kN occurred at 42 mm, Vector 2's estimate (460 kN peak) was hugely unconservative, highlighting that 2D analyses cannot replicate cover detachment and corner splitting. Like SA-50 there was clear delamination after the peak load as seen in Figure 4-14 and Figure 4-15.

Both the experimental and simulation curves rise steeply from the origin, showing good initial stiffness. Experimental curve flattens early, indicating significant damage or spalling before peak. Overestimation of stiffness, consistent with earlier SA-series results. No sign of brittle crack localization or sudden capacity drop in the simulation (which is expected in thick-cover failure cases). Spalling effect is likely severe and earlier than SA-50 and SA-25, based on early flattening of experimental curve. Increasing the cover to 75 mm in SA-series beams (which reduce core size) significantly impairs structural performance. The experiment shows earlier softening and reduced capacity compared to both simulation and lower cover specimens. Vector2 fails to capture this due to its 2D assumptions and neglect of spalling mechanisms.

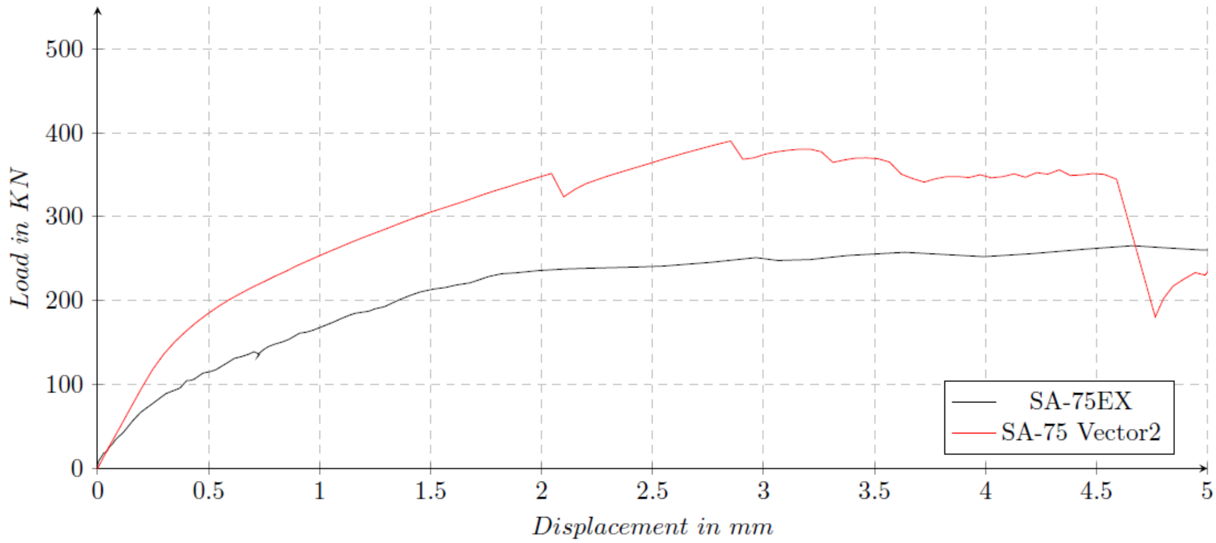

Figure 4-11 Load Vs. Mid-Span Deflection for SA-75 up to 5mm

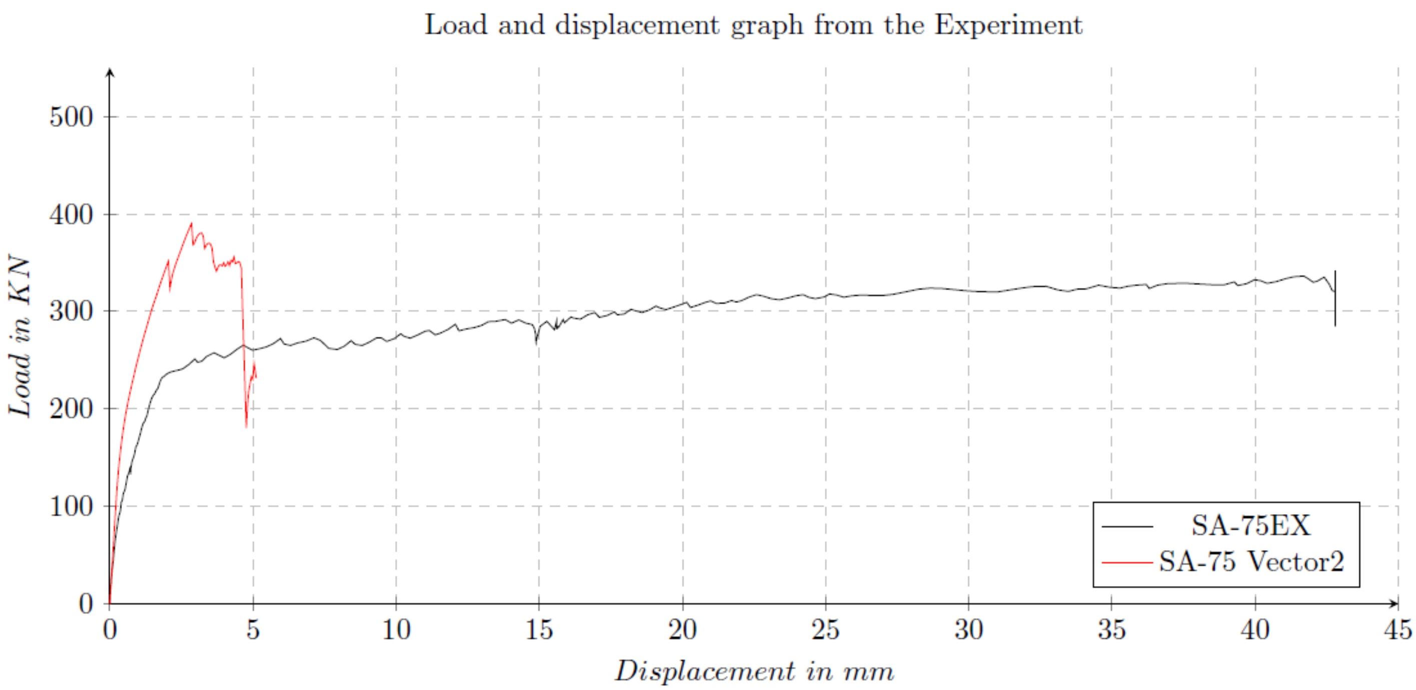

Figure 4-12 Load Vs. Mid-Span Deflection for SA-75 up to 45mm

Figure 4-13 Mid span cracking before peak load SA-75

Figure 4-14 Final State of the Beam SA-75

Figure 4-15 Final State of the Beam SA-75 top view

4.1.5 Test Observation - Specimen SB-50

By preserving the full core width and adding 50 mm of cover externally, SB-50 maintained high initial stiffness (95 kN/mm) and delayed nonlinearity until 1.1 mm as shown in Figure 4-16 and Figure 4-17. There were midspan cracks in the early phase of loading as shown in Figure 4-18. Its peak load of 425 kN at 13 mm nearly matched SA-25. Post-peak, SB-50 exhibited a mild softening plateau (400–420 kN to 30 mm), demonstrating excellent ductility. Spalling was minimal and occurred only slightly after peak load. These results confirm that maintaining core confinement preserves both strength and ductility, even with substantial side cover. Vector 2 predicted 470 kN—its closest match—yet still overestimated capacity and did not capture the slight post-peak softening observed.

Regarding post-peak behavior and spalling, the Vector2 curve shows a sudden drop around 2.2 mm subsequently recovers and stabilizes. In contrast, the experimental curve does not exhibit such a pronounced drop up to 5 mm, implying either that spalling did not occur as early as predicted by the model or that the model may be overly sensitive to crack propagation at that stage. This observation suggests that while Vector2 is effective in predicting crack initiation and failure progression, it may require further calibration for cover-related failure modes.

Lastly, the experimental results reveal a more gradual increase in displacement with load and less abrupt post-peak behavior, indicating that the actual beam likely exhibited greater ductility than modeled. The model maintains post-peak strength better than the test, which could occur due to assumptions regarding tensile stress capacity beyond cracking. Finally there were spalling as seen in Figure 4-19.

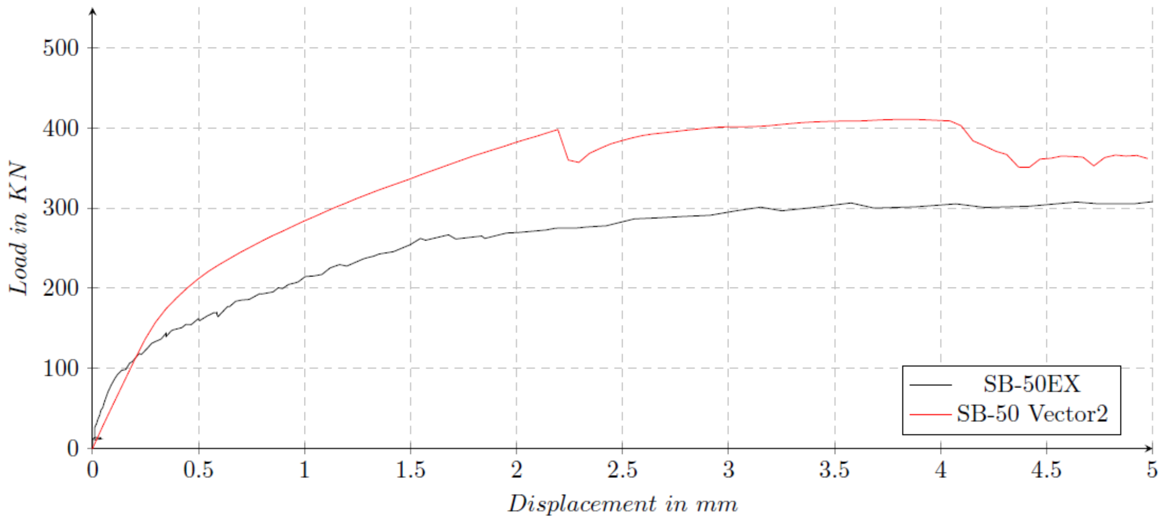

Figure 4-16 Load Vs. Mid-Span Deflection for SB-50 up to 5mm

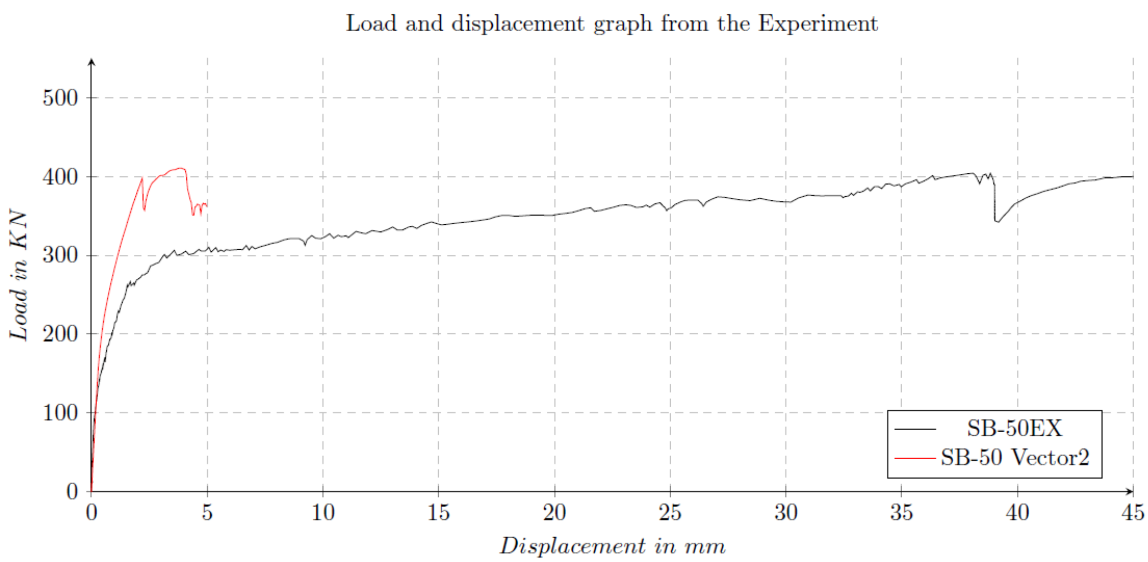

Figure 4-17 Load Vs. Mid-Span Deflection for SB-50 up to failure

Figure 4-18 Early Mid span cracking before peak load SB-50

Figure 4-19 Final State of the Beam SB-50

4.1.6 Test Observation - Specimen SB-75

Although SB-75 kept the core intact, its initial stiffness fell to 80 kN/mm and nonlinearity began near 1 mm as shown in Figure 4-20 and Figure 4-21. The beam peaked at 330 kN around 16 mm displacement and then held 300–320 kN up to 25 mm before a moderate decline. Moderate spalling occurred earlier than in SB-50, and the plateau was shorter but this was due to experimental setup in which we no longer were able to load the beam further. These findings show that once an optimal cover thickness is exceeded, additional cover provides little capacity gain and may encourage earlier spalling. This observation suggests that increased cover thickness may render the beam more vulnerable to premature spalling or crack propagation. This finding supports the hypothesis being explored: larger concrete cover may lead to pre-peak load spalling or reduced confinement, particularly when not accompanied by a proportionally larger core, as seen in the SB series where the core is fixed.

In terms of pre-peak instabilities, a small drop or plateau is observed in the Vector2 model around 2–3 mm displacement, potentially indicating early cracking or spalling in the outer concrete layers, as well as a local instability due to changes in internal force distribution caused by cracking. Regarding ductility and behavior beyond 5 mm, the experimental curve continues to rise or stabilize near the cutoff, suggesting that the full peak and softening phases were not visually captured. However, the known peak of 330.25 kN implies that the beam did not sustain load as effectively as SB-50. The Vector2 model appears to reach its peak slightly earlier than the experimental results and enters a more defined descending branch. The last state of the beam is shown in Figure 4-22, it doesn’t show extensive damage as other beams because of problems with the loading setup we were not able to increase the load to its full potential.

The effect of larger cover thickness may reduce effective confinement and induce earlier cracking, reinforcing the interpretation that, despite sharing the same core, SB-75's increased cover leads to greater tensile stress zones, resulting in early cracking or spalling. This supports the thesis objective that increased cover can diminish pre-peak strength and initiate localized failures in deep beams, even when internal reinforcement and core dimensions remain unchanged.

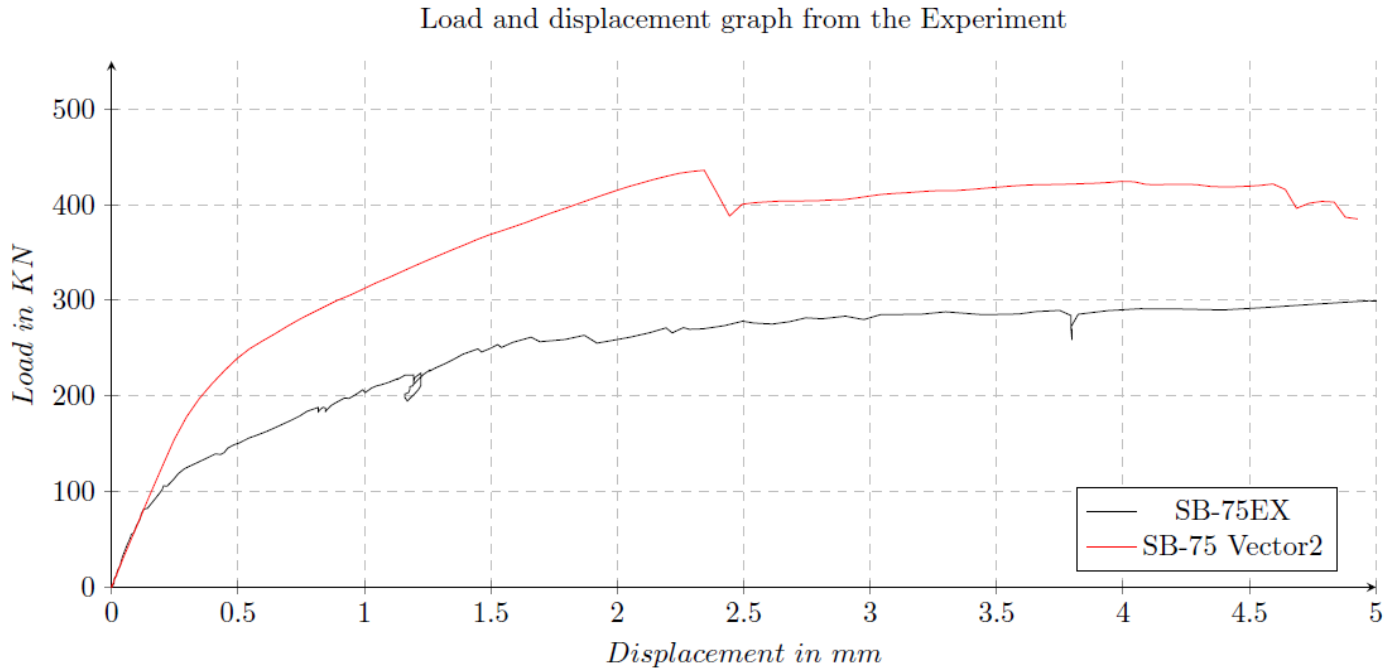

Figure 4-20 Load Vs. Mid-Span Deflection for SB-75 up to 5mm

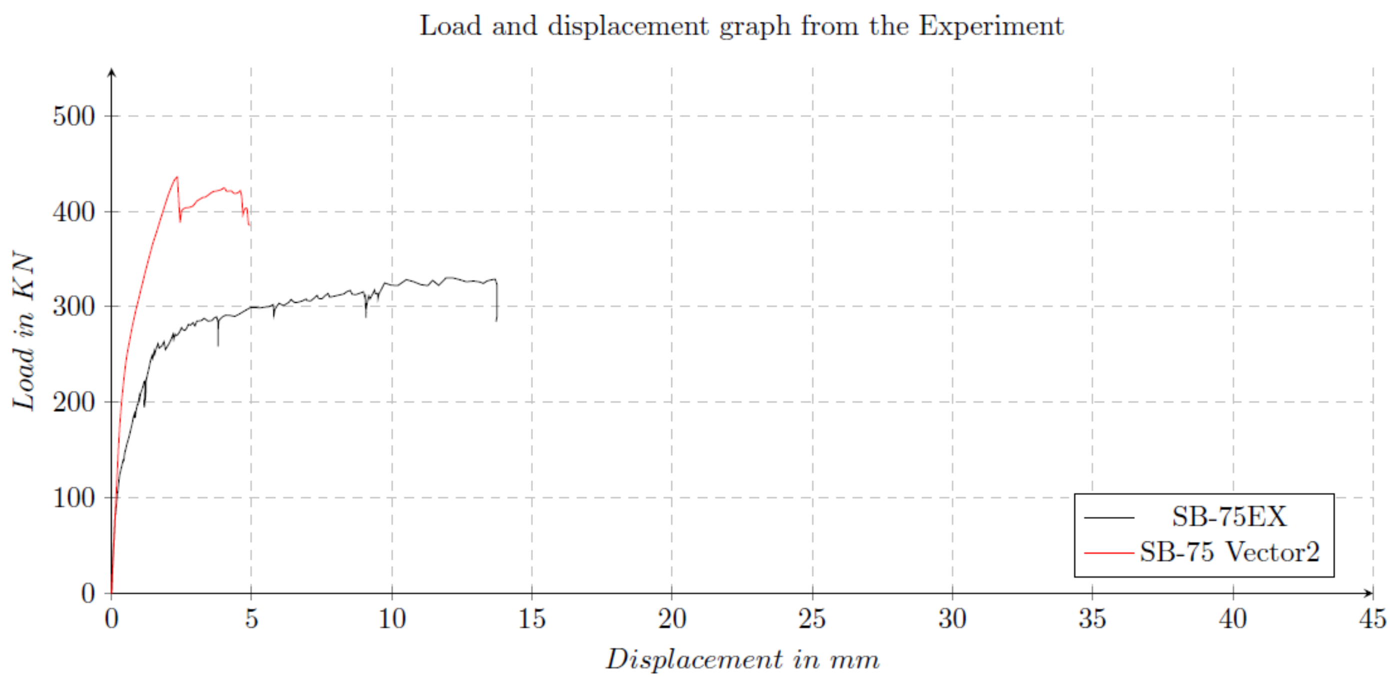

Figure 4-21 Load Vs. Mid-Span Deflection for SB-75 up to failure

Figure 4-22 Final state Mid span cracking just after peak load SB-75

4.1.7 Test Observation - Specimen SB-100

Figure 4-23 and Figure 4-24 shows that SB-100 matched SB-75's initial stiffness (85 kN/mm) and crack onset (1 mm), then reached 370 kN peak at 15 mm displacement. Post-peak, it maintained 340–360 kN to 25 mm before gradually dropping off. Spalling of the 100 mm cover appeared before peak but was less severe than in SA-series due to preserved core. Although SB-100EX performed better than SB-75EX, it still fell short of SB-50EX's optimal balance. These results reinforce that excessive side cover confers minimal benefit once core confinement is adequate. Vector 2 again overpredicted (465 kN) and could not simulate the early spalling that limited strength.

The Vector2 model demonstrates slightly higher initial stiffness compared to the experimental results. The experimental curve reflects a more gradual increase, which is typical when microcracking and cracking at the cover-core interface occur before the core fully engages. In terms of peak load comparison, the experimental peak load is approximately 369.65 kN, while the Vector2 model slightly overestimates the load-carrying capacity, peaking a bit higher than the experimental curve. The difference in peak load is less pronounced than in SB-50, suggesting improved simulation accuracy, potentially due to the larger cover behaving more elastically in the early stages.

Regarding post-peak behavior, both curves exhibit distinct softening after reaching their respective peaks. However, the experimental curve declines more rapidly, indicating a brittle failure that may be attributed to cover separation, spalling, or crack propagation around the steel core. Conversely, the Vector2 model shows a more gradual softening, which is characteristic of 2D models that cannot effectively capture three-dimensional spalling or out-of-plane failure mechanisms.

SB-100 exhibits lower ductility compared to SB-50 and possibly SB-75. Although it achieves a larger peak load than SB-75, the beam fails more abruptly, reinforcing the notion that a larger cover without additional confinement does not enhance performance. In summary, when compared with SB-50 and SB-75, the observations for each beam are as follows: SB-50 achieves a peak load of 424.88 kN, showcasing the best performance with greater stiffness and ductility; SB-75 reaches 330.25 kN, reflecting a decrease in strength and ductility due to increased cover thickness; and SB-100 peaks at 369.65 kN, which is higher than SB-75 but still below SB-50, exhibiting brittle post-peak behavior. Although SB-100 seems to regain some capacity relative to SB-75—possibly because the larger cover temporarily delays cracking—it ultimately fails due to insufficient confinement or out-of-plane instability. This result suggests a nonlinear relationship between cover thickness and performance, indicating that excessive cover may reduce effectiveness by delaying core engagement and increasing the risk of spalling. The early phase of loading causes tiny cracking in the middle bottom of the beam as shown in Figure 4-25 and extensive cracking and spalling at the bottom of the loading as shown in Figure 4-26 at the end of the loading.

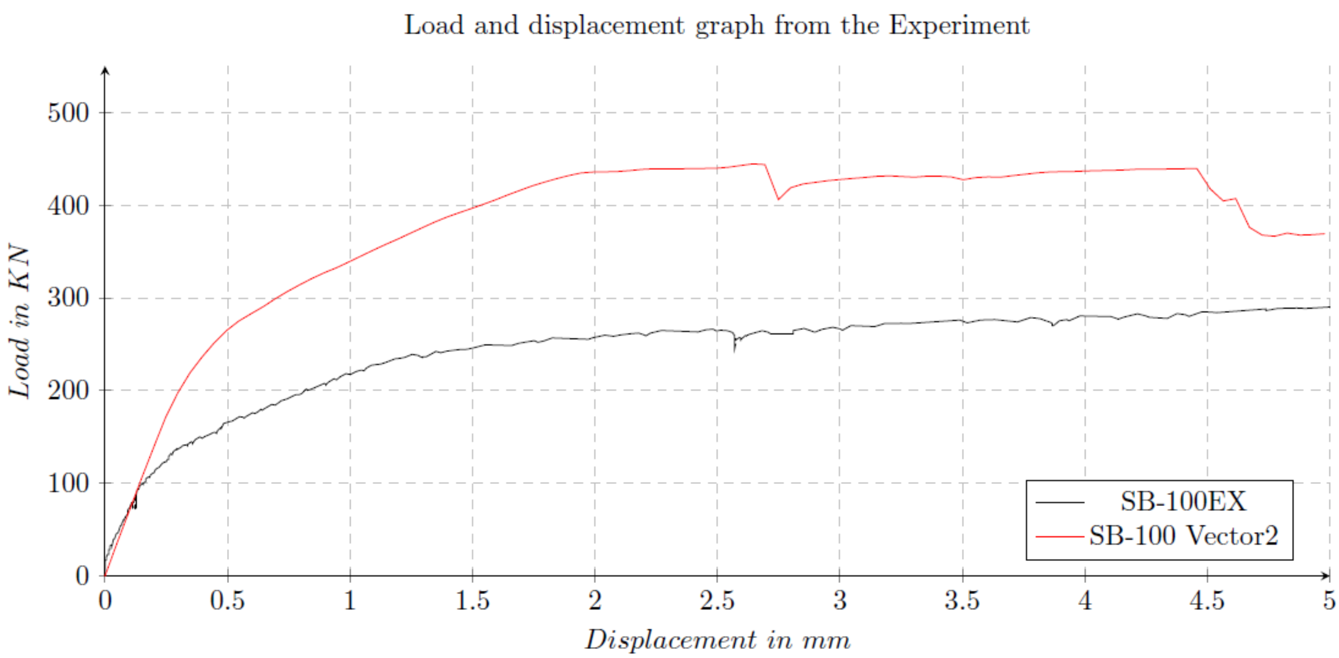

Figure 4-23 Load Vs. Mid-Span Deflection for SB-100 up to 5mm

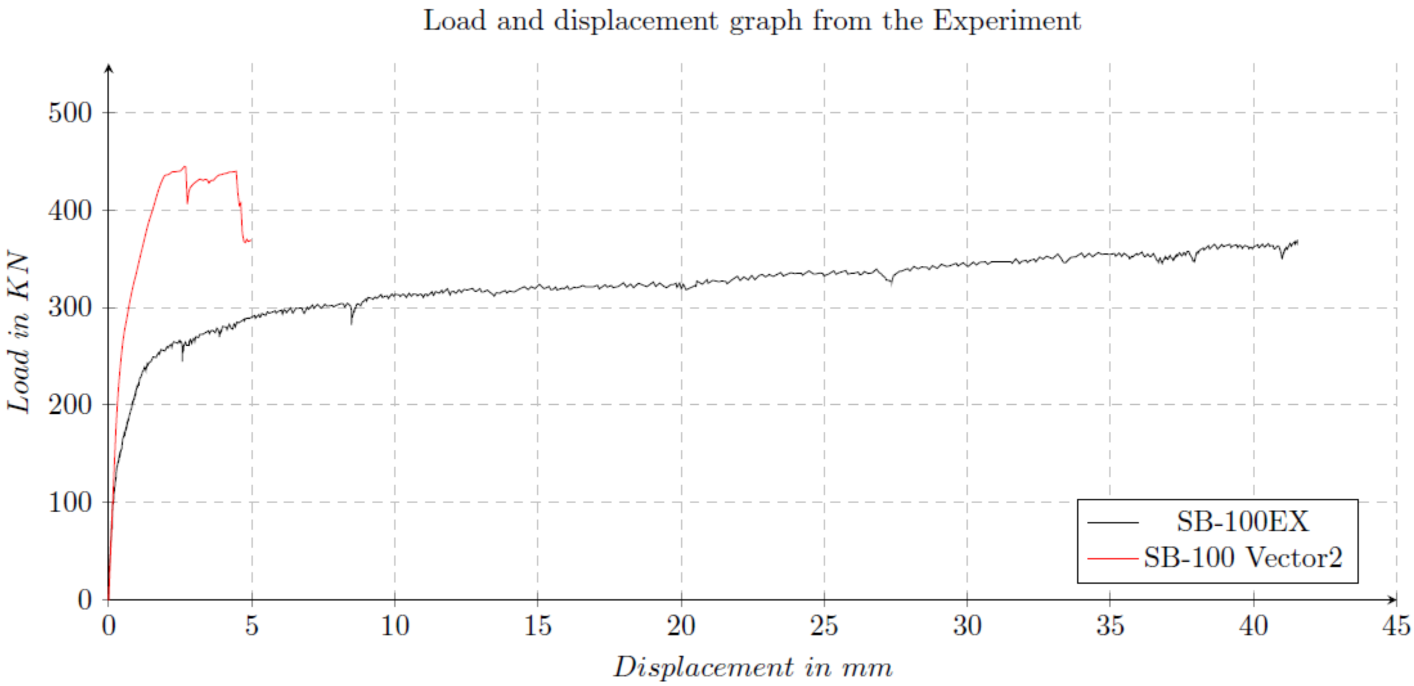

Figure 4-24 Figure 4 23 Load Vs. Mid-Span Deflection for SB-100 up to failure

Figure 4-25 Early Mid span cracking before peak load SB-100

Figure 4-26 Final state Mid span cracking just before peak load SB-100

4.1.8 SA-series and SB-series test observations

In all cases, the Vector 2 2D NLFEA model captured initial stiffness up to first cracking reasonably well but consistently overestimated ultimate capacity (by 10–35%) and failed to reproduce post-peak softening caused by side cover spalling. These discrepancies underscore the need for 3D modeling or experimental calibration when side cover behavior governs shear capacity. Figure 4-27 and Figure 4-28 compare the experimental load-displacement responses of three deep beams in the SA series (SA-25, SA-50, and SA-75) with predictions from a 2D nonlinear finite element analysis simulation (Vector2). There is a significant reduction in peak load with increasing concrete cover and decreasing core width, highlighting the negative impact of thicker covers on stirrup confinement. All three experimental curves demonstrated relatively gradual descending branches after peak load, indicating ductile behavior, although SA-75E showed a more flattened response, suggesting potential issues with spalling or bond degradation. The Vector2 simulation, however, significantly overestimated the capacity of all three beams likely due to the model's inability to capture out-of-plane effects and its single simulation approach that fails to account for variations in cover thickness.

The Figure 4-29 and Figure 4-30 compares the experimental performance of SB-series beams (SB-50, SB-75, and SB-100), which retain a constant core and add cover externally, against the benchmark SA-25. SA-25 again reaches the highest peak load outperforming all other beams. This indicates that while retaining the core is beneficial, excessively large covers may lead to premature spalling or ineffective confinement. Notably, increasing the concrete side cover in the SB-series does not result in a corresponding increase in stiffness or peak load capacity; SB-75 and SB-100 show reduced or plateaued performance compared to SB-50EX. This finding sharply contrasts with the assumptions in most building design codes, such as ACI 318 and Eurocode 2, which treat the entire cross-sectional width—including the cover zones—as fully effective in resisting shear.

The test results suggest that once the core (stirrup-confining zone) is sufficient, additional concrete cover adds little to structural performance and may even introduce weaknesses due to spalling risk. Additionally, SB-series beams display stable load-displacement behavior with limited softening after peak, indicating improved ductility compared to the SA-series. The consistent performance among SB beams suggests that preserving the core stirrup cage positively contributes to structural integrity. Despite having similar or larger total cross-section widths than SA-25, the peak capacities of the SB beams are generally lower, underscoring the importance of core width and confinement over total width in resisting shear and preventing spalling.

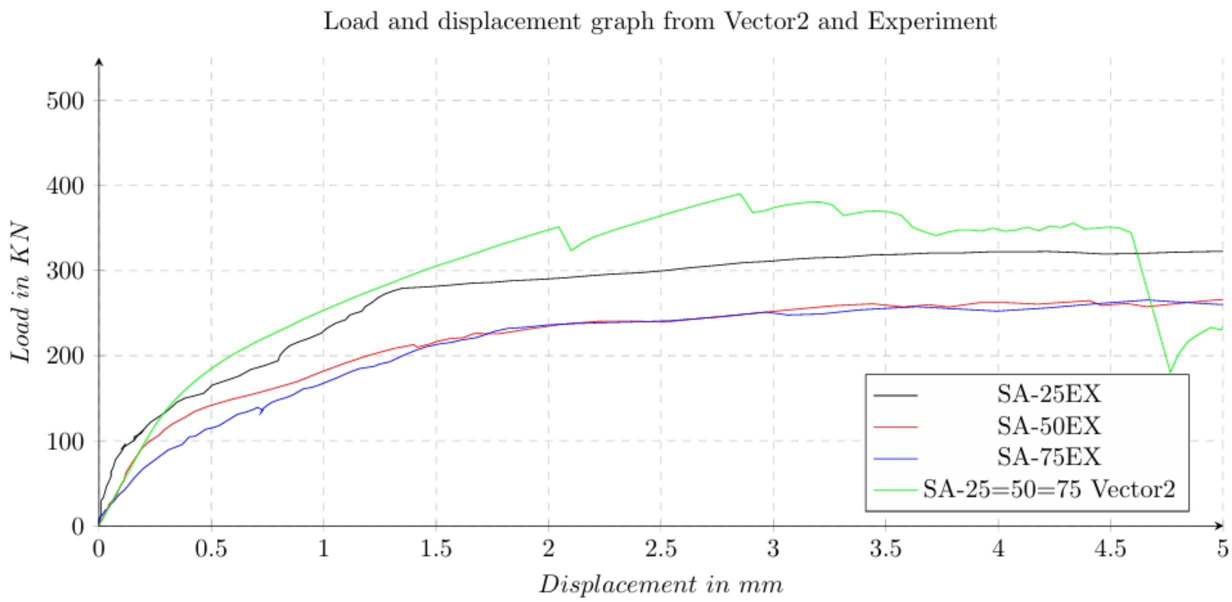

Figure 4-27 Load Vs. Mid-Span Deflection for SA series beams up to 5mm

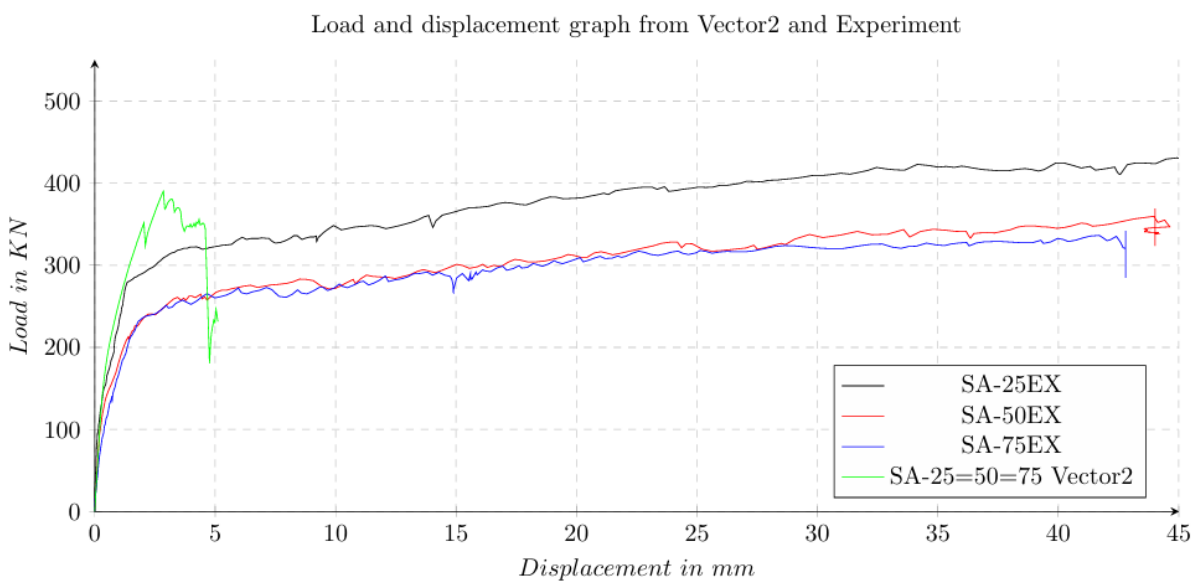

Figure 4-28 Load Vs. Mid-Span Deflection for SA series beams up to failure

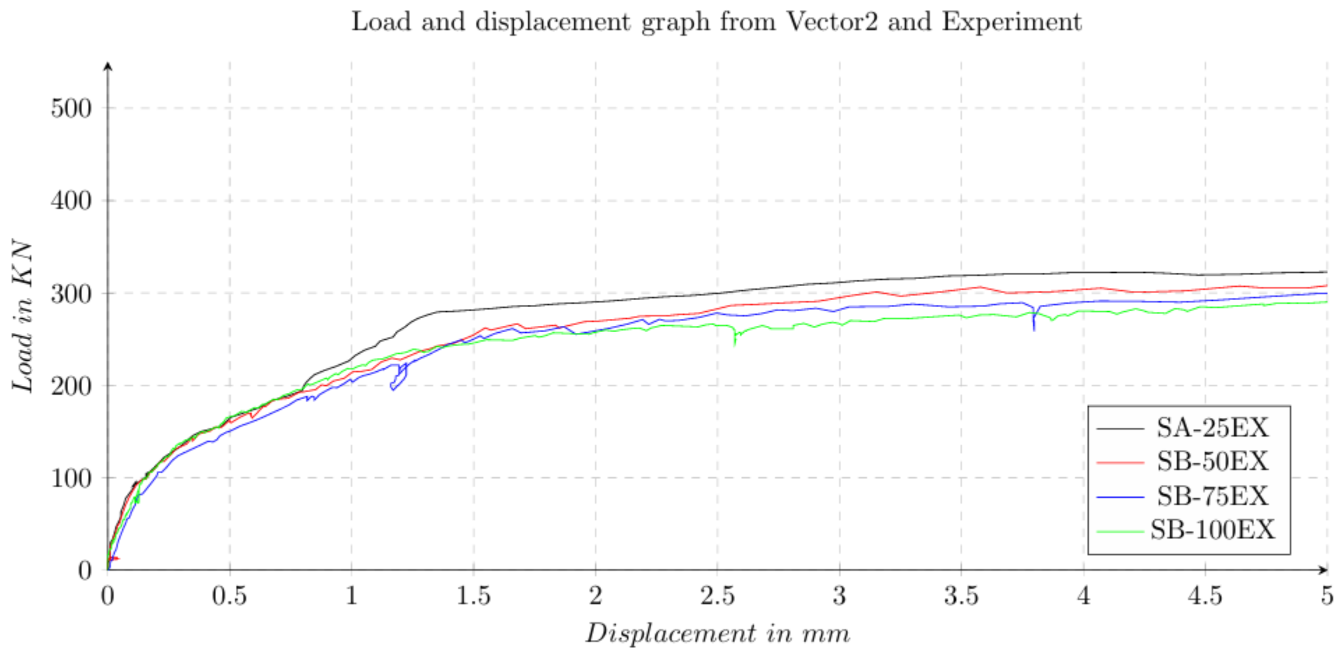

Figure 4-29 Load Vs. Mid-Span Deflection for SB series beams up to 5mm

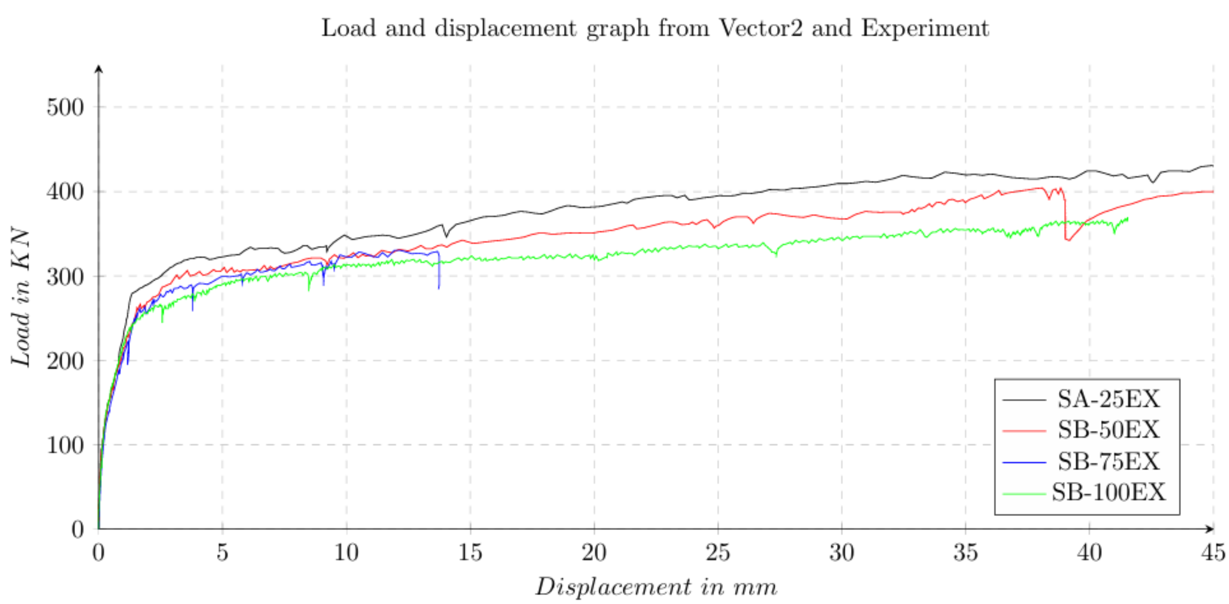

Figure 4-30 Load Vs. Mid-Span Deflection for SB series beams up to failure

4.2 Building Code Predictions

For building code predictions hand calculation procedures were followed while the program RESPONSE 2000 was used to determine predictions based on MCFT.

Table 6-1 below summarizes predictions made by ACI Standard (ACI), Vector 2 and the program RESPONSE 2000 which is based on MCFT.

Table 4-1 Building Code Prediction for Ultimate Load Resistance

	Experimental Results			Ultimate Static Failure Load Prediction (kN)				Remark
Specimen	fc (MPa)	fy (MPa)	Failure Load (kN)	MCFT (Response)	Ansys 3D	MCFT (Vector2)	STM with ACI 318-19	
SA-25	30.52	564.0	438.0	247.2	300.0	390.28	430.8	
SA-50			369.0	247.2	300.0	390.28	430.8	
SA-75			342.0	247.2	300.0	390.28	430.8	
SB-50			424.9	257.8	342.0	410.63	430.8	
SB-75			330.3	267.6	384.0	436.09	430.8	Not loaded to failure
SB-100			369.7	276.6	415.8	444.69	430.8	

Accordingly, the experimental test to prediction ratio is presented Table 4-2:

Table 4-2 Experimental Test to Prediction Ratio

Specimen	Ansys 3D	MCFT (Vector 2)	ACI STM
SA-25	1.46	1.12	1.017
SA-50	1.23	0.95	0.857
SA-75	1.14	0.88	0.794
SB-50	1.24	1.03	0.986
SB-100	0.89	0.83	0.858

4.3 Experimental Results

This section will present the full response of each specimen with respect to the different data obtained from the experiment. It will also elaborate on how the defined variables affected the failure and general behavior of each specimen. As the failure of most specimens was accompanied by spalling, this section will also explain the out of plane deformation of the specimens along with interesting findings.

4.3.1 Load Deformation Curves

Experiments show that all beams exhibited the expected three-point shear load–deflection response an initial linear branch up to first crack, a cracked-but-hardening branch, and a peak followed by softening. Beams with increased side cover or reduced stirrup cage width tended to be less stiff and reach peak load at larger deflections. For example, two companion beams with identical web reinforcement and full cage width (150 mm) but different cover (50 mm vs 75 mm) had very similar initial stiffness, but the beam with 75 mm cover (narrower effective cage) reached only about 80% of the peak load of the 50 mm cover beam. In contrast, when the stirrup cage width was held constant, varying cover from 25 mm to 100 mm produced negligible change in ultimate load. In our tests the beams designed in set I (cage width constant) all achieved the expected shear capacity, regardless of side cover thickness. Thus, overall shear capacity correlated with the effective shear width (distance between stirrups) rather than total beam width or cover.

4.3.2 Out of Plane Deformation/ Strain

Instrumentation on the side faces recorded out-of-plane (horizontal) strains during shear loading. All beams showed measurable out-of-plane deformation once shear cracks formed, regardless of cover thickness. In this study the spalling was expected at the strut but it happened right below the loading jack. This causes us to miss the spalling measurement at the spalled section. Nevertheless, the out of plane measurements collected are not reliable and not presented here due to error in the setup. But we can see that spalling began at the first flexural crack and intensified after the first diagonal shear crack. The measured transverse strain grew steadily with load and reached maximum values near the peak load, indicating that cover spalling or complete delamination was occurring at ultimate. Indeed, beams with thicker side cover began to peel off large segments of cover. Beams with 25–50 mm cover tended to spall "piece by piece" after the peak, whereas the 75 mm cover specimens delaminated a large patch in one piece. In short, increased cover thickness made the cover detach more abruptly, consistent with the notion that larger cover promotes a single-plane split. These observations agree with prior studies: tensile splitting strains develop in the thin cover after flexural cracking and grow until spalling near ultimate load.

4.4 Effect of Varying Side Cover Thickness and Stirrup Cage Width

Varying the concrete cover thickness alone (with full cage width) had little effect on ultimate shear capacity. In the first two test series, all beams had the same 150 mm cage width but covers of 25, 50 or 75 mm. This result aligns with Rahal [25], who found that series I specimens actually increased in strength as cover went from 25→50→75 – the 75 mm cover beam was stronger than the 50 mm one, since spalling occurred only at peak.

However, when cover thickness was increased by narrowing the stirrup cage, strength fell sharply. Two pairs of specimens illustrate this. In each pair the stirrup spacing and reinforcement ratio were identical, so code shear calculations (based on full beam width) predicted equal capacity. This underscores that the effective width of the concrete core (stirrup cage width) governs shear resistance. The tests of Rahal and others imply that simply adding cover (reducing core width) offers no strength benefit.

A clear correlation was established between side cover thickness and structural performance in beams. Specifically, beams with larger cover thicknesses ranging from 75 to 100 mm exhibited several detrimental characteristics, including higher crack spacing and width, earlier onset of spalling, lower post-cracking stiffness, and reduced effective shear capacity. In contrast, beams with covers between 25 and 50 mm demonstrated delayed spalling, effective crack control, and improved interaction between the core and side concrete. These findings align with the research conducted by Rahal [25] and Arbesman [26], highlighting the critical influence of cover thickness on the structural integrity of concrete beams.

5 CONCLUSION AND RECOMMENDATION

5.1 Conclusion

Pre-peak load spalling was more prevalent in beams with larger concrete cover, especially in SA-series specimens where the increase in cover was at the expense of core concrete. The SA-75 beam, for instance, exhibited lower peak load capacity and showed brittle spalling before reaching its full load-carrying potential. The SB-series beams, which retained core dimensions, demonstrated better ductility and load resistance despite having thicker covers. This highlights that the loss of core integrity in SA-series beams due to increased cover significantly compromises structural performance. In both series, an overall decrease in peak load was observed as the cover increased. However, the rate of reduction was more pronounced in the SA-series, reinforcing the negative impact of reducing the core to achieve thicker covers. Experimental and numerical results consistently showed that increased concrete cover alters the crack initiation zones, and in cases of excessive cover, it promotes cover separation and premature spalling, which may shift the failure mode from ductile shear compression to brittle cover peeling.

5.2 Recommendations

Based on the findings of this study, the following recommendations are proposed for future research and practical design:

1. Preserve Core Concrete Dimensions:
   If thicker covers are required (e.g., for fire resistance or environmental exposure), they should be added externally (as in the SB-series), without compromising the structural core dimensions.
2. Design Guidelines Should Address Pre-Peak Spalling:
   Current design standards, including ACI 318, do not explicitly account for pre-peak spalling due to large covers in deep beams. Additional provisions should be considered to limit the cover thickness or provide detailing that mitigates brittle failure.
3. Further Studies on Confinement and Reinforcement Anchorage:
   Additional research is encouraged to explore how varying transverse reinforcement and anchorage detailing can reduce spalling tendencies in beams with large covers.
4. Three-Dimensional Modeling and Parametric Studies:
   While this study used 2D NLFEA, future investigations using 3D finite element models could capture out-of-plane effects and local failures more accurately, particularly in beams with large widths or multiple layers of reinforcement.
5. Long-Term Durability vs. Structural Performance Trade-Off:
   For structures exposed to aggressive environments, a balance must be achieved between providing sufficient cover for durability and maintaining structural efficiency. This trade-off should be evaluated case-by-case in both design and retrofit scenarios.

References

[1] İ. Saribaş And M. Akar, "The Seismic Performance Of Reinforced Sustainable Concrete Low-Rise Structures," *Academic Platform Journal Of Natural Hazards And Disaster Management*, Vol. 3, No. 1, Pp. 32–44, Jun. 2022, Doi: 10.52114/Apjhad.1126565.

[2] K. Tesfaye, "An Experimental Investigation On The Effect And Mechanism Of Side Cover Spalling For Slender Beams Subjected To Shear," Master's Thesis, Addis Ababa University, Addis Ababa , 2021.

[3] Y. Dong, D. M. Frangopol, And D. Saydam, "Time-Variant Sustainability Assessment Of Seismically Vulnerable Bridges Subjected To Multiple Hazards," 2013. Doi: 10.1002/Eqe.2281.

[4] S. Saha, M. Serati, C. Maluk, And D. R. Sahoo, "Synergies Between Heat- And Stress-Induced Spalling Theory Applied To Rock And Concrete In Tunnel Applications," 2023. Doi: 10.1088/1755-1315/1124/1/012076.

[5] A. M. Gil, B. Fernandes, F. L. Bolina, And B. F. Tutikian, "Experimental Analysis Of The Spalling Phenomenon In Precast Reinforced Concrete Columns Exposed To High Temperatures," 2018. Doi: 10.1590/S1983-41952018000400011.

[6] M. Tahershamsi, K. Zandi, K. Lundgren, And M. Plos, "Anchorage Of Naturally Corroded Bars In Reinforced Concrete Structures," 2014. Doi: 10.1680/Macr.13.00276.

[7] D. A. Kuchma And K. S. Kim, "Stress Limits And Minimum Reinforcement Requirements In Shear Design Provisions," 2001. Doi: 10.1002/Pse.94.

[8] © Esa, "Compulsory Ethiopian Standard Design Of Concrete Structures-Part 1-1: General Rules And Rules For Buildings Ces 149," Addis Ababa, 2015.

[9] A. Committee, "Building Code Requirements For Structural Concrete (Aci 318-19) Commentary On Building Code Requirements For Structural Concrete (Aci 318r-19)," 2019.

[10] A. A. Of S. H. And T. Officials, *Lrfd Bridge Design Specifications*, 9th Edition. Washington, Dc: American Association Of State Highway And Transportation Officials, 2020.

[11] Y. Murad, E. Saleh, A. Tarawneh, G. Almasabha, And A. Alghossoon, "Shear Strength Prediction Of Concrete Beams Reinforced With Frp Bars And Stirrups Using Gene Expression Programming," *Sustainability*, Vol. 15, No. 8, P. 6335, 2023, Doi: 10.3390/Su15086335.

[12] L. Jian And B. Mihaylov, "Shear Strength Of Rc Deep Beams With Web Openings Based On Two-Parameter Kinematic Theory," *Structural Concrete*, Vol. 21, No. 1, Pp. 349–361, 2019, Doi: 10.1002/Suco.201800356.

[13] J. K. Wight, F. E. Richart, And J. G. Macgregor, *Reinforced Concrete : Mechanics And Design*. Pearson Prentice Hall, 2012.

[14] B. Kamaran Sulaiman Ismail, "Shear Behaviour Of Reinforced Concrete Deep Beams," 2016.

[15] B. Singh, S. K. Kaushik, K. F. Naveen, And S. Sharma, "Design Of A Continuous Deep Beam Using The Strut And Tie Method," 2006. [Online]. Available: Www.Sid.Ir

[16] T. T. C. Hsu And Y. L. Mo, "Unified Theory Of Concrete Structures," 2010.

[17] W. Ritter, "Die Bauweise Hennebique (Hennebiques Construction Method)," 1899.

[18] F. J. Vecchio And M. P. Collins, "The Modified Compression-Field Theory For Reinforced Concrete Elements Subjected To Shear.," *Aci J.*, Vol. 83, No. 2, Pp. 219–231, 1986.

[19] D. Mitchell And M. P. Collins, "Diagonal Compression Field Theory-A Rational Model For Structural Concrete In Pure Torsion," In *Journal Proceedings*, 1974, Pp. 396–408.

[20] F. J. Vecchio And M. P. Collins, "Predicting The Response Of Reinforced Concrete Beams Subjected To Shear Using Modified Compression Field Theory," *Aci Struct J*, Vol. 85, No. 3, Pp. 258–268, 1988.

[21] E. C. Bentz, *Sectional Analysis Of Reinforced Concrete Members*. University Of Toronto Toronto, 2000.

[22] S. Nagataki, S. H. Lee, And T. Okamoto, "A Study On Mechanism Of Torsional Resistance Of Reinforced Concrete Members," *Doboku Gakkai Ronbunshu*, Vol. 1988, No. 390, Pp. 179–188, 1988.

[23] M. Sirage, M. Sirage Ibrahim, And E. Gebreyouhannes, "Spalling Of Concrete Cover Due To Torsion: Examination Of Advanced Theoretical Models." [Online]. Available: Https://Www.Researchgate.Net/Publication/346970156

[24] K. N. Rahal And M. P. Collins, "Interaction-An Experimental Investigation," *Aci Struct J*, 1995.

[25] K. N. Rahal, "Shear Behavior Of Reinforced Concrete Beams With Variable Thickness Of Concrete Side Cover," *Aci Mater J*, Vol. 103, No. 2, P. 171, 2006.

[26] B. Arbesman, *The Effects Of Stirrup Cover And Amount Of Reinforcement On Shear Capacity Of Reinforced Concrete Beams*. University Of Toronto, 1975.

[27] A. W. Fisher, E. C. Bentz, And M. P. Collins, "Response Of Heavily Reinforced High-Strength Concrete Coupling Beams.," *Aci Struct J*, Vol. 114, No. 6, 2017.

[28] M. Zakaria, T. Ueda, Z. Wu, And L. Meng, "Experimental Investigation On Shear Cracking Behavior In Reinforced Concrete Beams With Shear Reinforcement," *Journal Of Advanced Concrete Technology*, Vol. 7, No. 1, Pp. 79–96, 2009.

[29] F. Moccia, M. Fernández Ruiz, And A. Muttoni, "Spalling Of Concrete Cover Induced By Reinforcement," *Eng Struct*, Vol. 237, Jun. 2021, Doi: 10.1016/J.Engstruct.2021.112188.

[30] A. Dinku, *Construction Materials - Labratory Manual*. 2002. Accessed: May 04, 2025. [Online]. Available: Https://Www.Scribd.Com/Document/367440779/Construction-Materials-Labratory-Manual-By-Abebe-Dinku-Pdf

Appendix A NON-LINEAR FINITE ELEMENT ANALYSIS

A.1 2D NLFEA Using Vector 2

The experimental specimens were simulated using a two-dimensional non-linear finite element analysis (NLFEA) tool known as Vector 2. This software is based on the Modified Compression Field Theory (MCFT) and the Disturbed Stress Field Model, enabling the prediction of the structural behavior of reinforced concrete elements subjected to in-plane normal and shear stresses under both quasi-static and dynamic loading conditions.

The modeling process incorporates FormWorks, a pre-processing application of the finite element model. Post-processing and visualization of analysis results are conducted using Augustus, a dedicated tool for interpreting outputs such as load-displacement curves, stress and strain distributions, crack developments, and other response characteristics. For each loading step, Vector 2 generates detailed output files describing the condition of nodes and elements. These results also include material characteristics, modeling assumptions, and other relevant analytical information.

A.1.1 Material Definition

A.1.1.1 Concrete

Two types of concrete materials were defined for each model, plain concrete used for concrete covers and concrete with smeared reinforcement for part of the beam that includes web reinforcement. Concrete regions were modeled with plane stress rectangular elements with uniform thickness in the out-of-plane direction. The width of the beams was therefore defined as thickness. both compressive and tensile strength of concrete were taken from the experimental program.

A.1.1.2 Reinforcement

Two reinforcement approaches were used. Longitudinal flexural and web reinforcement was modeled explicitly using discrete ductile truss elements, while the web reinforcement was represented as smeared reinforcement within the concrete matrix by specifying the corresponding reinforcement ratio. Material properties such as yield strength and ultimate strength were determined from tensile tests on reinforcement bars performed in the laboratory. Additionally, out-of-plane smeared reinforcement was defined in the plain concrete cover zones to mitigate localized failure effects.

A.1.1.3 Structural Steel

To accurately represent the experimental boundary conditions, steel supports used in the physical tests were also modeled. Structural steel was defined as a separate material in the finite element setup, with its width specified to match the beam width.

A.1.2 Modelling

In modelling the specimens, first, geometry of the element is defined by creating regions. Regions are created by defining four nodes, assigning material and defining mesh parameters. For a moreaccurate result a finer mesh grid of 15mm by 15mm (x, y) was defined for each specimen. Then reinforcements were defined as truss elements between two nodes by assigning previously defined reinforcement material. Finally, the mesh was created and added to the defined structure.

Boundary conditions were set for the defined structure before analysis by adding support restraints at the two sides where structural steel supports were defined. Aimed to create a simply supportedone pin and roller supports were used at alternative supports of the beam model. Monotonic loading was applied by assigning a fixed support displacement.

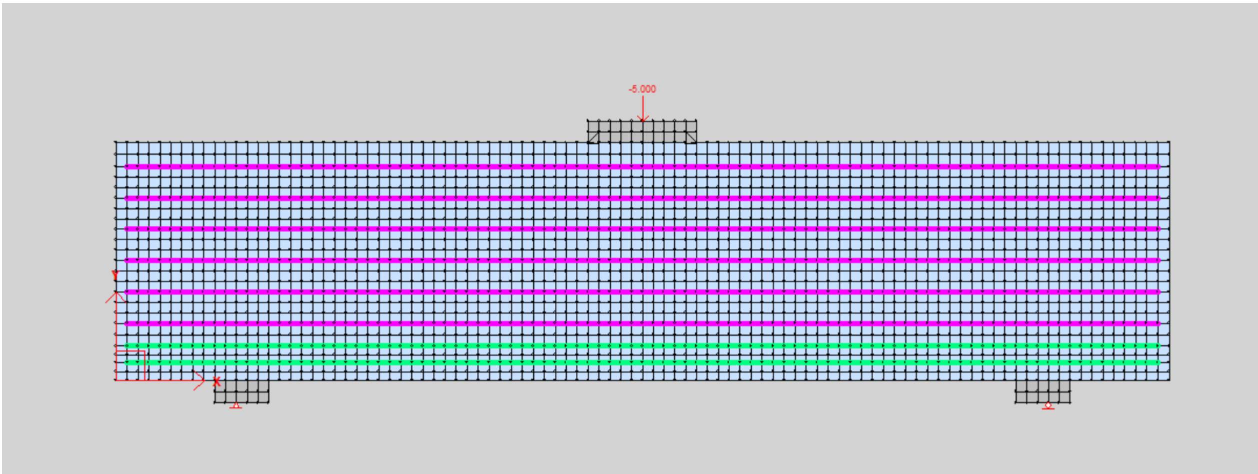

Figure A-1 VecTor 2 Modelling for Specimens

One load case with a monotonic loading type with an iteration of 100 load stages was defined. Vector processor is then run for analysis and results were graphically illustrated by the post processor, Augustus.

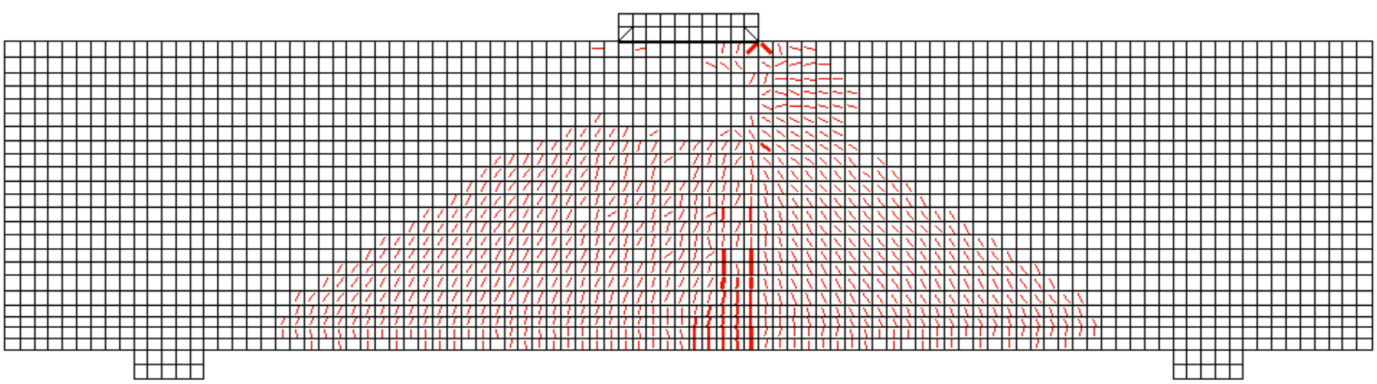

Figure A-2 Crack pattern as simulated by Augustus

Appendix B SURFACE STRAIN MEASUREMENTS

B.1 Location and direction of surface strain measurements

Each surface strain gauge covers 300mm of length.

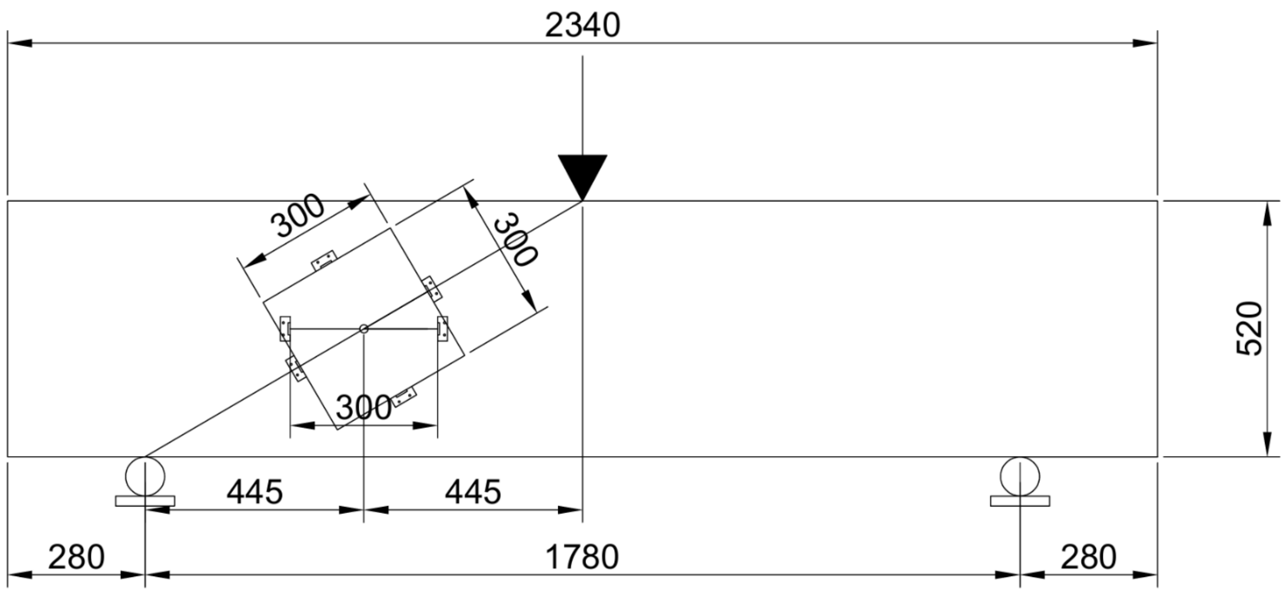

Figure B-1 All surface strain gauges

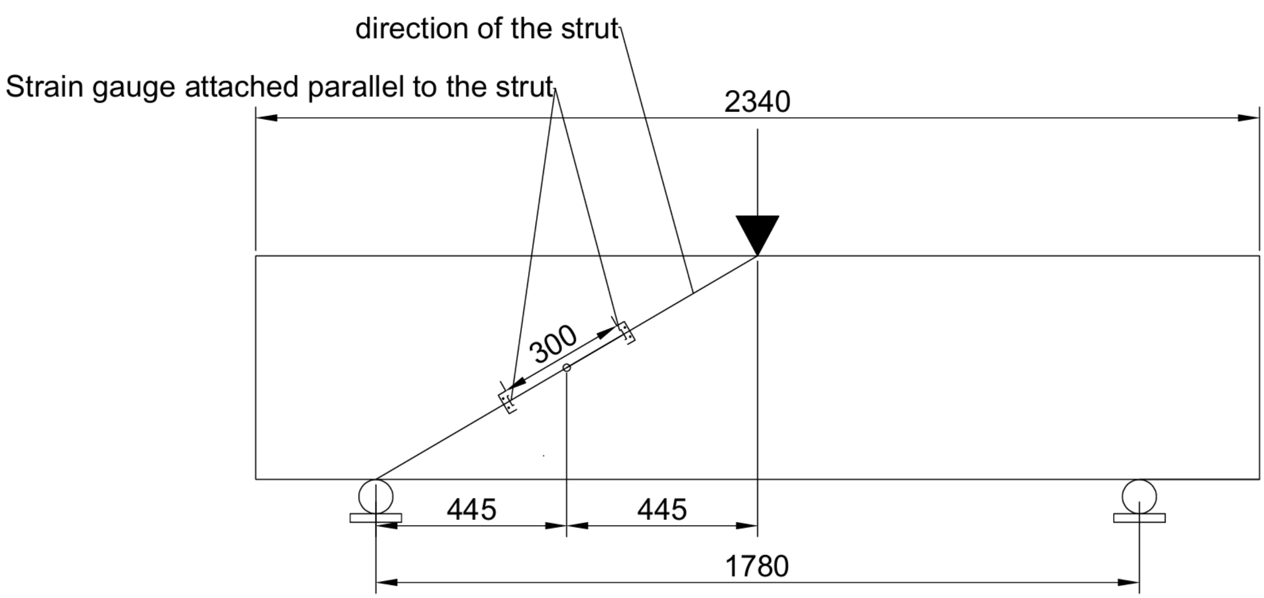

Figure B-2 Surface strain gauge parallel to the strut

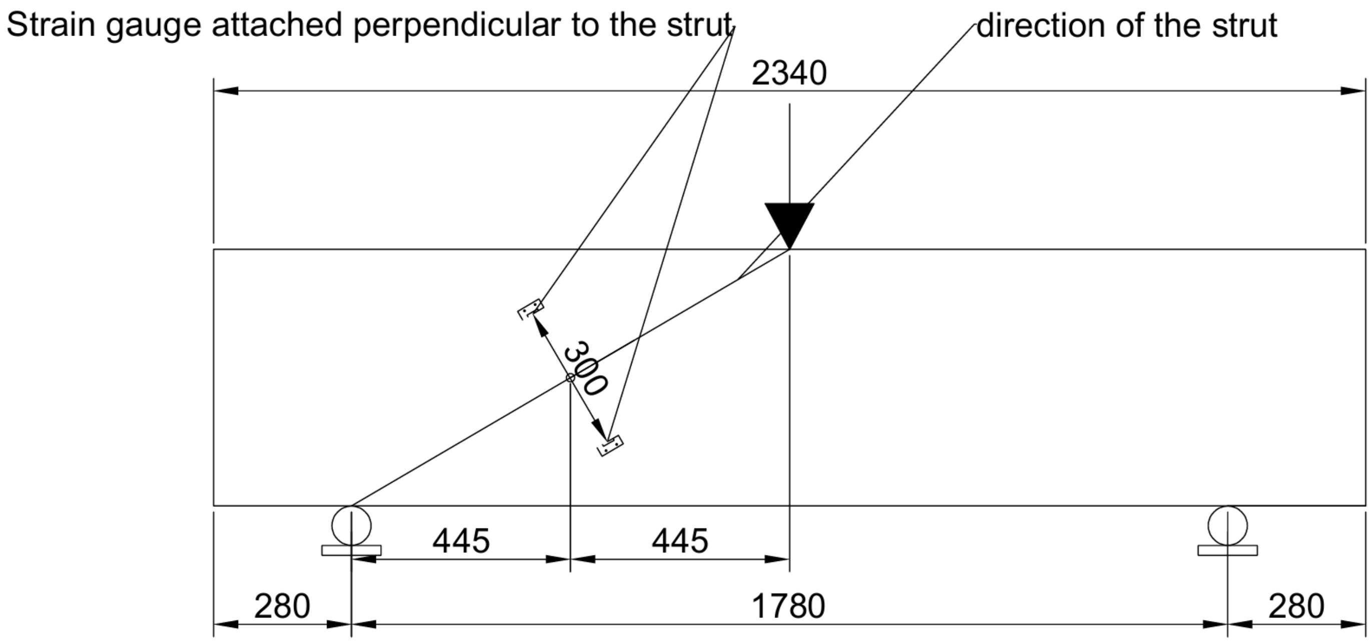

Figure B-3 Surface strain gauge perpendicular to the strut

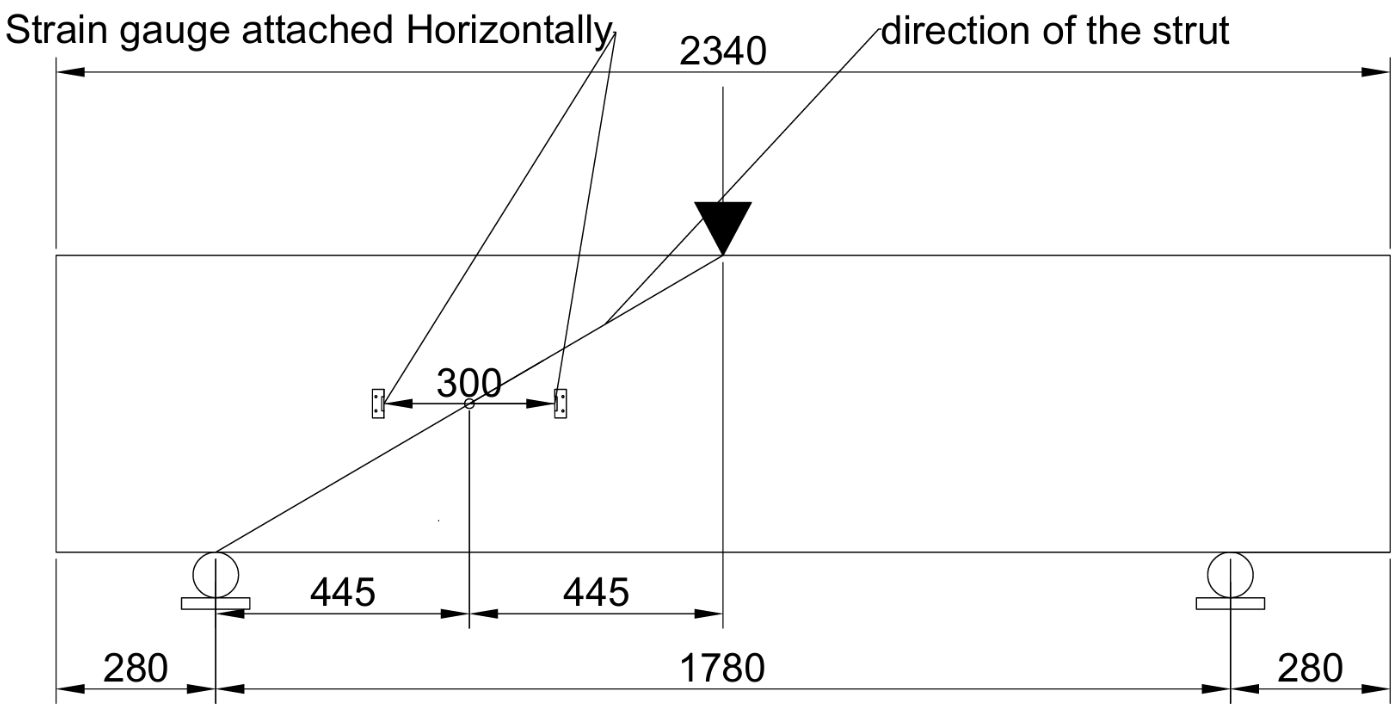

Figure B-4 Surface strain gauge attached horizontally

B.2 SA-25 Surface strain measurements

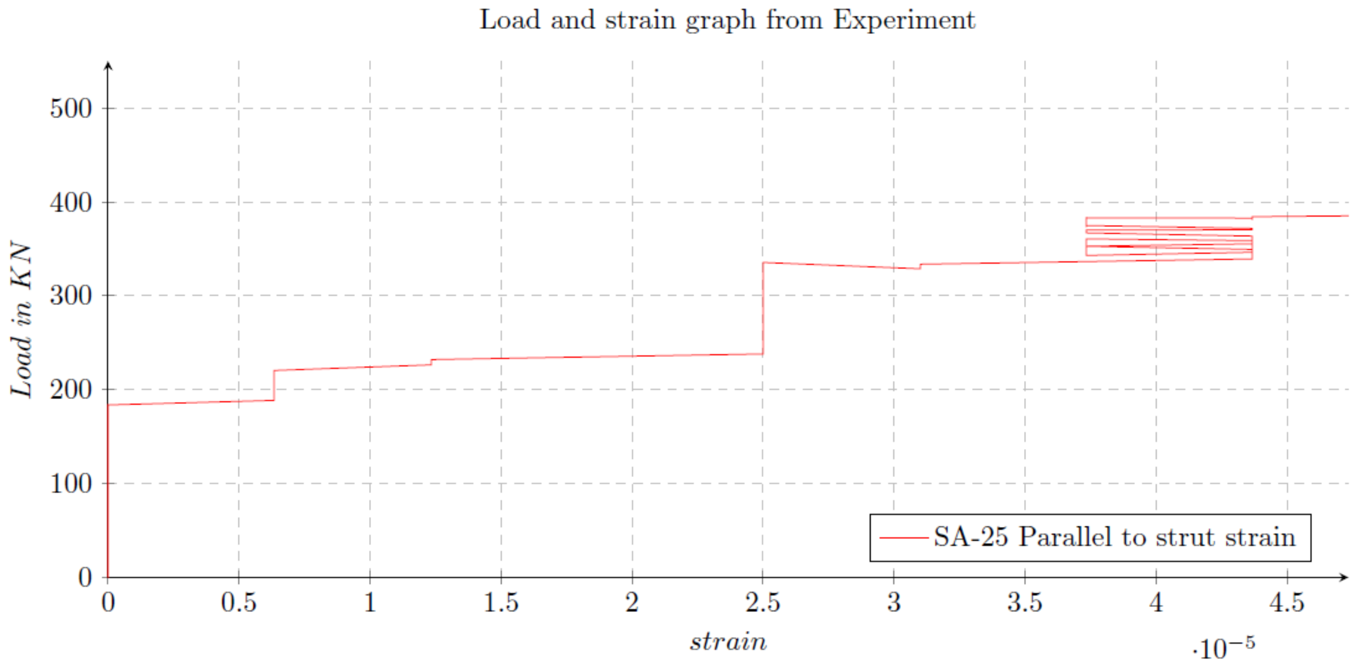

Figure B-5 Surface strain measurements - Parallel to the strut for SA-25

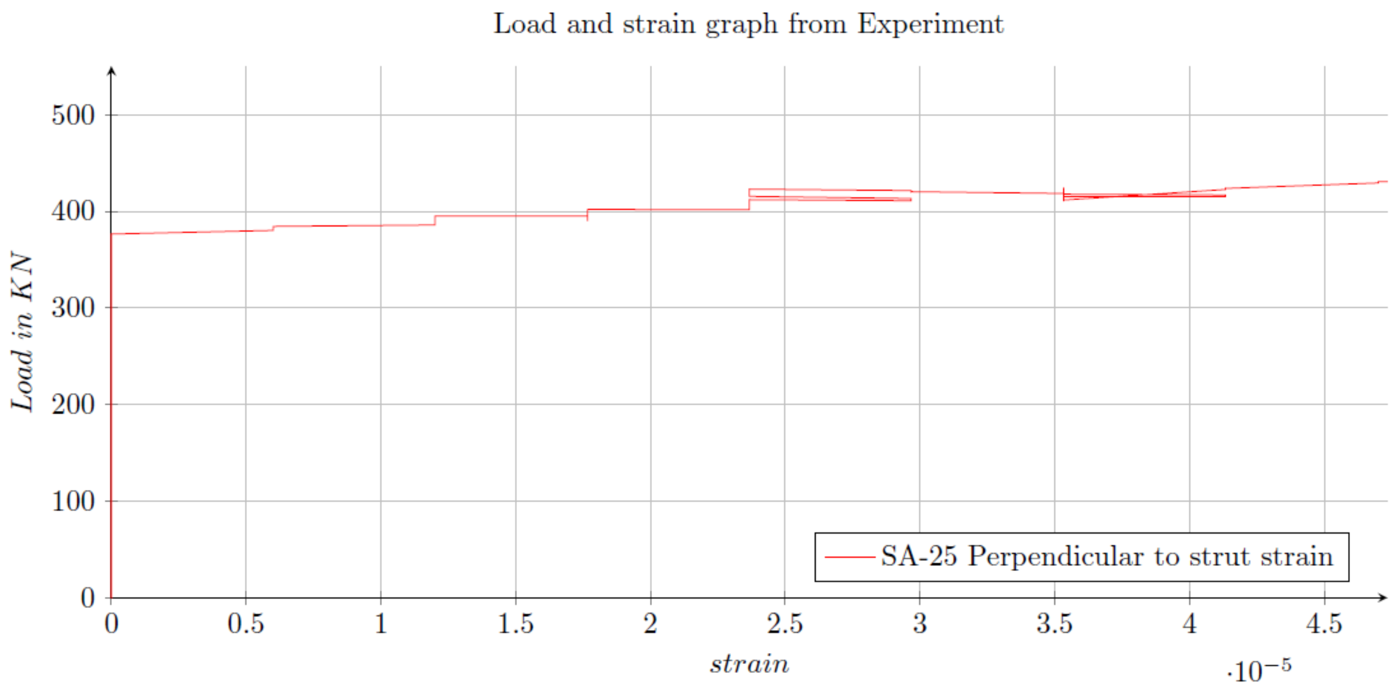

Figure B-6 Surface strain measurements - perpendicular to the strut for SA-25

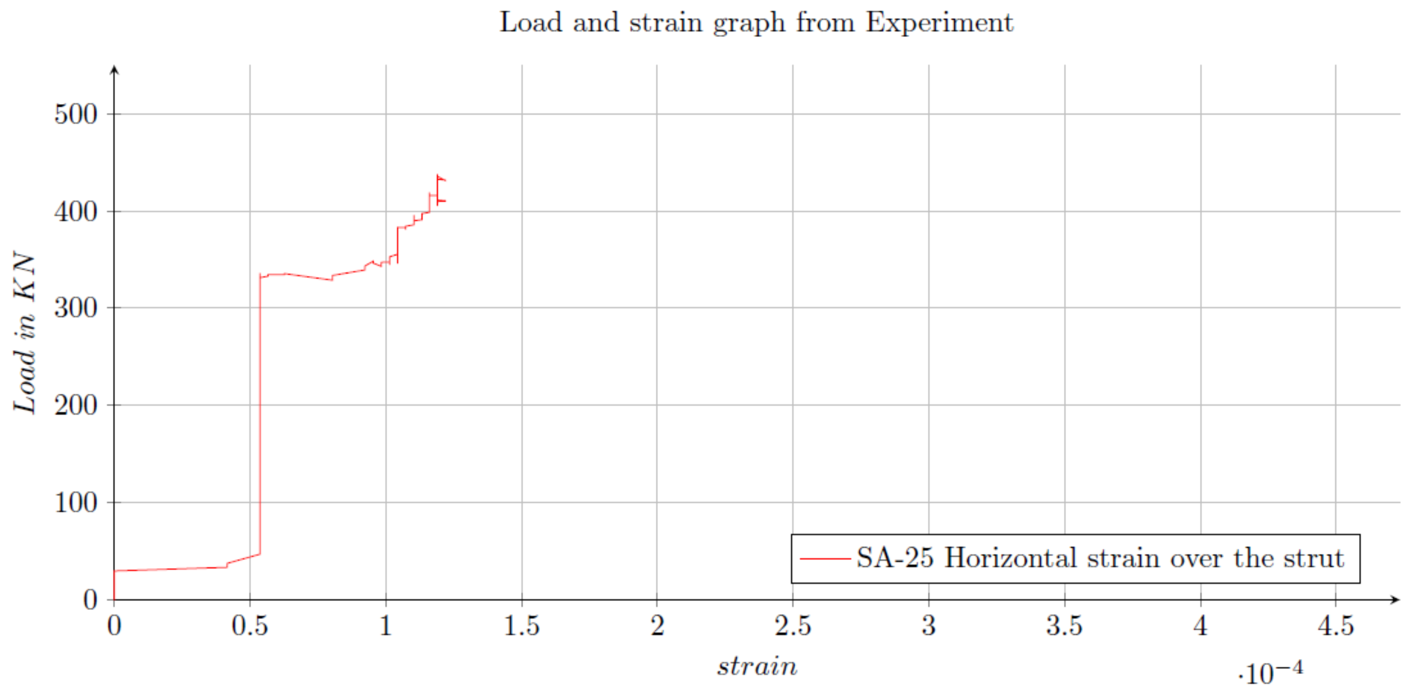

Figure B-7 Surface strain measurements - Horizontal for SA-25

B.3 SA-50 Surface strain measurements

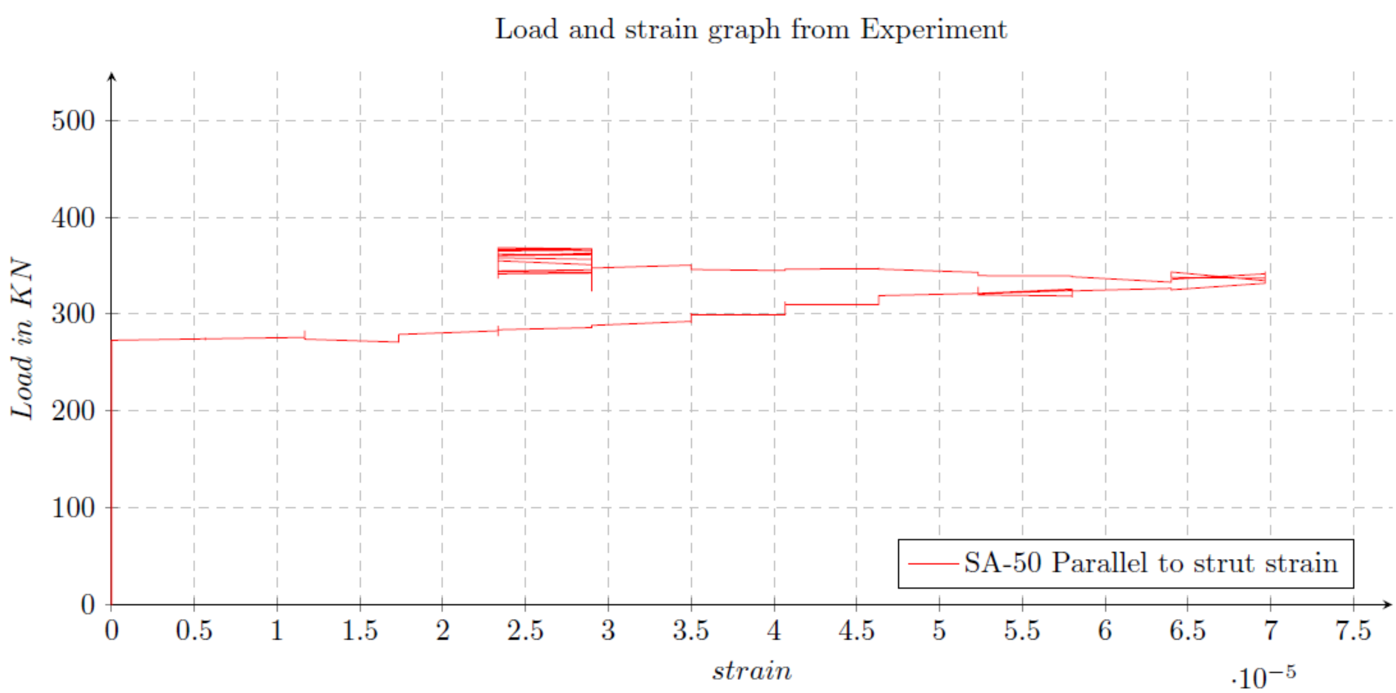

Figure B-8 Surface strain measurements - Parallel to the strut for SA-50

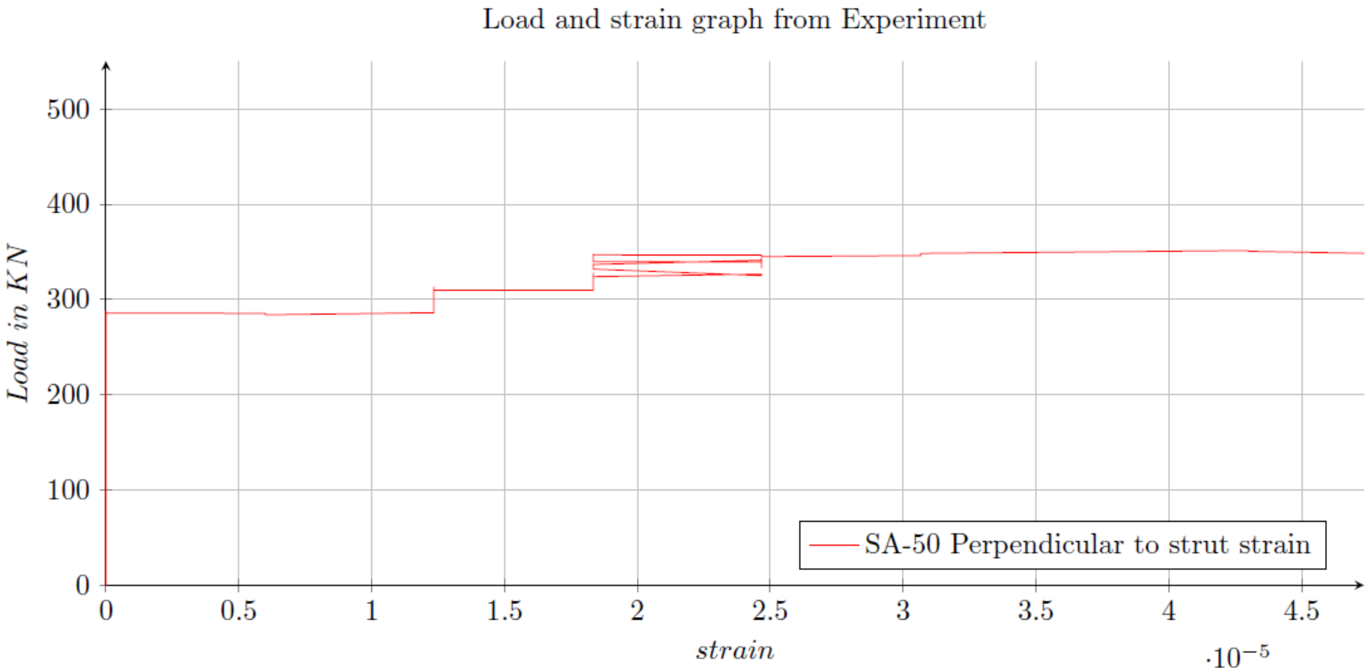

Figure B-9 Surface strain measurements - perpendicular to the strut for SA-50

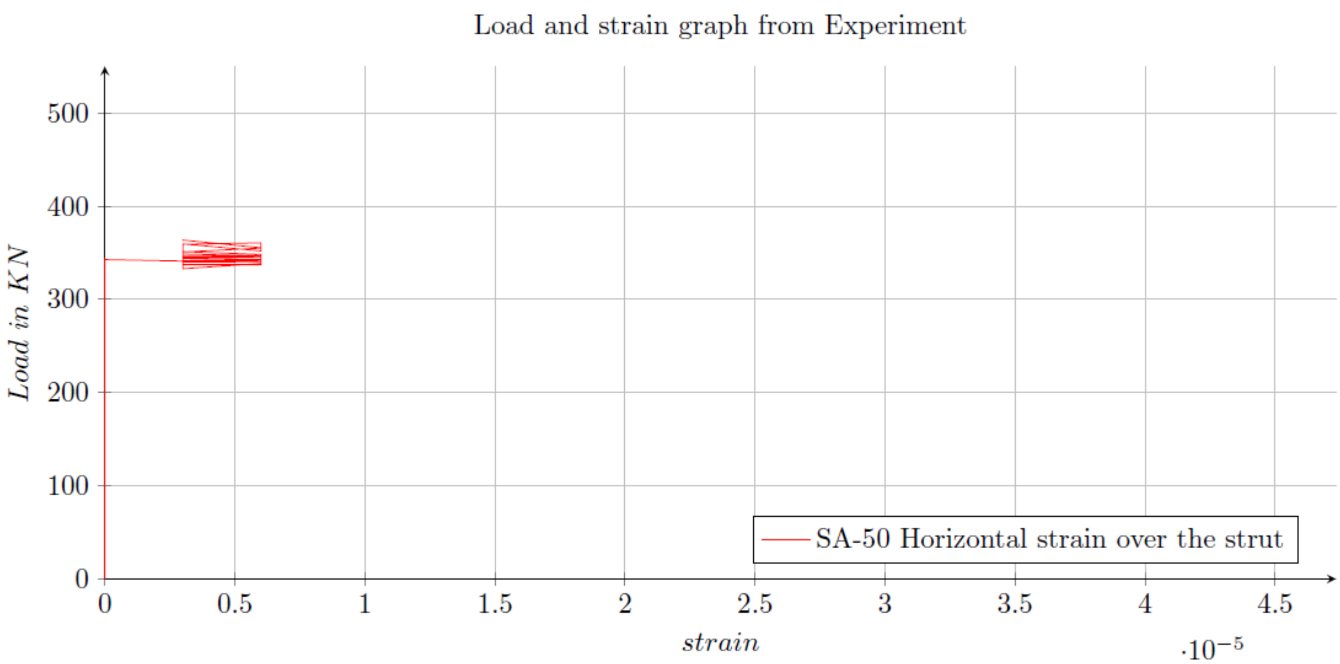

Figure B-10 Surface strain measurements - Horizontal for SA-50

B.4 SA-75 Surface strain measurements

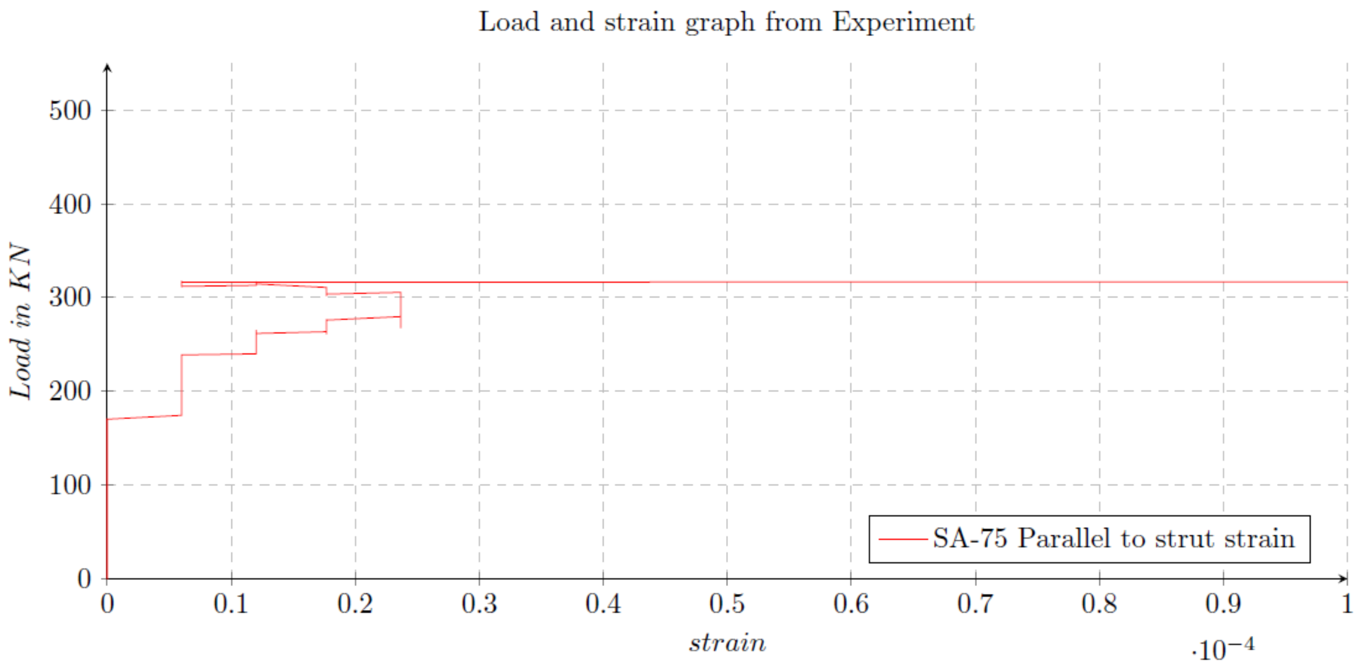

Figure B-11 Surface strain measurements - Parallel to the strut for SA-75

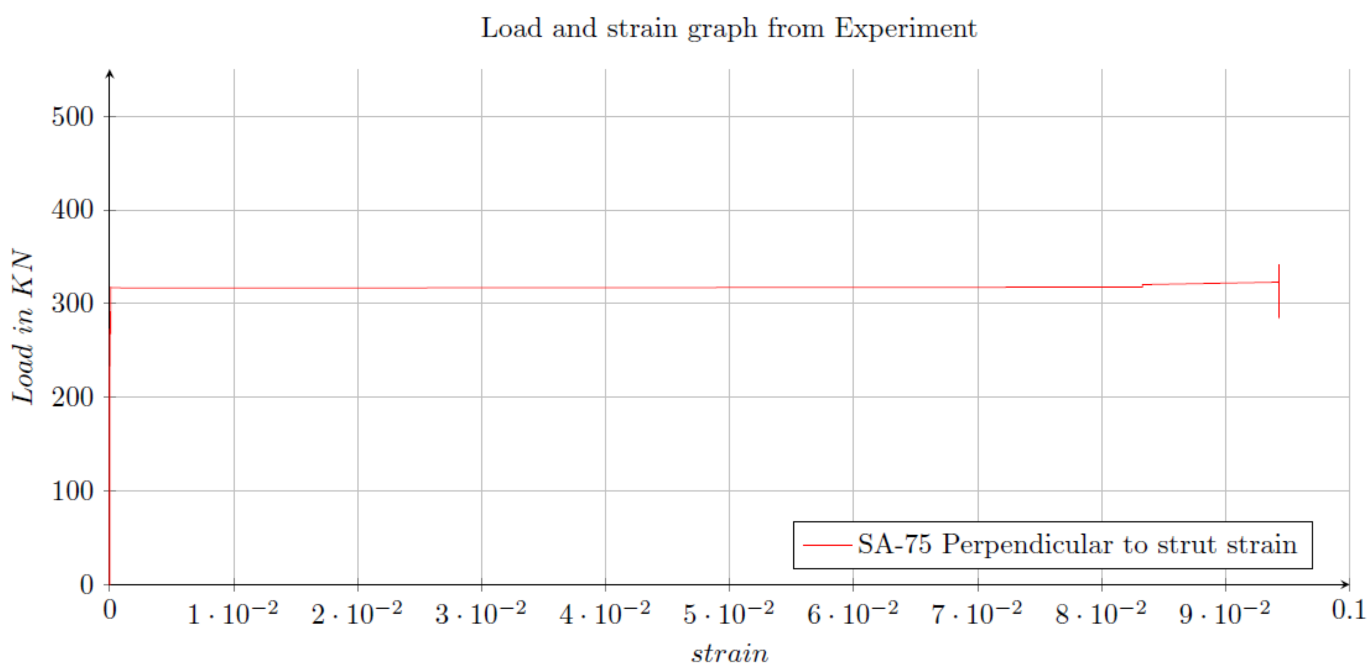

Figure B-12 Surface strain measurements - perpendicular to the strut for SA-75

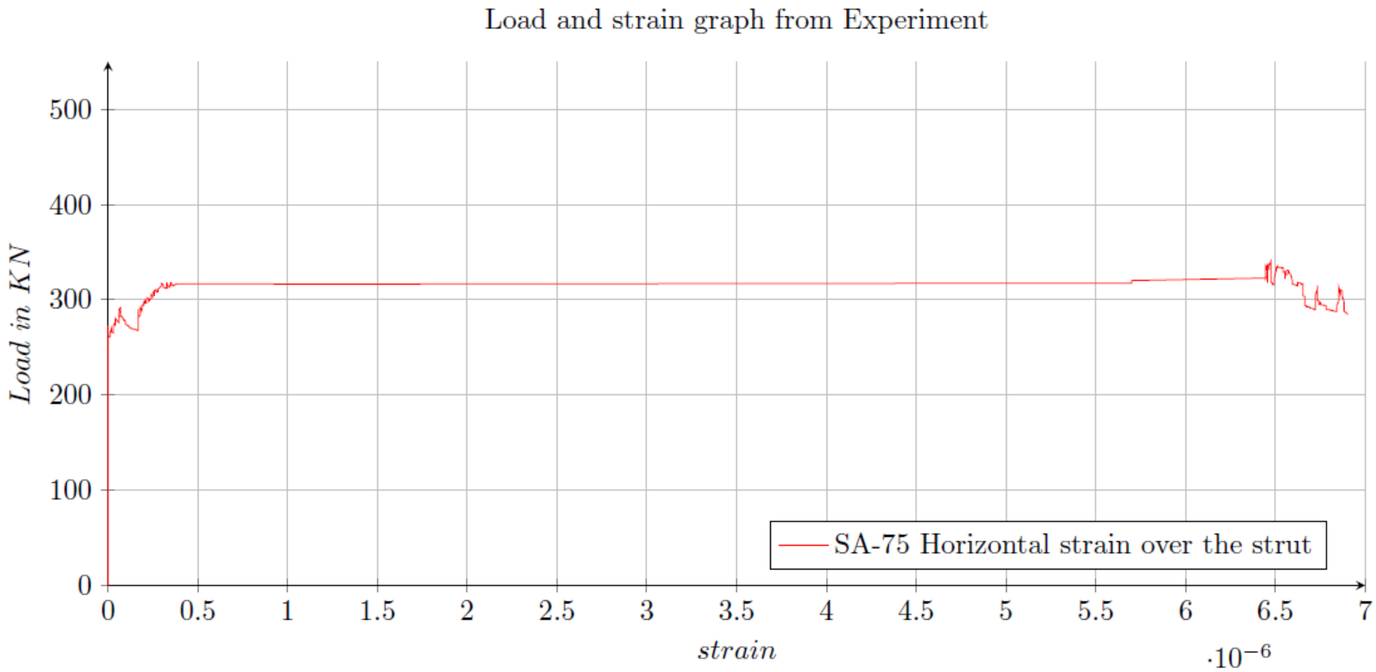

Figure B-13 Surface strain measurements - Horizontal for SA-75

B.5 SB-50 Surface strain measurements

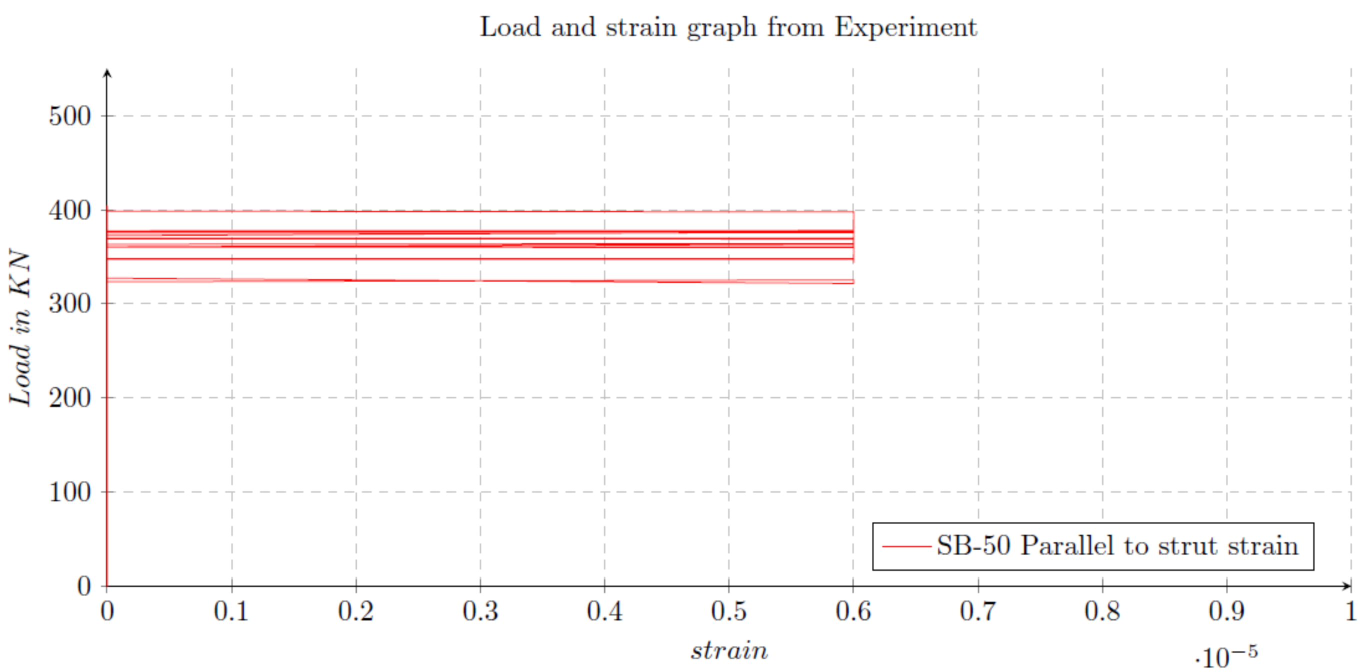

Figure B-14 Surface strain measurements - Parallel to the strut for SB-50

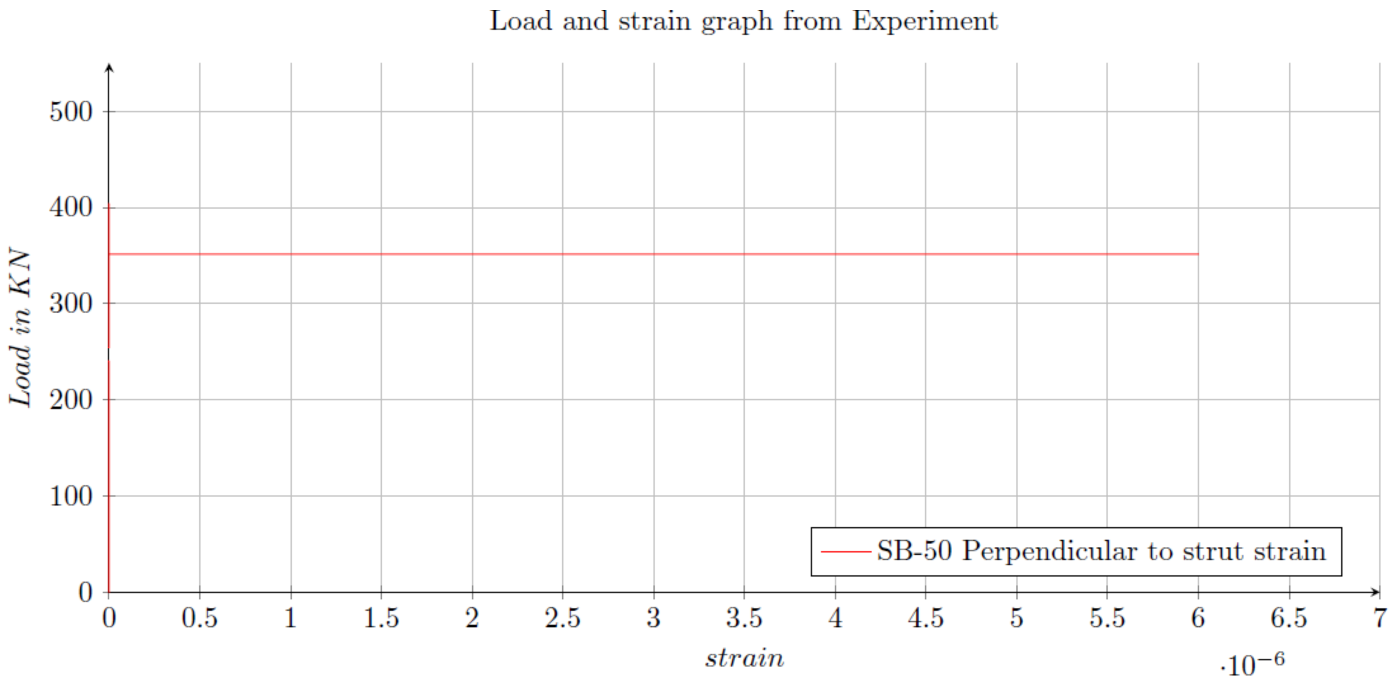

Figure B-15 Surface strain measurements - perpendicular to the strut for SB-50

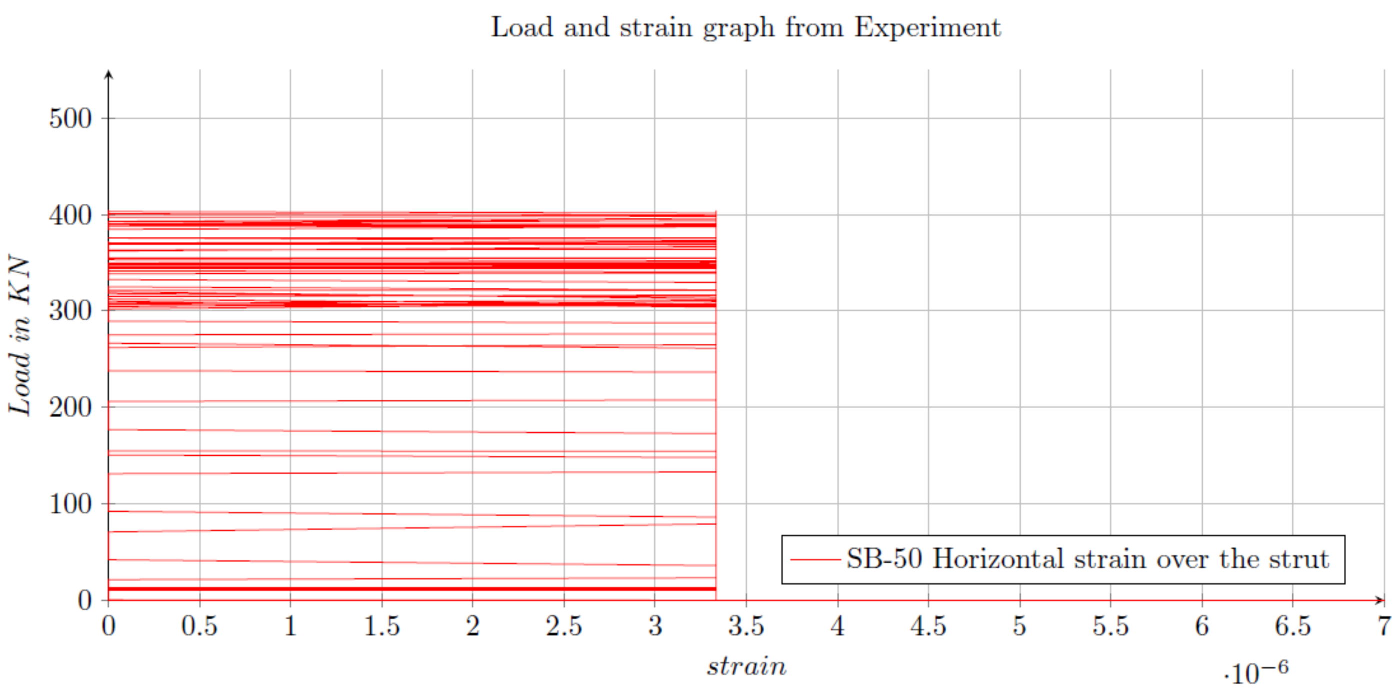

Figure B-16 Surface strain measurements - Horizontal for SB-50

B.6 SB-75 Surface strain measurements

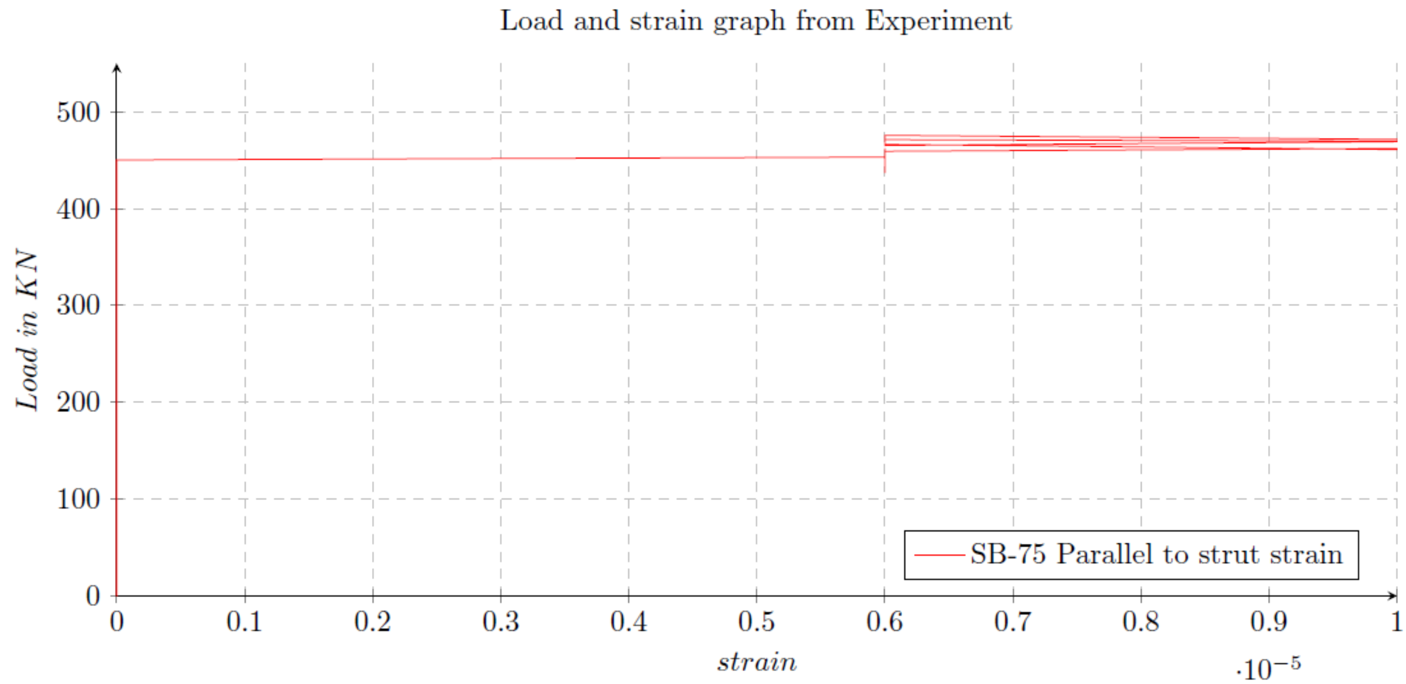

Figure B-17 Surface strain measurements - Parallel to the strut for SB-75

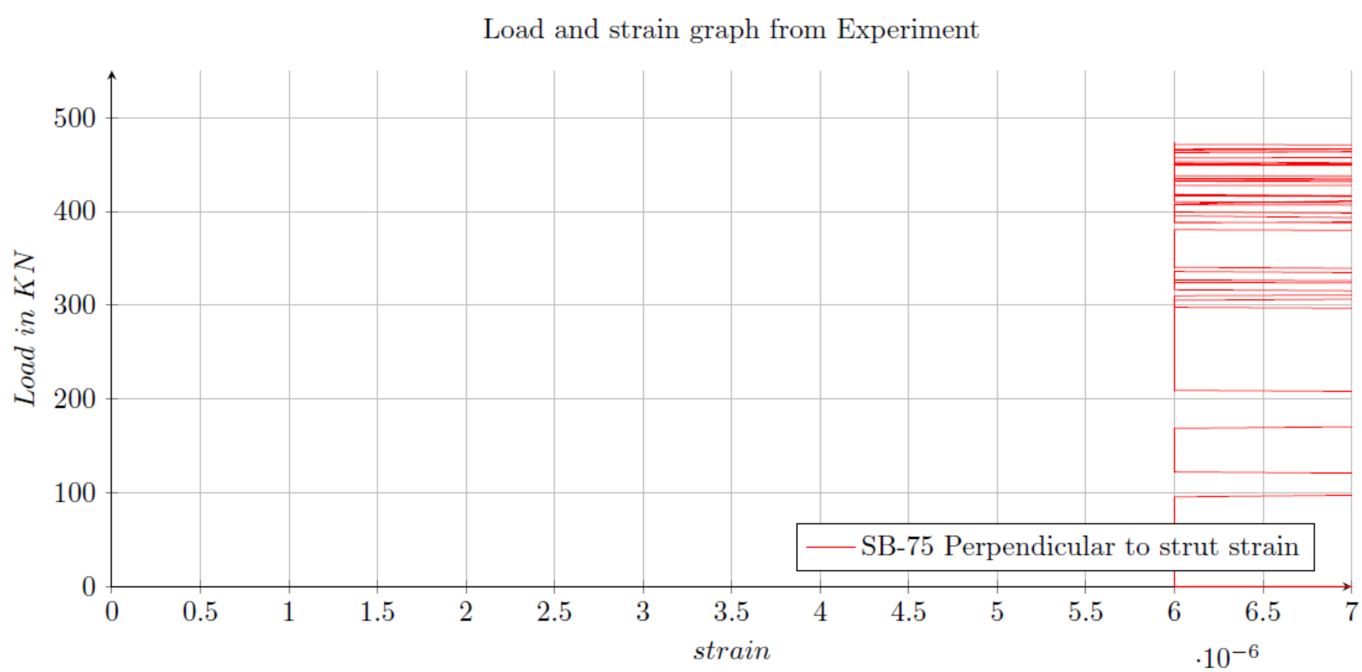

Figure B-18 Surface strain measurements - perpendicular to the strut for SB-75

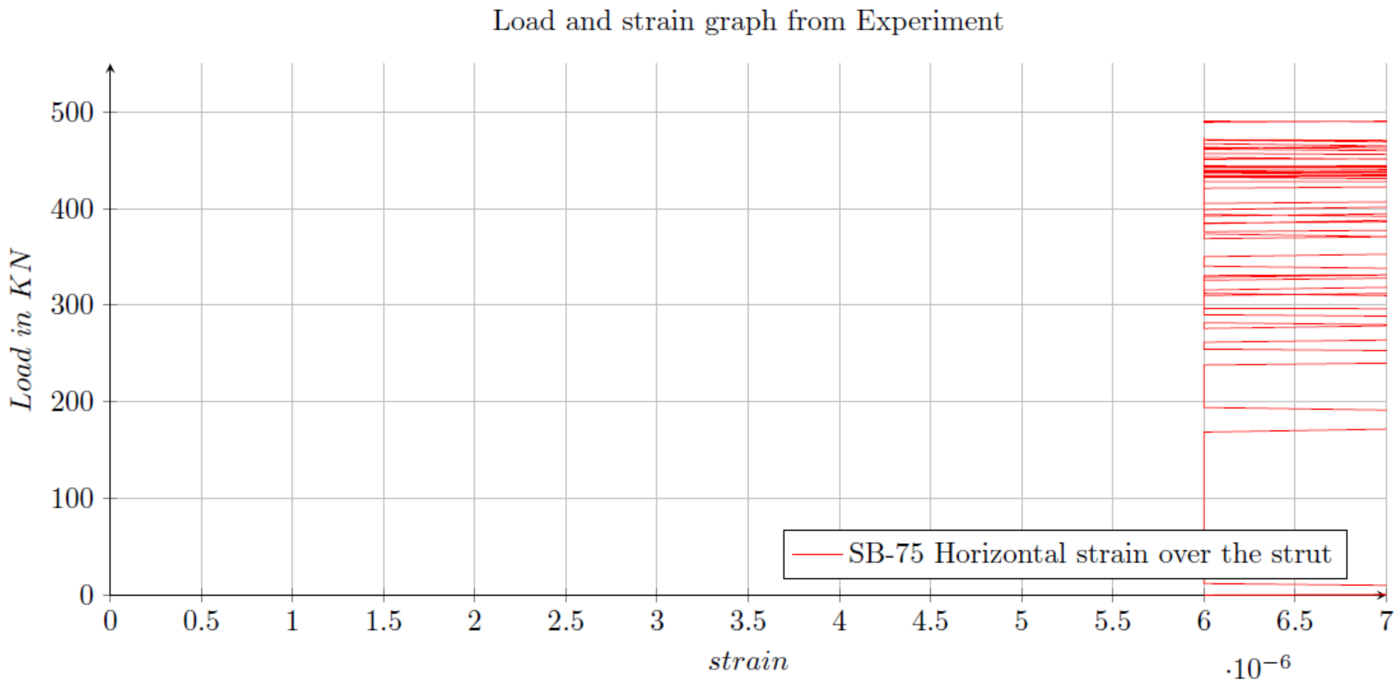

Figure B-19 Surface strain measurements - Horizontal for SB-75

B.7 SB-100 Surface strain measurements

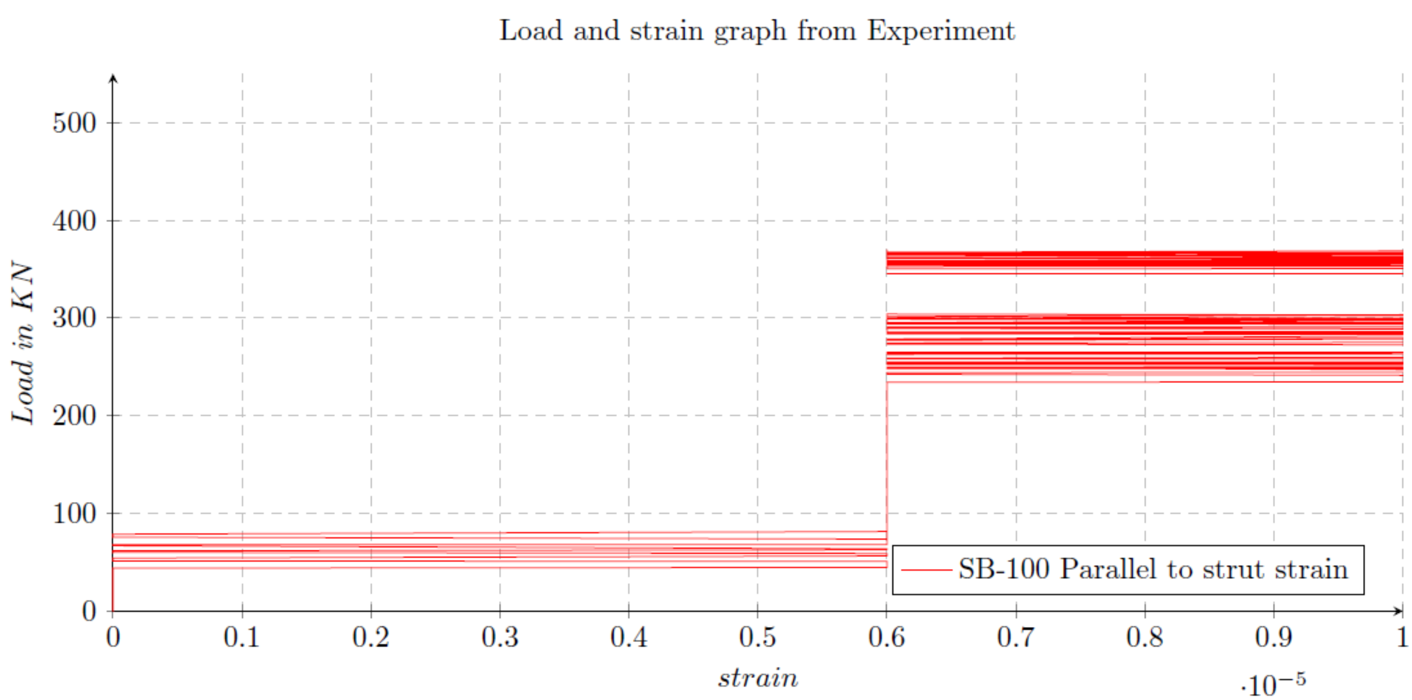

Figure B-20 Surface strain measurements - Parallel to the strut for SB-100

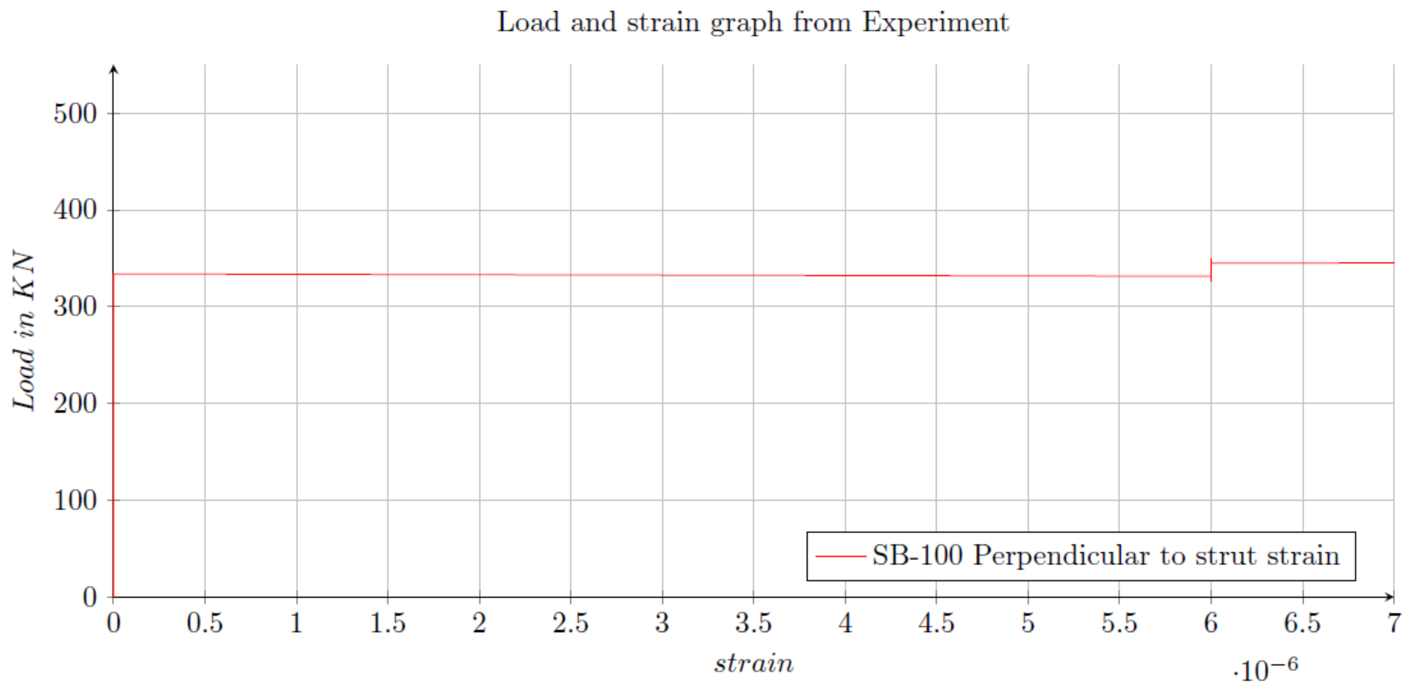

Figure B-21 Surface strain measurements - perpendicular to the strut for SB-100

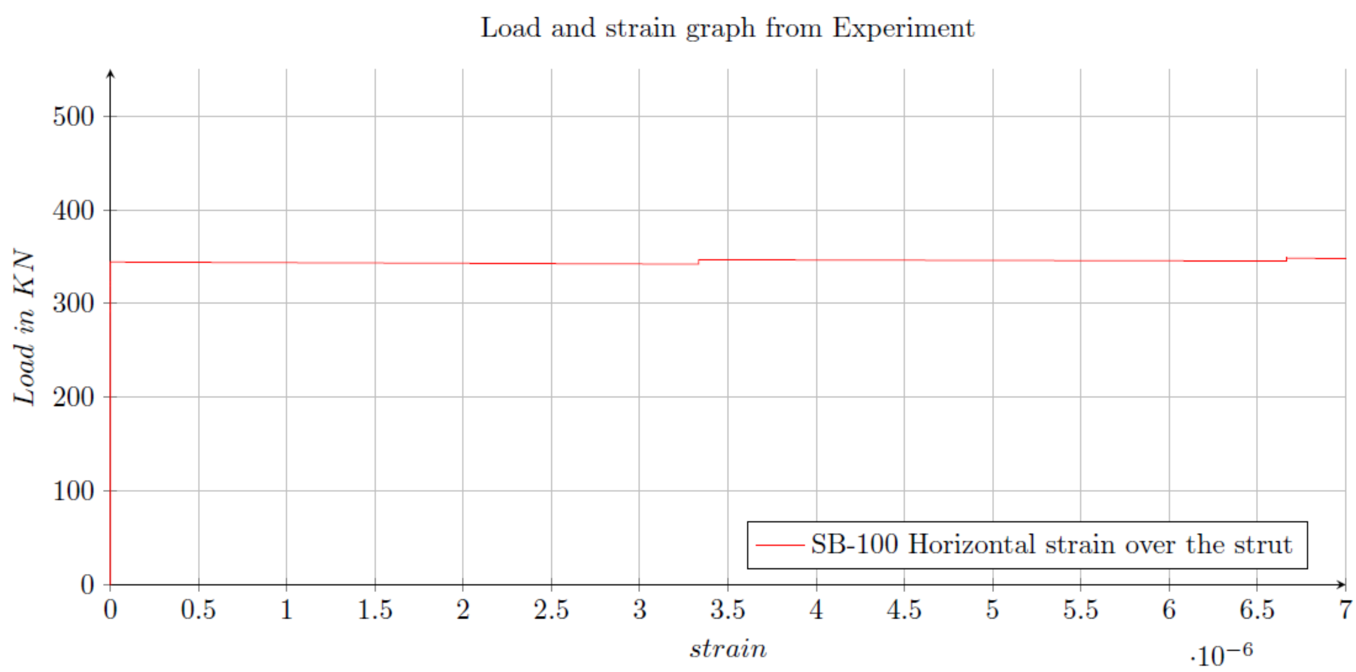

Figure B-22 Surface strain measurements - Horizontal for SB-100

Appendix C MECHANICAL PROPERTIES OF REBAR USED

Table C-1 mechanical properties of rebar used

Nominal diameter	**Diameter (d_1) (mm)**	**Diameter (d_2) (mm)**	**Yield load (kN)**	**Failure load (kN)**	**Elongation (%)**	**Mass/length (kg)**	**Length (m)**
8	7.4	8.59	23.9	29.4	5.3	0.243	0.69
8	7.47	8.58	24.2	28.7	5.3	0.25	0.68
8	7.5	8.59	23.7	29.4	5.6	0.245	0.7
Average	**7.46**	**8.59**	**23.93**	**29.17**	**5.40**	**0.25**	**0.69**
10	9.57	10.84	41.9	54.6	7.7	0.453	0.7
10	9.56	10.92	40.3	50.4	8	0.459	0.7
10	9.55	10.9	39.3	55.3	7.6	0.455	0.7
Average	**9.56**	**10.89**	**40.50**	**53.43**	**7.77**	**0.46**	**0.70**